SPHERICAL SCATTERING OF SUPERPOSITIONS OF LOCALIZED WAVES

DESMOND POWER

Spherical Scattering Of Superpositions Of Localized Waves

By
© Desmond Power, B.Eng.

A thesis submitted to the School of Graduate Studies in partial fulfilment of the requirements for the degree of Master of Engineering

Faculty of Engineering and Applied Science
Memorial University of Newfoundland
St. John's, Newfoundland, Canada

The three pages of release forms should precede this title page.

ISBN 0-315-91638-9

Table of Contents

List of Figures

List of Tables

Nomenclature

The following list of terms appears throughout the body of this document. They are defined here approximately in the order in which they appear in the text:

Term, Variable	Definition
LW	Localized Wave
MPS	Modified Power Spectrum Pulse
FWM	Focus Wave Mode
HWE	Homogeneous Wave Equation
L	Rayleigh distance, diffraction length
f	frequency in Hz
λ	wavelength, (also used as a free parameter)
R_a	aperture radius
A	aperture area
p	pressure
m	mass
$\mathbf{F}$	force vector
V	volume
ϱ	density
$\mathbf{v}$	velocity vector
$\mathbf{a}$	acceleration vector
S	closed surface

Term, Variable	Definition
$\mathbf{S}$	vector normal to surface S
c	speed of sound
$\psi(\mathbf{r},t)$	space-time waveform that satisfies the HWE
$\Psi(\mathbf{k},\omega)$	three dimensional spatial and temporal Fourier transform of ψ
$\mathbf{r}$	spatial observation coordinate, $\mathbf{r} = (x,y,z)$ (cartesian), $\mathbf{r} = (\rho,\phi,z)$ (cylindrical), $\mathbf{r} = (r,\theta,\phi)$ (spherical)
r	magnitude of $\mathbf{r}$, $r = \sqrt{x^2 + y^2 + z^2}$
$\mathbf{r}'$	spatial source coordinate
r'	magnitude of $\mathbf{r}'$
t	time
$\mathbf{k}$	transform variable corresponding to the spatial vector $\mathbf{r}$, $\mathbf{k} = (k_x, k_y, k_z)$ (cartesian), $\mathbf{k} = (\kappa,\varphi,k_z)$ (cylindrical), $\mathbf{k} = (r,\vartheta,\varphi)$ (spherical)
k	wavenumber, magnitude of $\mathbf{k}$, $k = \sqrt{k_x^2 + k_y^2 + k_z^2}$
ω	frequency in radians/second, spatial transform variable corresponding to t
Ξ	a weighting function
$\mathrm{sgn}(x)$	signum function, $\mathrm{sgn}(x) = \begin{cases} 1 & x < 0 \\ 0 & x = 0 \\ 1 & x > 0 \end{cases}$
β, z_0, γ, B, b, τ, T	free parameters
J	Bessel function
H	Hankel function
P	Legrendre polynomial
j	spherical Bessel function
h	spherical Hankel function

Term, Variable	Definition
$g(\mathbf{r},\mathbf{r}')$	Propagator function, $1/4\pi R$
I	field intensity
$\Im$	field fluence
$\mathscr{E}$	total energy, field energy
HWHM, ρ^{HWHM}	half waist at half maximum
w	pulse waist
W	window function
Γ	gamma function, array efficiency
ω_{rad}, Ω_{rad}, ω_{meas}, Ω_{meas}, f_{eff}	defined effective frequencies
θ	beam divergence (also used in spherical coordinate system)
α_n, γ_n	variables defined to simplify plane wave scattering expression
δ	delta function
Λ	spherical backscatter spectrum (temporal Fourier transform of signal backscattered from a sphere)
u	unit step function
κ	compressibility, cylindrical spatial Fourier transform coordinate
υ	reconstructed backscatter signal
Υ	reconstructed backscatter spectrum, spatial Fourier transform of υ
ς_n	backscatter signal from n^{th} transmit element

Abstract

Localized wave (LW) solutions to the homogeneous wave equation represent broadband focused interference patterns whose focusing properties have been demonstrated to be superior to those of equivalent monochromatic (i.e. CW) solutions, in the context of multi-time-derivative transmit-receive systems. The focused, broadband nature of these pulses make them ideal candidates for use in remote sensing. The broadband nature of these LWs allows for enhanced target parameter extraction while the superior focusing properties ensure that a relatively large amount of energy reaches the target.

The spherically backscattered spectra of acoustic realizations of LWs are investigated for purposes of remote sensing. The LWs are acoustically launched with a synthetic hydrophone array. The backscattered spectra of several different sized steel and aluminum spheres have been obtained. Analysis indicates that the sphere radius can be readily extracted from these spectra. The backscattered spectra of steel sphere pairs have also been obtained. Preliminary analysis indicates that the single-sphere and double-sphere backscattered spectra have similar characteristics. However, it is questionable whether or not analysis of multi-sphere backscattered spectra will produce useful experimental data for a practical LW remote sensing system.

Acknowledgements

I wish to thank sincerely my thesis supervisor, Dr. Rod Donnelly, for his important contribution to this work. It is through his patience, understanding and advice that this work stands finished. Thanks are also due to Dr. Richard Ziolkowski of the University of Arizona. His original research and experiments paved the way to the success of this project. I also thank him for his patience in replying to my endless E-mail questions.

I am deeply indebted to the Canadian Centre for Marine Communications (CCMC) for the extended use of their acoustic tank and equipment at the Marine Institute, St. John's, Newfoundland. I also thank Bob MacIsaac, who was the initial contact person with CCMC. Bob also provided very helpful advice in the use of CCMC's hydrophones and equipment. I also thank Brian McGraw of CCMC for his technical assistance, and Leo Spurrell and Humphrey Dye of Memorial University's Technical Services for the machined spheres.

Finally, I would like to thank my wife Brenda for her patience and understanding throughout the duration of my graduate studies. Brenda put up with my many late nights and weekends at the Marine Institute and the University, and I thank her for her kindness and love.

1 Introduction

It is inherently true that all classical aperture launched space-time waveforms diffract as they propagate. This diffraction causes the maximum amplitude of the waveform to decay, generally with a $1/r^2$ decrease in the field's energy as the energy spreads out over an increasing volume. Certain spatially localized energy beams have the ability to retain their localization before attaining the $1/r^2$ energy decay. This phenomenon may be given in terms of a diffraction length or Rayleigh distance, L_R, which describes the distance before which a spatially localized beam attains a $1/r^2$ decay. For example, a CW piston beam consisting of circular aperture uniformly driven with a continuous wave (CW) signal of frequency $f=c/\lambda$, will have natural focussing properties. For the CW piston with aperture radius R_a and area $A = \pi R_a^2$, the diffraction length may be given by the classical Rayleigh distance [Ziolkowski, 1991]

$$L_{\text{Piston}} = \frac{A}{\lambda} = \frac{\pi R_a^2}{\lambda} . \qquad \textbf{(1.1)}$$

Over the past few years, there has been great interest in space-time waveforms which have extended regions of localization, i.e. they have associated diffraction lengths which exceed classical Rayleigh distances. These waveforms, called *Localized Waves* (LWs), were first introduced by Brittingham [1983] and were studied in detail later by Ziolkowski [1985, 1988, 1989, 1990, 1991]. These waveforms do not defy the laws of physics since their physical realizations eventually attain a $1/r^2$ energy decay. However, LWs have interesting propagation characteristics and their regions of extended localization have been demonstrated using acoustical transmit arrays in water.

This work addresses possible uses of the LWs for remote sensing purposes. The broadband nature of the FWMs allow for the ability to extract target parameters. In order to test this possible application, backscatter experiments were performed on a number of steel and aluminum spheres using an acoustic LW realization.

In chapter two, the background theory of localized waves is discussed in a literature review. Since the fundamental LW is an infinite energy pulse, this chapter includes discussion on designing finite energy LWs from the fundamental infinite energy pulse. A particular finite energy LW called the *Modified Power Spectrum Pulse* (MPS) is described in detail. The results from Ziolkowski's [1989, 1990] localized wave experiments are also given. Using these results, Ziolkowski verified the superior propagation characteristics of LWs.

In chapter three, the predicted MPS spherical backscatter spectrum is calculated using techniques described in chapter two. The predicted backscattered spectrum is further analyzed to show a method of extracting the radius of the sphere. In chapter four, the methodology of obtaining the experimental backscattered spectrum is detailed. The acoustical launching array, along with the data acquisition system, is described in detail. In chapter five, the obtained spherical backscattered spectrum is analyzed. A computer algorithm is used to extract the radius of the sphere from the spectrum. In chapter six, the two ball experiments are described. In the next few sections, some relevant preliminary theory is presented for the purpose of completeness.

1.1 Preliminary Theory

Since the main body of this work centres around acoustic scattering in a compressible fluid, it is necessary to discuss some fluid dynamics theory. The material which is presented may be found in a variety of texts including [Morse & Ingard, 1968; Bowman, Senior & Uslenghi, 1969; Wyld, 1976]. Ultimately, the discussion will lead to the derivation of the wave equation for a pressure field. The fact that a pressure field satisfies the wave equation has important repercussions for the research presented here. If one wishes to launch a particular pressure field, $p(\mathbf{r},t)$, then the equation describing the pressure field should be a solution to the wave equation.

1.3.1 Hydrodynamics

Consider first a small volume element of fluid, dV, to which Newton's second law may be applied:

$$\mathbf{F} = m\mathbf{a} = \varrho dV\frac{d\mathbf{v}}{dt} \tag{1.2}$$

In (1.2), $m=\varrho dV$ is the mass of the fluid element, ϱ is its density, $\mathbf{a}=d\mathbf{v}/dt$ is its acceleration, and $\mathbf{v}$ is the velocity. In general, the density and velocity are functions of both space and time, $\varrho=\varrho(\mathbf{r},t)$, $\mathbf{v}=\mathbf{v}(\mathbf{r},t)$, thus the time derivative of the velocity may be written as

$$\frac{d\mathbf{v}}{dt} = \frac{\partial\mathbf{v}}{\partial t} + \frac{\partial x}{\partial t}\frac{\partial\mathbf{v}}{\partial x} + \frac{\partial y}{\partial t}\frac{\partial\mathbf{v}}{\partial y} + \frac{\partial z}{\partial t}\frac{\partial\mathbf{v}}{\partial z} = \frac{\partial\mathbf{v}}{\partial t} + (\mathbf{v}\cdot\nabla)\mathbf{v}\ , \tag{1.3}$$

where ∇ is the operator $(\partial/\partial x,\ \partial/\partial y,\ \partial/\partial z)$ in cartesian coordinates. The force, $\mathbf{F}$, and

fluid pressure, p, may also be related through

$$\mathbf{F} = -\nabla p \, dV \, . \tag{1.4}$$

Hence Newton's second law may be re-written as

$$\varrho \left[\frac{\partial \mathbf{v}}{\partial t} + (\mathbf{v} \cdot \nabla)\mathbf{v} \right] = -\nabla p \, . \tag{1.5}$$

In (1.5) it is assumed that the fluid is non-viscous and hence there is no energy loss by the forces of friction between molecules of the fluid.

We will also need the continuity equation for fluids:

$$-\oint_S d\mathbf{S} \cdot \varrho \mathbf{v} = -\int_V dV \nabla \cdot \{\varrho \mathbf{v}\} = \int_V dV \frac{\partial \varrho}{\partial t} \, , \tag{1.6}$$

where the volume integral on the RHS of (1.6) determines the rate of change of matter in volume V, while the surface integral on the LHS of (1.6) determines the flow of matter across the surface S enclosing V. This can also be written in the form

$$\frac{\partial \varrho}{\partial t} + \nabla \cdot \{\varrho \mathbf{v}\} = 0. \tag{1.7}$$

1.3.2 Wave Motion In A Compressible Fluid

In this section we will consider small oscillations (e.g. sound vibrations) in a compressible fluid of uniform average pressure and density, p_0 & ϱ_0. As such, the pressure and density may be denoted as $p = p_0 + p'$ & $\varrho = \varrho_0 + \varrho'$, where p' & ϱ' are the small oscillations in the medium pressure and density. If it is assumed that the pressure and density oscillations are small compared to their respective average values, then

Newton's second law (1.5) can be approximated by

$$\varrho_0 \frac{\partial \mathbf{v}}{\partial t} = -\nabla p' \ , \tag{1.8}$$

where the nonlinear terms $(\mathbf{v}\cdot\nabla)\mathbf{v}$ and $\varrho'\mathbf{v}$ are assumed negligible. The continuity equation becomes

$$\frac{\partial p'}{\partial t} = \varrho_0 \nabla \cdot \mathbf{v} \ . \tag{1.9}$$

If the pressure is assumed to be a function of density only, then the pressure and density fluctuations are related by the square of the speed of sound in the medium,

$$p' = c^2 \varrho' \ . \tag{1.10}$$

Hence, the homogenous wave equation may now be derived for the pressure fluctuations by taking the divergence of (1.8) and using (1.9) and (1.10) to eliminate $\mathbf{v}$ and ϱ'.

$$\nabla^2 p' - \frac{1}{c^2}\frac{\partial^2 p'}{\partial t^2} = 0 \tag{1.11}$$

In the next chapter, interesting localized wave solutions to the HWE will be discussed, along with their methods of design. Given an initial pressure field, p, one can easily determine the scattered field from objects of simple shapes. The research presented in chapters 3-6 focuses on the backscattered signal from spheres of arbitrary size and acoustical impedance.

2 Relevant Background

Although this chapter is devoted to a literature review, it will be seen that a great portion of other authors' research is given here, rather than brief summaries of their work. This is deliberately done so that the reader may get a full picture of the objective of the new research presented later. It will be seen how naturally the previous research flows into the context of that presented in the chapters following.

2.1 Focus Wave Modes

Focus Wave Modes (FWMs) were first introduced by Brittingham in 1983. In his work, he described a family of three-dimensional, source free, non-diffracting pulses which propagate at the speed of light in free space. These FWMs are localized both along, and transverse to, the axis of propagation. Since the FWM is theoretically non-diffracting, the pulse envelope remains fixed as it propagates.

Brittingham's original work spurred on an number of papers related to the concept of transmitting focused energy beams. Of particular note is the work of Ziolkowski, who has investigated in depth the possibility of launching focused waves from a finite aperture [Ziolkowski, 1985, 1988, 1989, 1990, 1991]. Recent work by Donnelly & Ziolkowski [1992, 1993] has detailed a framework for constructing localized waves (LWs). This review will concentrate on the FWM pulses, and mainly on the research listed above.

2.1 Designing Localized Waves

Of particular importance to this research is a systematic method of constructing LW solutions. Such a method could be used to construct the original FWM as well as other LWs with different propagation characteristics. Donnelly & Ziolkowski [1992, 1993] introduced such a method of obtaining solutions to constant coefficient homogeneous partial differential equations, such as the wave equation, the damped wave equation, and the Klein-Gordon equation, for example. This method is particularly important in the context of this thesis, and will now be described.

Consider the free space homogeneous wave equation (HWE),

$$\left[\nabla^2 - \frac{1}{c^2}\frac{\partial^2}{\partial t^2}\right]\psi(\mathbf{r},t) = 0 \ . \tag{2.1}$$

A three dimensional spatial and temporal Fourier transform may be performed on (2.1) using the transform relationship

$$\Psi(\mathbf{k},\omega) \equiv \mathcal{F}_{\mathbf{r},t}\{\psi\}(\mathbf{k},\omega) = \int_{\mathbf{R}} d\mathbf{r} \int_{-\infty}^{\infty} dt\, \psi(\mathbf{r},t)\, e^{-i\mathbf{k}\cdot\mathbf{r}} e^{i\omega t} \ , \tag{2.2}$$

where $\mathbf{k} = (k_x, k_y, k_z) \equiv k_x\hat{x} + k_y\hat{y} + k_z\hat{z}$, to give

$$(k^2 - \omega^2/c^2)\Psi(\mathbf{k},\omega) = 0 \ . \tag{2.3}$$

One may readily design solutions to (2.3) using the generalized function relationship

$$f(\mathbf{v})\,\delta(\mathbf{v} - \mathbf{v}_0) = f(\mathbf{v}_0)\,\delta(\mathbf{v} - \mathbf{v}_0) \ . \tag{2.4}$$

In this case, Ψ may be designed using appropriate delta functions that force the function $(k^2-\omega^2/c^2)$ to become identically zero.

In describing LWs, it is most convenient to use a cylindrical coordinate system. As such, (2.3) may be re-written as

$$(\kappa^2 + k_z^2 - \omega^2/c^2)\Psi(\mathbf{k},\omega) = 0 \ , \tag{2.5}$$

where $\kappa = \sqrt{k_x^2 + k_y^2}$ is the transform variable corresponding to the transverse coordinate ρ. Consider now the function

$$\Xi(\kappa,\beta)\ \delta[k_z - f(\kappa,\beta)]\ \delta[\omega + cg(\kappa,\beta)] \ . \tag{2.6}$$

If the functions f and g are set such that $\kappa^2 + f^2(\kappa,\beta) - g^2(\kappa,\beta) = 0$, then the delta functions will force $(k^2 - \omega^2/c^2)$ to be identically zero. As such, the function (2.6) will be a solution of (2.5). The choice of the weighting function in (2.6) determines the amount of transverse localization. If the weighting function is set to be

$$\Xi(\kappa,\beta) = \frac{\pi^2}{i\beta} e^{-\kappa^2 z_0/4\beta}, \tag{2.7}$$

and the functions f and g are set to $(\beta - \kappa^2/4\beta)$ and $-(\beta + \kappa^2/4\beta)$ respectively, the resultant function is

$$\Psi_{\mathrm{FWM}}(\mathbf{k},\omega,\beta) = \frac{\pi^2}{i\beta} e^{-\kappa^2 z_0/4\beta}\, \delta[k_z - (\beta - \kappa^2/4\beta)]\, \delta[\omega + c(\beta + \kappa^2/4\beta)] \ . \tag{2.8}$$

The above equation is the three dimensional spatial and temporal Fourier transform of the FWM solution originally given by Ziolkowski [1985],

$$\psi_{\mathrm{FWM}}(\mathbf{r},t,\beta) = \mathcal{F}_{k,\omega}^{-1}\{\Psi_{\mathrm{FWM}}\}(\mathbf{r},t) = e^{i\beta(z+ct)} \frac{e^{-\rho^2\beta/[z_0 + i(z-ct)]}}{4\pi i[z_0 + i(z-ct)]} \ . \tag{2.9}$$

In (2.7), (2.8) and (2.9), β, $z_0 > 0$ are free parameters.

The method described above provides a means of controlling both the non-separable nature and the localization of the designed solutions, ψ. The non-separability is determined by the delta function constraints, while the localization is determined through the weighting function, $\mathcal{Z}$. The question which remains is how does one effectively manipulate the delta functions to produce solutions with desirable propagation characteristics.

Consider again the effect of the delta functions on equation (2.5). For example, the delta functions in equation (2.8) have the effect of forcing any of the transform variables (κ,k_z,ω) to lie on the surface

$$\kappa^2 + k_z^2 - (\omega/c)^2 = 0 \ . \qquad \textbf{(2.10)}$$

This surface is illustrated in figure 2.1. The delta functions of (2.8) force the transform variables to lie on the line described by the two equations, $k_z=\beta-\kappa^2/4\beta$ and $\omega/c=-(\beta+\kappa^2/4\beta)$. The projection of this line onto the k_z, ω/c plane is given in figure 2.2.

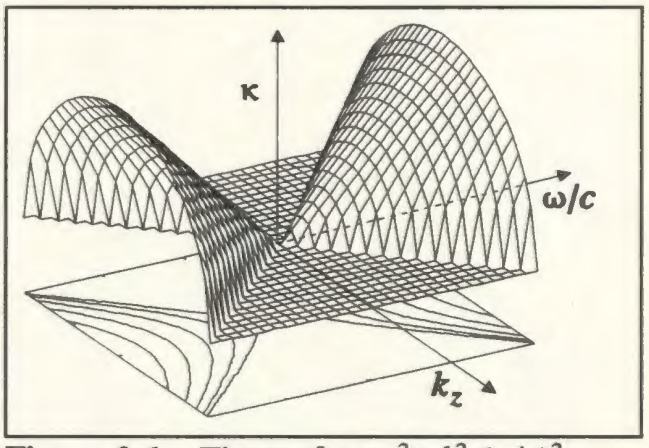

Figure 2.1: The surface $\kappa^2+k_x^2-(\omega/c)^2$.

When the free parameter, β, is set to 0, the projection line of figure 2.2 coincides with the solution line given now by the two equations $\omega/c=k_z$, $\kappa=0$. In this case there is no transverse localization and the ψ_{FWM} solution becomes a superposition of plane waves, each with frequency ω and speed c, travelling the k_z direction. With this interpretation, Donnelly and Ziolkowski [1993] state that the FWMs represent the next

generalization of HWE solutions from plane waves; the plane wave superposition support line is $\omega/c=k_z$, $\kappa=0$, while the FWM support line is simply the parallel translation of the plane wave support line onto the surface of figure (2.1).

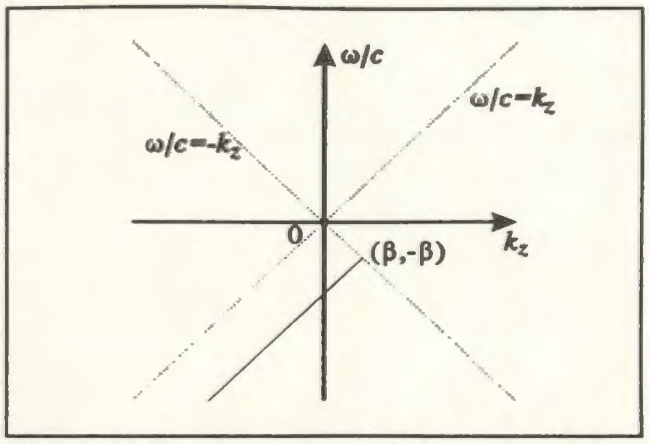

Figure 2.2: Projection of the support line of $\Psi_{FWM}(\mathbf{k},\omega)$, as given in (2.8) onto the k_z, ω/c plane (projection shown as solid line segment).

As shown further by Donnelly & Ziolkowski [1993], the form of the LW solutions is due not only to the support line, but also to the weighting function Ξ along the line. Combinations of different support lines and weighting functions lead to LWs with enhanced localization properties and different propagation characteristics. For instance, if a different weighting function is chosen, such as

$$\Xi(\kappa,\lambda,\beta) = \frac{z_0 4\pi^2}{\beta} I_0\left[\frac{\lambda z_0 \kappa}{2\beta}\right] e^{-\lambda^2 z_0/4\beta} e^{-z_0\kappa^2/4\beta}, \qquad (2.11)$$

with the same delta function support as the FWM solution, the solution becomes the zeroth order "Bessel-Gauss" pulse [Overfelt, 1991; Donnelly & Ziolkowski, 1992; 1993],

$$\psi_{BG,0}(\mathbf{r},t,\beta,\lambda) = \frac{z_0}{z_0 + i(z-ct)} J_0\left[\frac{\lambda z_0 \rho}{z_0 + i(z-ct)}\right] e^{i\beta(z+ct)} e^{-\beta\rho^2/[z_0+i(z-ct)]} \times e^{-i\lambda^2 z_0(z-ct)/4\beta[z_0+i(z-ct)]}. \qquad (2.12)$$

In (2.12) and (2.13) β, z_0 & $\gamma>0$ are free parameters.

Now, if the solution support line on surface (2.10) is changed such that the projection line on the k_z, ω/c plane becomes a straight line with slope $1/\gamma$ emanating from the origin (figure 2.3), the Fourier transform of the solution is obtained, given by

$$\Psi_{\text{SUPER}}(\mathbf{k},\omega,\gamma) = \Xi(\kappa,\gamma)\,\delta\left[k_z - \frac{\gamma\kappa}{\sqrt{1-\gamma^2}}\right]\delta\left[\omega - \frac{c\kappa}{\sqrt{1-\gamma^2}}\right] . \qquad (2.13)$$

Note that according to figure 2.3 the value of γ should lie in the range (-1,1) so that the projection line will correspond to a line on the surface of (2.10). If the weighting function

$$\Xi(\kappa,\gamma) = \frac{(2\pi)^3\gamma^2}{1-\gamma^2}\, e^{-z_0|\gamma|\kappa(1-\gamma^2)^{1/2}} \qquad (2.14)$$

is now chosen, the resultant solution is

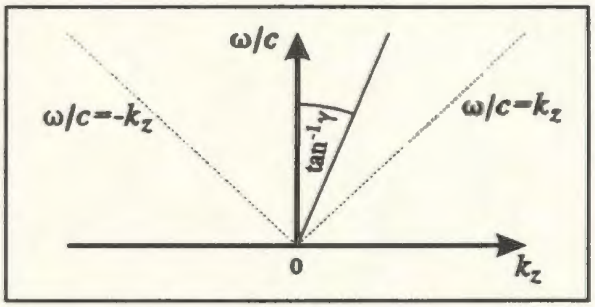

Figure 2.3: Projection of the support line of $\Psi_{\text{SUPER}}(\mathbf{k},\omega)$, as given in (2.13) onto the k_z, ω/c plane (projection shown as solid line segment).

$$\psi_{\text{SUPER}}(\mathbf{r},t,\gamma) = \frac{[z_0 - i\,\text{sgn}(\gamma)(z - ct/\gamma)]}{\left\{\rho^2(1-\gamma^2)/\gamma^2 + [z_0 - i\,\text{sgn}(\gamma)(z - ct/\gamma)]^2\right\}^{3/2}} . \qquad (2.15)$$

Since γ lies in the range (-1,1), it is easily seen that this solution represents a waveform travelling in the either the positive or negative z direction with speed $|c/\gamma| > c$. In other words, the pulse is superluminal with speed depending on γ.

As illustrated by Donnelly & Ziolkowski [1993], many other choices of the solution support and the weighting function can be made to form other interesting solutions to the HWE. The authors also extend the HWE methodology described above

to the damped wave and the Klein-Gordon equations. In this review, emphasis will be placed on the FWM solution (2.8).

2.2 Obtaining Finite Energy Solutions

As shown by Ziolkowski [1985], the FWM solution given by (2.9) has finite energy density but infinite total energy. If the LW solutions are to be physically launched, it is desirable that they have finite energy. Finite energy LW solutions may be formed from the infinite energy FWM solutions using superposition. Consider that if a function $\psi(\beta)$ is a solution to the HWE, where β is an arbitrary parameter, then a weighted superposition of the function $\psi(\beta)$, over the parameter β, will also be a solution the HWE. Using this reasoning, the superposition

$$\int_0^\infty d\beta\, F(\beta)\, \psi_{\text{FWM}}(\mathbf{r}, t, \beta) \tag{2.16}$$

is also a solution to the HWE [Ziolkowski, 1985; Donnelly & Ziolkowski 1992; 1993], where F is an arbitrary weighting function. Ziolkowski [1985] first showed that the superposition in (2.16) will lead to a finite energy solution provided that

$$\int_0^\infty d\beta\, \frac{|F(\beta)|}{\beta} < \infty \,. \tag{2.17}$$

This constraint on F will change for different LW solutions depending the choice of the delta function support and the weighting function Ξ used to extract a LW solution. Donnelly & Ziolkowski [1993] outline a method for determining these constraints. If the

superposition of an arbitrary HWE solution ψ is denoted by

$$\Theta(\mathbf{r},t) = \int_0^\infty d\beta F(\beta)\psi(\mathbf{r},t,\beta) \ , \tag{2.18}$$

then the total energy of this solution may be given by

$$\mathscr{E} = \int_{\mathbf{R}^3} d\mathbf{r} |\Theta(\mathbf{r},t)|^2 \ . \tag{2.19}$$

This expression can be shown [Donnelly & Ziolkowski, 1992] to be re-written as

$$\mathscr{E} = \frac{1}{(2\pi)^4} \int_0^\infty d\beta |F(\beta)|^2 \int_0^\infty d\kappa \frac{\kappa}{|\partial f(\kappa,\beta)/\partial\beta|} |\Xi(\kappa,\beta)| \ . \tag{2.20}$$

where the function f was given in (2.6). If the integrals in (2.20) converge, then the superposition has produced a function Θ with finite energy. In the case of the LW pulses, $f(\kappa,\beta)=\beta-\kappa^2/4\beta$ and $|\Xi(\kappa,\beta)| = e^{-\kappa^2 z_0/2\beta}$, hence the total energy of the superposed LW is given by

$$\mathscr{E}_{LW} = \frac{1}{16} \int_0^\infty d\beta |F(\beta)| \int_0^\infty d\kappa \frac{\kappa}{\kappa^2 + 4\beta^2} e^{-\kappa^2 z_0/2\beta} \ . \tag{2.21}$$

As shown in [Donnelly & Ziolkowski, 1993], this integral will lead to the result previously given in (2.17) for finite total energy.

For the general FWM superposition, a finite energy solution may be written as

$$\psi_{LW}^{FINITE} = \frac{1}{4\pi i[z_0 + i(z - ct)]} \int_0^\infty d\beta F(\beta) e^{-\beta s} , \tag{2.22}$$

where $s = \rho^2/[z_0 + i(z - ct)] - i(z + ct)$, assuming the energy criterion of (2.17) is met. Examination of (2.22) reveals that the integral is in the form of a Laplace transform [Ziolkowski, 1985], i.e.

$$\psi_{LW}^{FINITE} = \frac{1}{4\pi i[z_0 + i(z - ct)]} \mathcal{L}_\beta\{F\}(s) . \tag{2.23}$$

Hence interesting finite energy LW solutions may be obtained by simply consulting a table of Laplace transforms. One such solution introduced by Ziolkowski [1985] is called the *Modified Power Spectrum* (MPS) pulse. Its name is derived from the power spectrum $F(\beta) = \beta^{(T-1)} e^{-\tau\beta}$ appropriately scaled and truncated to give the spectral weighting

$$F(\beta) = \begin{cases} 4\pi i B(B\beta - b)^{T-1} \dfrac{e^{-\tau(B\beta - b)}}{\Gamma(T)}, & \beta > \dfrac{b}{B} \\ 0, & 0 \le \beta < \dfrac{b}{B} \end{cases} \tag{2.24}$$

The parameters, τ, b, T, B in the above expression are free parameters. Performing the superposition leads to the space-time expression for the MPS pulse,

$$\psi_{MPS}(\mathbf{r}, t) = \frac{1}{z_0 + i(z - ct)} \frac{1}{(s/B + \tau)^T} e^{-bs/B} . \tag{2.25}$$

The MPS has some interesting propagation properties, as outlined in [Ziolkowski, 1985]. For instance, if $B \gg 1$ and $T = 1$ in (2.25), the real part of Ψ_{MPS} is given by

$$\psi_{MPS}(\rho=0, z=ct) = \frac{\cos(2bz/B) - (2z/B\tau)\sin(2bz/B)}{1 + (2z/B\tau)^2} \frac{1}{\tau z_0}$$

$$\approx \begin{cases} 1/\tau z_0 & \text{when } 2z/B\tau < 1 \text{ and } 2bz/B \ll 1 \\ \cos(2bz/B) / \tau z_0 & \text{when } 2z/B\tau < 1 \\ [\sin(2bz/B) / (2z_0/B)]\,(1/z) & \text{when } 2z/B\tau > 1\ . \end{cases} \quad \textbf{(2.26)}$$

From (2.26) it can be seen that the MPS pulse centre retains a contant amplitude when $2bz/B \ll 1$ and $2z/B\tau < 1$. The pulse centre then begins to oscillate with period $\pi B/b$ in the region $B/2b < z < B\tau/2$, and begins to decay in the region $z > B\tau/2$. Figures 2.4-2.7 show plots of $\mathbf{Re}\{\psi_{MPS}\}$ for the various regions given above, using the parameters $z_0=0.004$ m, $T=1$, $\tau=1.0$ m, $B=300$ and $b=750$ m^{-1}.

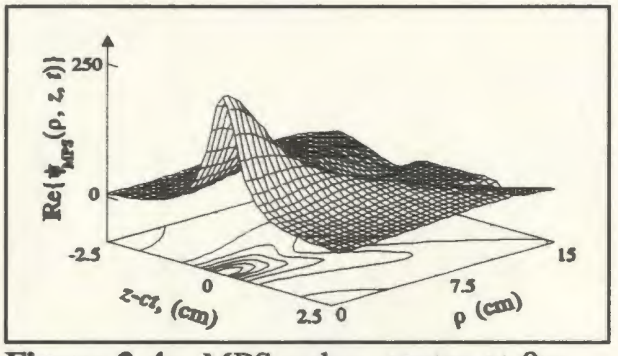

Figure 2.4: MPS pulse, centre at 0m

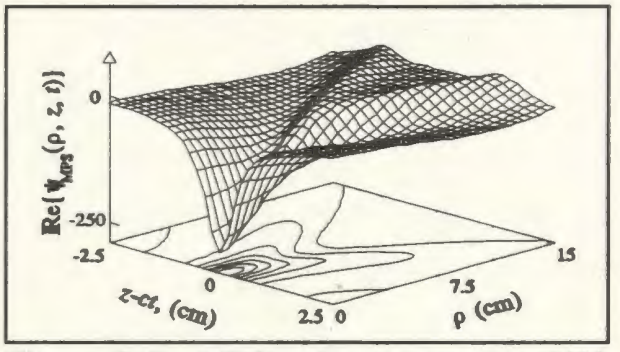

Figure 2.5: MPS pulse, centre at $\pi B/2b$

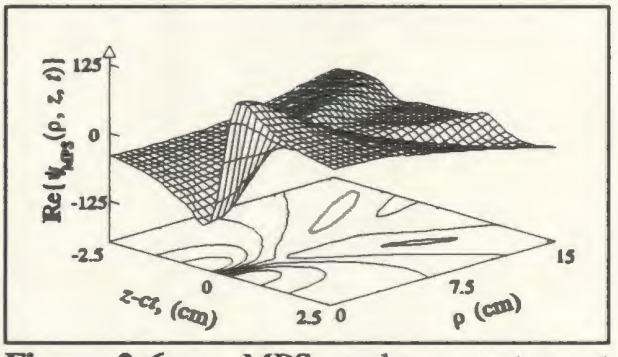

Figure 2.6: MPS pulse, centre at $3\pi B/4b$.

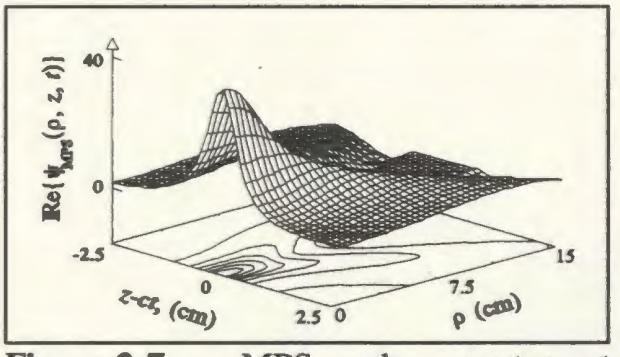

Figure 2.7: MPS pulse, centre at $301\pi B/4b$.

2.3 Launching a Localized Wave

Several successful attempts have been made to launch approximations to LW pulses [Ziolkowski, 1985; 1991; Ziolkowski & Lewis, 1989; 1990; Donnelly *et al*, 1994], both in numerical simulations and in acoustic realizations. The realization of these pulses is made possible through the use of Huygens' representation [Jones 1964],

$$\psi(\mathbf{r},t) = \oint_S \{ g(\mathbf{r},\mathbf{r}')\,\partial_{n'}[\psi(\mathbf{r}',t-R/c)] - \psi(\mathbf{r}',t-R/c)\,[\partial_{n'}g(\mathbf{r},\mathbf{r}')] + g(\mathbf{r},\mathbf{r}')\,\partial_{ct}[\psi(\mathbf{r}',t-R/c)]\,\partial_{n'}R \}\, dS' \quad , \tag{2.27}$$

where ψ is a scalar field satisfying the HWE, S is a closed surface ($\mathbf{r}$ lies inside S), n' is the inward pointing normal to S, $R=\sqrt{(x-x')^2+(y-y')^2+(z-z')^2}$ is the distance between the source coordinates (x',y',z') on S and the observation coordinates (x,y,z) contained within S, and $g(\mathbf{r},\mathbf{r}')=1/4\pi R$. This equation can be interpreted as follows: the HWE solution scalar field ψ inside any closed volume S can be reconstructed by simply knowing the normal derivative of ψ, the time derivative of ψ and the value of ψ on the surface S. Hence if the surface S is excited with the function given inside the integrand of (2.27), ψ will be exactly reconstructed at the point $\mathbf{r}$ for all time. Using this interpretation of (2.27), it is possible, with a few approximations, to launch a facsimile of a scalar field LW into a region of space.

Consider first S being the surface consisting of a circle on the plane $z=0$ and the *top* half of a spherical shell, the half pointing towards positive z (figure 2.8). Both the sphere and the circle are centred at the origin and both have radius r_1. If $r_1\to\infty$, the surface S encloses the region $z>0$ and the reconstruction point $\mathbf{r}$ is contained in the region $z>0$. Since the LW pulses have most of their energy contained within a small

region about the axis of propagation, an approximation to the reconstruction of ψ at $\mathbf{r}$ can be made by exciting a small aperture on the surface S centred at the origin. This is essentially Kirchhoff's approximation [Jones, 1964]. As such, (2.27) may be re-written as

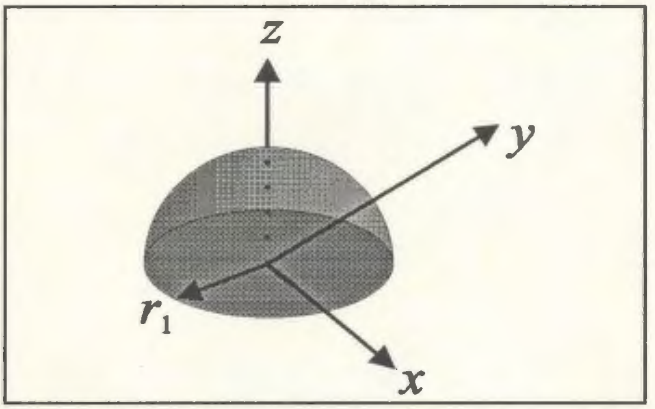

Figure 2.8: Hemisphere of radius r_1 on the $z=0$ plane projecting into $z>0$ plane.

$$\psi(\mathbf{r},t) = -\int_A dS'\, \Phi(\mathbf{r}',t - R/c)\frac{1}{4\pi R}, \qquad \textbf{(2.28)}$$

where A is the area of the aperture on the plane $z'=0$, and the driving function Φ is given by

$$\Phi(\mathbf{r}',t - R/c) = [\partial_{z'}\psi] - [\partial_{ct}\psi]\frac{z}{R} - [\psi]\frac{z}{R^2}\ . \qquad \textbf{(2.29)}$$

The square brackets in (2.29) indicate that the function inside is to be evaluated at the retarded time, t-R/c. Since the driving function Φ depends on the observation coordinate $\mathbf{r}$, it seems that it may be possible to reconstruct the LW only at a single point. However, if it is assumed that the reconstruction point is sufficiently far away from the aperture and close enough to the z-axis to assume that $R \approx z$, the driving function may be approximated by $\Phi \approx 2\partial_{ct}\psi$. Hence a LW pulse may now be reconstructed by approximating (2.28) by

$$\psi(\mathbf{r},t) \approx \sum_{n=1}^{N} \Phi(\mathbf{r}_n, t - R/c)\frac{A_n}{4\pi R} , \qquad (2.30)$$

where N is the number of transducers placed uniformly on the aperture A, $\mathbf{r}_n$ is the discrete location of each transducer on the aperture, and A_n is an area weighting for each element, replacing dS' in (2.28). For a uniform array of equally spaced elements, A_n is constant for all n. The function Φ now becomes the driving function for point source transducers whose impulse response is modelled by

$$h(\mathbf{r}, \mathbf{r}_n, t) = \delta(t-R/c)/4\pi R . \qquad (2.31)$$

Equation (2.31) gives the impression that the radiation pattern of the point sources should be spherically symmetric. However, it is assumed that the observation point is far from the array and close to the z-axis. This means that the angle between the transducer's axis and the observation point will be small. This allows the use of certain transducers with directive radiation patterns. For instance, Ziolkowski [1991] uses disk transducers having radiation pattern described by $2J_1(ka\sin\theta)/(ka\sin\theta)$ where a is the radius of the disk and k is the wavenumber of the sinusoid driving the disk. Since θ is assumed to be small when reconstructing near the z-axis and far from the array, the radiation pattern term may be set to unity. In using such an approximation, it is assumed that the sidelobe levels of the array are not adversely affected (i.e. they do not increase).

2.4 Localized Wave Performance Bounds

In the previous sections, a method of designing and launching localized wave solutions, which are non-separable in space and time, has been discussed. It will be shown in this section that this non-separability provides for extended regions of localization over their CW counterparts.

In order to launch a LW, a finite array of point sources may be driven with the broadband LW signals given in (2.30). Conventionally, a focused pulse is produced by driving an array of point sources with a gated CW signal. The inherent differences between the signals launched make it difficult to compare their propagation characteristics and beam qualities. For instance, traditional performance criteria such as Rayleigh distance, beam spread, beam intensity and beam energy are based on narrowband concepts and are not readily applicable to the broadband case. However, in [Ziolkowski, 1991], performance bounds are derived based on the measurement of an effective frequency for the LW arrays. All of the theoretical analysis presented in this section is taken from [Ziolkowski, 1991]. Experimental data which supports this theoretical analysis can be found in [Ziolkowski, 1991; Ziolkowski & Lewis, 1989; 1990]

Consider an array of N independently addressable radiating elements placed on an aperture as illustrated in figure 2.9. Each element has radiating area A_n and is excited with the driving function $\Phi_n(t)=\Phi(\mathbf{r}_n,t)$. The total area the array is $A = \sum_{n=1}^{N} A_n$. The experiments discussed in [Ziolkowski & Lewis, 1989; 1990] employed small disk transducers which have the approximate transmit/receive characteristics illustrated in figures 2.10 and 2.11. Further analysis of these transducers may be found in many texts,

including Ristic [1983].

In figure 2.10, it is assumed that the characteristic length, l, of each element is not large in comparison with the shortest significant wavelength, λ_{min}, driven into each element, or $2\pi l/\lambda_{min} = k_{max} l \lesssim 1$. A voltage signal driven into a transmitting transducer will experience a single time derivative from the electro-mechanical energy conversion. The signal then experiences a second time derivative from the radiation process, which converts energy near the transducer's face to energy far from the transducer. A third time derivative occurs from electro-mechanical energy conversion at the receiving transducer. In this case, the *radiated field* is defined as the field near the transducer face and is indicated in figure 2.10.

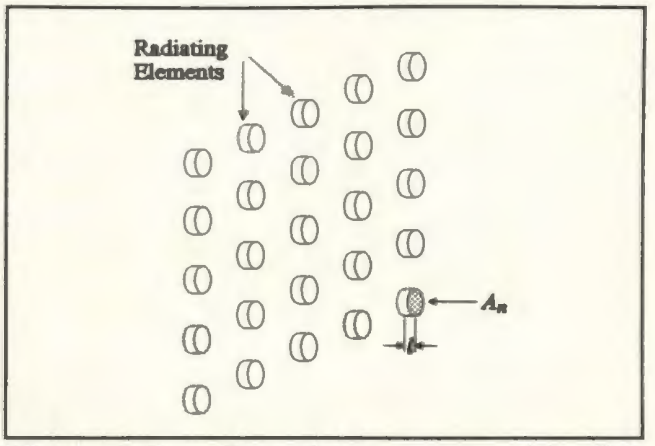

Figure 2.9: Transducer array with disk type elements.

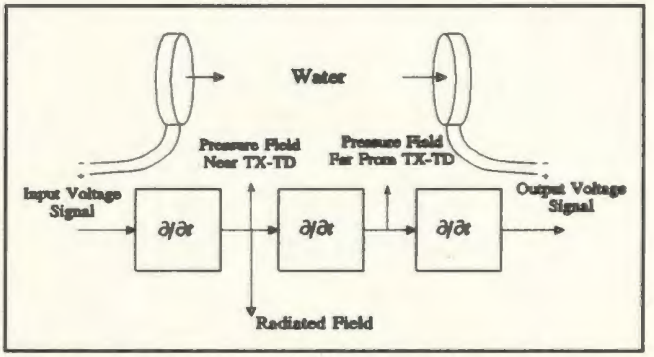

Figure 2.10: Disk transducer system response for $k_{max} l \lesssim 1$.

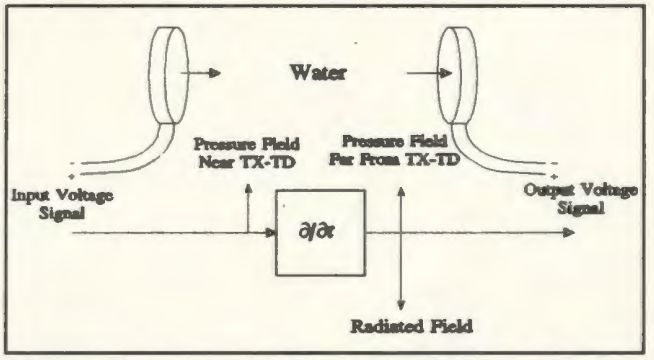

Figure 2.11: Disk transducer system response for $k_{max} l \gg 1$.

Next, consider the case in which the array elements are large in comparison with the shortest significant wavelength, i.e. $k_{max} l \gg 1$. In this case, the transducer's electro-

mechanical conversion process does not have any effect on the signal; the system will impart a single time derivative on the signal due to the radiation process. In this case, the *radiated field* is defined as the field far from the transducer face and is indicated in figure 2.11.

For both the small and large transducer models, the input driving functions experience a single time derivative when being transmitted from the input to the radiated field. Then, according to the previous section, an approximate LW may be launched as the *radiated field* if the transducers are instead driven with the new set of functions, $\psi_n = \psi(\mathbf{r}_n,t)$ (Note that the factor of two has been dropped). The driving fuctions will consitute the *input field*. The units of an input signal are taken to be $(W/m^2)^{1/2}$. The expression for the total *radiated field* may be approximated using (2.30) in conjunction with the radiated field model in figures 2.10 and 2.11,

$$\psi_{\text{rad}}(\mathbf{r},t) \approx \sum_{n=1}^{N} \frac{A_n}{2\pi c|\mathbf{r}-\mathbf{r}_n|} \partial_t \psi_n(\mathbf{r}_n, t-|\mathbf{r}-\mathbf{r}_n|/c). \qquad \textbf{(2.32)}$$

When the transducers are small, i.e. when $k_{\max} l \lesssim 1$, the radiated field is not the same as *measured field*, the field given at the output of the receiving transducers. The time derivatives caused by the radiation and measurement process should be taken into account (c.f. figure 2.10), hence

$$\psi_{\text{meas}}(\mathbf{r},t) \approx C \sum_{n=1}^{N} \frac{A_n}{2\pi c|\mathbf{r}-\mathbf{r}_n|} \partial_t^3 \psi_n(\mathbf{r}_n, t-|\mathbf{r}-\mathbf{r}_n|/c). \qquad \textbf{(2.33)}$$

The constant C is introduced by the conversion from radiated to measured fields as detailed in [Ziolkowski, 1991].

In order to evaluate the beam quality of the LWs, the quantities of input field energy, $\mathscr{E}$, beam intensity, I, and fluence, $\Im$, will now be defined:

$$\mathscr{E}_{\text{field}} = \int_{A_n} dS' \int_{-\infty}^{\infty} dt\, |\psi_{\text{field}}(\mathbf{r},t)|^2, \quad [\text{J}] \tag{2.34}$$

$$I_{\text{field}}(\mathbf{r},t) = |\psi_{\text{field}}(\mathbf{r},t)|^2, \quad [\text{W/m}^2] \tag{2.35}$$

$$\Im_{\text{field}}(\mathbf{r}) = \int_{-\infty}^{\infty} dt\, I_{\text{field}}(\mathbf{r},t). \quad [\text{J/m}^2] \tag{2.36}$$

These quantities are readily derivable for each of the array driven field quantities: input, radiated and measured.

2.4.1 Radiated Field Efficiency

In this section, the efficiency of the radiated fields of the LW and CW driven arrays will be compared. In this case, the efficiency of the array will be defined as the ratio of radiated to input field fluence,

$$\Gamma_{\text{rad}} = \frac{\Im_{\text{rad}}}{\Im_{\text{in}}}. \tag{2.37}$$

The input and radiated field fluence can be calculated for the array of transducers as,

$$\Im_{\text{in}} = \frac{\mathscr{E}_{\text{in}}}{A} = \frac{1}{A}\left[\sum_{n=1}^{N} A_n \int_{-\infty}^{\infty} dt\,|\psi_n(\mathbf{r}_n,t)|^2\right] , \tag{2.38}$$

$$\Im_{\text{rad}}(\mathbf{r}) \le \left[\frac{A}{2\pi cz}\right]^2 \frac{U_{\text{rad}}}{A} , \tag{2.39}$$

where

$$U_{\text{rad}} = \sum_{n=1}^{N} U_n = \sum_{n=1}^{N} A_n \int_{-\infty}^{\infty} dt\,|\partial_t \psi_n(\mathbf{r}_n,t)|^2 . \tag{2.40}$$

First, consider the CW driven array. The array is uniformly spaced with each of the sources having the same area, i.e $A_n = A_0$ and $A = NA_0$. Each element is driven with the same CW signal having angular frequency ω_{CW} so that $\int dt\,|\partial_t\psi|^2 = \omega_{\text{CW}}^2 \int dt\,|\psi|^2$, and the input energy is the same for each element, $\mathscr{E}_n^{\text{in}} = \mathscr{E}_0^{\text{in}}$. The input fluence, radiated fluence and far field efficiency are given by

$$\Im_{\text{in}}^{\text{CW}} = \frac{\mathscr{E}_0^{\text{in}}}{A_0} , \tag{2.41}$$

$$\Im_{\text{rad}}^{\text{CW}} \le \left[\frac{A}{2\pi cz}\right]^2 \frac{U_0}{A_0} , \tag{2.42}$$

$$\Gamma_{\text{rad}}^{\text{CW}} \le \left[\frac{L_{\text{CW}}}{z}\right] , \tag{2.43}$$

where the *diffraction length* $L_{\text{CW}} = A/\lambda_{\text{CW}}$ has been introduced.

Next, consider the far field efficiency of the same array driven with a set of LW functions. Here one has

$$\Gamma_{\text{rad}}^{\text{LW}} \leq \left[\frac{A}{2\pi cz}\right]^2 \frac{U_{\text{rad}}^{\text{LW}}}{\mathscr{E}_{\text{in}}^{\text{LW}}} \tag{2.44}$$

Note that the CW array efficiency is conveniently given in (2.43) in terms of the CW diffraction length. However, for the LW driven array, the concept of a diffraction length is not readily applied since the LW consists of broadband frequency components. However, one may define an *effective frequency* that provides a quantitative measure of the frequency content of the LW beam. This effective frequency may then be used to determine the diffraction length, $L_{\text{LW}}=Af_{\text{eff}}/c=A/\lambda_{\text{eff}}$, where λ_{eff} is the effective wavelength. Consider the effective frequency of the radiated field ω_{rad}, which is defined as

$$\omega_{\text{rad}}^2 = \frac{U_{\text{rad}}^{\text{LW}}(\text{far field})}{\mathscr{E}_{\text{in}}^{\text{LW}}} = \frac{\sum_{n=1}^{N} A_n \int_{-\infty}^{\infty} dt\, |\partial_t \psi_n(\mathbf{r}_n, t)|^2}{\sum_{n=1}^{N} A_n \int_{-\infty}^{\infty} dt\, |\psi_n(\mathbf{r}_n, t)|^2} = \frac{\sum_{n=1}^{N} A_n \int_{-\infty}^{\infty} d\omega\, \omega^2 |\Psi_n(\mathbf{r}_n, \omega)|^2}{\sum_{n=1}^{N} A_n \int_{-\infty}^{\infty} d\omega\, |\Psi_n(\mathbf{r}_n, \omega)|^2} . \tag{2.45}$$

In (2.45), the term *far field* refers to the situation where the approximation $R \approx z$ is valid. Because the measurement process alters the frequency content of the beam, an effective frequency will also have to be described for the measured field as well. This will be discussed later.

Now that the concept of effective frequencies has been defined for the LW radiated field, the efficiency of the LW radiated field may be given in terms of the diffraction length.

$$\Gamma_{\text{rad}}^{\text{LW}} \leq \left\lceil \frac{L_{\text{rad}}}{z} \right\rceil , \tag{2.46}$$

where the wavelength $\lambda_{\text{rad}}=2\pi c/\omega_{\text{rad}}$ and the Rayleigh distance is defined as $L_{\text{rad}}=A/\lambda_{\text{rad}}$. Hence, the radiated field efficiency of the LW pulse can be measured in relation to that of the CW pulse by taking the ratio of two efficiencies

$$\frac{\Gamma_{\text{rad}}^{\text{LW}}}{\Gamma_{\text{rad}}^{\text{CW}}} \approx \left(\frac{\omega_{\text{rad}}}{\omega_{\text{CW}}} \right)^2 . \tag{2.47}$$

The question is whether or not this ratio is greater than one. In order to determine this, the value of ω_{CW} that makes a fair comparison of the CW and LW pulses should be quantified. For instance, the effective frequency radiated field very close to array, Ω_{rad}, may also be defined in the same way that ω_{rad} was,

$$\Omega_{\text{rad}}^2 = \frac{U_{\text{rad}}^{\text{LW}}(\text{near field})}{\mathscr{E}_{\text{in}}^{\text{LW}}} = \frac{\sum_{n=1}^{N} A_n \int_{-\infty}^{\infty} dt \, |\Phi_n(\mathbf{r}_n, t)|^2}{\sum_{n=1}^{N} A_n \int_{-\infty}^{\infty} dt \left| \int_{-\infty}^{t} d\tau \, \Phi_n(\mathbf{r}_n, \tau) \right|^2} . \tag{2.48}$$

In (2.45), it was assumed that the observation point is located spatially far away from the array (i.e. $R \approx z$) and that the transducer driving functions may be given by ψ_n, where $\Phi_n \approx 2\partial_{ct}\psi_n$. In this case, the observation point is located spatially near the array (i.e. is located in the array's *near field*), where Φ must be given by (2.29). In this case, the driving functions are given by $\int_{-\infty}^{t} d\tau \, \Phi(\mathbf{r}_n, \tau)/2$. The value Ω_{rad} is an array weighted accumulation of the input LW signal spectra and is thus a measure of the input field

spectra. Hence Ω_{rad} may be considered a fair substitute for ω_{CW} in (2.47). Note that it can be shown that $\Omega_{rad} < \omega_{rad}$. The standard engineering criterion of the 3dB frequency, ω_{3dB}, may also be used in place of ω_{CW}, in which case $\omega_{3dB} < \omega_{rad}$. Other substitutions for ω_{CW} may be made, however, as a demonstration, Ziolkowski [1991] chose the value of Ω_{rad} for comparison, in which case

$$\frac{\Gamma_{rad}^{LW}}{\Gamma_{rad}^{CW}} \approx \left[\frac{\omega_{rad}}{\omega_{CW} = \Omega_{rad}} \right]^2 \geq 1. \tag{2.49}$$

Hence, one can claim that the LW beam is more efficient in transmitting its energy than the corresponding CW one. In an optimal design, one would try and maximize the value of the ratio given in (2.49).

2.4.2 Measured Field Efficiency

The above radiated field analysis can also be performed on the measured field. As was discussed earlier, the measured field will differ from the radiated field by two time derivatives and a constant (equations (2.32) and (2.33)). In the same sense as described above, a measured field effective frequency can be quantified

$$\omega_{meas}^4 = \frac{\sum_{n=1}^{N} A_n \int_{-\infty}^{\infty} dt \, |\partial_t^3 \psi_n(\mathbf{r}_n, t)|^2}{\sum_{n=1}^{N} A_n \int_{-\infty}^{\infty} dt \, |\partial_t \psi_n(\mathbf{r}_n, t)|^2}. \tag{2.50}$$

If the array were driven with the same CW signal, ω_{meas} would be simply equal to ω_{CW}.

The ratio of the LW to CW measured efficiencies is

$$\frac{\Gamma_{meas}^{LW}}{\Gamma_{meas}^{CW}} \approx \left[\frac{\omega_{rad}}{\omega_{CW}}\right]^2 \left[\frac{\omega_{meas}}{\omega_{CW}}\right]^4 . \tag{2.51}$$

Hence the condition for the LW array to be more efficient than the CW array is given by

$$\omega_{meas}^2 > \frac{\omega_{CW}^3}{\omega_{rad}} . \tag{2.52}$$

If the CW frequency is conservatively set to ω_{rad} then (2.52) becomes

$$\omega_{meas} > \omega_{rad} . \tag{2.53}$$

Ziolkowski has shown that the above criterion is readily achieved with a variety of LW solutions, as well as other broadband driving signals. As will be discussed here, Ziolkowski's experiments [Ziolkowski & Lewis, 1989; 1990] showed that more than an order of magnitude increase in the measured field energies can be achieved.

2.4.3 Beam Divergence

Another performance measure which can quantify the beam quality of a LW is the rate of beam divergence or spread. This can be quantified by examining the fluence profile of the beam. In this case, when the centre of the beam has propagated a distance, z, the radius at which the fluence profile has decreased to half its maximum is measured. This radius is called the half width at half maximum, $\rho^{HWHM}(z)$, and is a good measure of beam's transverse localization. The HWHM radius can be calculated from the appropriate array fluence expression. For instance, the HWHM radius of the far field measured energy profile occurs at

$$\rho_{meas}^{HWHM} \approx \left[\frac{\lambda_{meas}}{4d_{max}}\right] z \ , \tag{2.54}$$

where d_{max} is the radius of the aperture. Hence the rate of beam divergence is given by $\theta_{meas} = \partial_z \rho_{meas}^{HWHM} \approx \lambda_{meas}/4d_{max}$. Using the same analysis, the radiated field HWHM radius occurs at,

$$\rho_{rad}^{HWHM} \approx \left[\frac{\lambda_{rad}}{4d_{max}}\right] z \ . \tag{2.55}$$

Thus the beam generated by a LW array will have beam divergence given by $\theta_{rad}^{LW} \approx \lambda_{rad}/4d_{max}$, while the beam generated by a CW driven array is given by $\theta_{rad}^{CW} = \theta_{meas}^{CW} \approx \lambda_{CW}/4d_{max}$. The ratio of the LW and CW beam divergence is given by

$$\frac{\theta_{meas}^{LW}}{\theta_{meas}^{CW}} \approx \frac{\omega_{meas}^{CW}}{\omega_{meas}^{LW}} \ . \tag{2.56}$$

As was discussed in the previous section, the ratio given (2.56) can be made much less than one by properly designing the correlation properties of the LW time signals. Hence, the beam generated by a LW array can be made more localized than a beam generated by a corresponding CW array.

2.5 Experimental Results

2.5.1 Simple Array

Ziolkowski [1991] first considered the case of driving a circular aperture (radius R_a) with the real part of the MPS solution, ψ_{MPS} previously given in (2.25). His experiments used the parameters $z_0=4.5\times10^{-4}$ m, $T=1$, $\tau=1.0$ m, $B=300$ and $b=600$ m^{-1}.

In order to write compactly the diffraction lengths of the various beams, the waist, w, of the beam is introduced. The waist is usually defined as the beam radius at half maximum of the beam's intensity profile, $|\psi_{MPS}|^2$. The waist should not be confused with ρ^{HWHM}, which evaluates the transverse localization of the radiated and measured fields using the fluence profile. The initial waist of the MPS is given by $w=(Bz_0/b)^{1/2}=1.5$ cm. The maximum effective frequency, f_{max}, of the MPS is also introduced and is defined as the $1/e$ fall off point in the Fourier amplitude of the MPS. This frequency is derived by examining the temporal Fourier transform of the MPS at $z=0$,

$$\Psi_{MPS}(\rho,z=0,\omega) \approx \frac{1}{z_0\tau}\frac{2\pi}{\omega_{max}}\, u(\omega-\omega_{min})\, e^{-(\omega-\omega_{min})/\omega_{max}}\, J_0\left(2(\rho/c)[\omega_{min}(\omega-\omega_{min})]^{1/2}\right), \quad (2.57)$$

where u is the unit step function, $\omega_{min}=bc/B$, and $\omega_{max}=c/z_0$ is the $1/e$ fall off point. For the MPS parameters listed above, $f_{max}\approx0.53$ MHz. Again, f_{max} should not be confused with the radiated

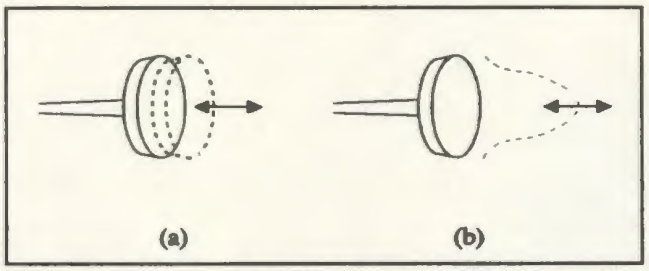

Figure 2.12: (a) Piston and (b) Gaussian beam.

and measured effective frequencies, f_{rad} & f_{meas}.

In these experiments, two different types of beams are compared with the MPS: a simple piston beam (aperture is uniformly illuminated with a CW signal) and a gaussian piston beam (aperture amplitude is tapered with a gaussian function in the transverse direction) as illustrated in figure 2.12. Using the expressions for the radiated field of an array from the previous section, the diffraction lengths of each of the particular beams can be derived,

$$L_{\text{MPS}} = \frac{\pi w R_a}{\lambda_{\text{min}}}, \tag{2.58a}$$

$$L_{\text{Gauss}} = \frac{\pi w^2}{\lambda_{\text{min}}}, \tag{2.58b}$$

$$L_{\text{Piston}} = \frac{\pi R_a^2}{\lambda_{\text{min}}}. \tag{2.58c}$$

where $w \leq R_a$. For the piston array, the entire aperture is illuminated with the CW signal having frequency, f_{max}, while for the gaussian array, the aperture is driven with the transverse tapered CW signal, f_{max}. From (2.58), it is seen that the MPS will have a longer diffraction length than the Gaussian piston if $w < R_a$, while if this holds the regular piston will have the longest diffraction length.

As Ziolkowski [1991] points out, the diffraction length says nothing about the quality of the beam. While the CW piston has a longer diffraction length, its near field contains large regions of constructive and destructive interference, hence the beam quality is poor. In contrast, the Gaussian and MPS beam quality is pencil like, highly superior to that of the piston array. The theoretical waists of the piston and Gaussian

beams are given by

$$w_{\text{Gauss}} \approx \frac{wz}{L_{\text{Gauss}}} = \frac{\lambda_{\min} z}{\pi w}, \tag{2.59a}$$

$$w_{\text{Piston}} \approx \frac{\lambda_{\min} z}{4R_a}. \tag{2.59b}$$

Now consider the comparison of the MPS, Gaussian and piston beams using the radiated and measured diffraction lengths given in the previous section. The effective radiated and measured frequencies can be calculated, for the given MPS parameters, as

$$\omega_{\text{rad}}^2 \approx \frac{3}{16}\omega_{\max}^2, \tag{2.60a}$$

$$\omega_{\text{meas}}^4 \approx \left[\frac{R_a^2}{2w^2}\right]^3 \omega_{\max}^4. \tag{2.60b}$$

Hence the radiated and measured field diffraction lengths are given by,

$$L_{\text{rad}}^{\text{MPS}} = \frac{A}{\lambda_{\text{rad}}} = \frac{\pi R_a^2}{\lambda_{\text{rad}}} \approx \sqrt{3/16}\, L_{\text{Piston}} = \sqrt{3/16}\left[\frac{R_a}{w}\right]^2 L_{\text{Gauss}}, \tag{2.61a}$$

$$L_{\text{meas}}^{\text{MPS}} = \left[\frac{\omega_{\text{meas}}}{\omega_{\text{rad}}}\right]^2 L_{\text{rad}} \approx \sqrt{16/3}\left[\frac{R_a^2}{2w^2}\right]^{3/2} L_{\text{Piston}} = \sqrt{2/3}\left[\frac{R_a}{w}\right]^5 L_{\text{Gauss}}. \tag{2.61b}$$

These theoretical results show that if $w < R_a$, the MPS radiated field diffraction length can be made larger than that of the Gaussian array and the MPS measured field diffraction length can be made longer than the corresponding piston and Gaussian diffraction lengths. Similarly, the theoretical waists of the MPS beams are given by

$$w_{rad}^{MPS} \approx \frac{\lambda_{rad}}{4R_a} = \frac{4}{\sqrt{3}} w_{Piston}(z) = \frac{1.81w}{R_a} w_{Gauss}(z) \qquad \textbf{(2.62a)}$$

$$w_{meas}^{MPS} \approx \frac{\lambda_{meas}}{4R_a} = \left[\frac{2w^2}{R_a^2}\right]^{3/4} w_{Piston}(z) = 1.32\left[\frac{w}{R_a}\right] w_{Gauss}(z) \qquad \textbf{(2.62b)}$$

Again, these results show that if $w<R_a$ the waist of the MPS radiated field can be made smaller than that of the Gaussian array and the waist of the MPS measured field can be made smaller the corresponding piston and Gaussian waists.

The experiments were carried out on a 6cm square array consisting of 21×21 elements. The array was synthetic; a single transmitting element was used to synthesize an entire array. A circular array was obtained by zeroing the signals of the elements outside R_a=3cm. Hence, the effective radiated and measured frequency values are calculated as f_{rad}=0.23MHz, f_{meas}=0.89MHz. The frequency of the piston and Gaussian beams is set to f_{max}=0.53MHz. The theoretical measured Rayleigh distances for the MPS, Piston, and Gaussian beams compare[1] as $L_{meas}^{MPS} = (\omega_{meas}/\omega_{rad})^2 L_{rad} = 6.54L_{Piston} = 26.14L_{Gauss} = 6.53$m. The measured Rayleigh distances for the piston and Gaussian beams are equal to their radiated field values. The experimentally measured Rayleigh distance of the MPS array was actually 150 cm. Although there is a large discrepancy between the predicted and measured values of L_{meas}^{MPS}, the measured MPS Rayleigh distance exceeds the piston Rayleigh distance by a factor of 1.5, $L_{meas}^{MPS} = 1.5L_{Piston}$. The folded array results presented in the next section produced experimental diffraction

[1]Ziolkowski {1991} in his original paper mistakenly writes $L_{meas}^{MPS} = (\omega_{meas}/\omega_{CW})^2 L_{rad}$. This has been corrected here.

lengths that more closely resemble the predicted diffraction lengths.

The theoretical waists of the three beams compare as $w_{meas}^{MPS} = 0.59 w_{meas}^{Piston} = 0.23 w_{meas}^{Gauss}$. Note that the beam divergence can be calculated from the waists by differentiating the waist with respect to z (or in this case dividing by z). Hence the ratio of the MPS beam divergence to Gaussian beam divergence is approximately 4.29. Experimentally this value was determined to be 6.29. The discrepancy between theoretical and experimental values was attributed to experimental error.

2.5.2 Folded Array

One of the most important aspects of Ziolkowski's LW research involved determining how far beyond the classical Rayleigh distance, L_{Piston}, the localized wave diffraction length would reach. As discussed previously, a larger array leads to a longer diffraction length for a given localized wave. Hence, Ziolkowski proposed squeezing a larger array into a smaller one using a folded array scheme [1989] as depicted in figure 2.13. As shown in the figure, the aperture size is set to R_{max}. Driving functions outside of the aperture can be folded onto the aperture using the conformal map $\rho \rightarrow R_{max}^2/\rho$. Although the folded array produces better results than the simple array, the tradeoff is a much more

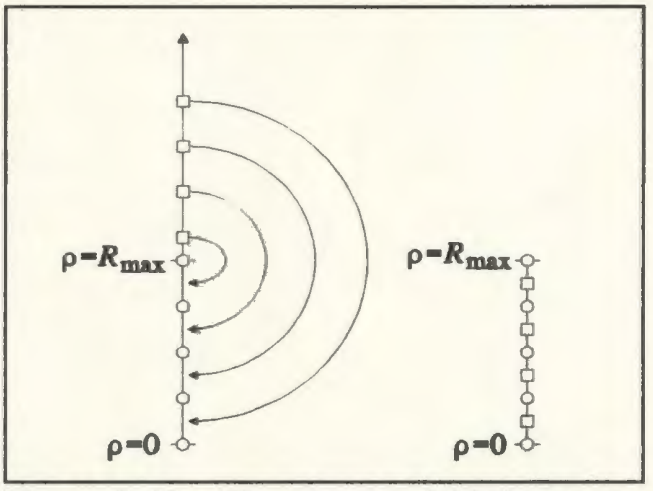

Figure 2.13: Elements are folded onto the aperture (left) to produce a folded array (right).

complex driving source distribution. Hence it is much more difficult to derive the theoretical waists and Rayleigh distances in closed form as was done for the simple array. As Ziolkowski demonstrated, this tradeoff produced a ten-fold enhancement in the measured diffraction length.

As discussed in [Ziolkowski, 1991; Ziolkowski & Lewis, 1990], the folded array was tested on a 25 element, (5×5) array. Array elements were spaced at 2.5mm such that the array was 1.25 cm on a side with $A=1.5625$ cm^2. The array elements were driven with the folded scheme driving function

$$\Phi(\rho,t)=\begin{cases} W(t)\psi_{\mathrm{MPS}}(\rho,z=0,t) & \rho=0 \\ W(t)\left[\psi_{\mathrm{MPS}}(\rho,z=0,t)+(R_{\max}/\rho)^4\,\psi_{\mathrm{MPS}}(R_{\max}^2/\rho,z=0,t-t_d)\right] & \rho\neq 0, \end{cases} \tag{2.63}$$

where $t_d=\left[(z_d^2+(R_{\max}^2/\rho)^2)^{1/2}-(z_d^2+\rho^2)^{1/2}\right]/c$ is the position dependent delay time, z_d is the constant delay distance 3.0 cm, and W(t) is a window function that removes the Mach cones characteristic to the MPS pulse (see figures 2.4-2.7).

The effective frequency values and diffraction lengths were calculated numerically. The radiated field effective frequency is given by, $f_{\mathrm{rad}}=0.33$ MHz. For comparison, the piston CW frequency is set to $f_{\mathrm{CW}}=1.52f_{\mathrm{rad}}=0.5$MHz (Ziolkowski chooses this more conservative choice of f_{CW} over setting $f_{\mathrm{CW}}=f_{\mathrm{rad}}$ to illustrate the superior beam characteristics of the MPS). The LW radiated field Rayleigh distance can be calculated as $L_{\mathrm{rad}}^{\mathrm{MPS}}=0.66L_{\mathrm{Piston}}=3.44$cm. The effective frequency of the measured field is given as $f_{\mathrm{meas}}=1.435$ MHz. From this, the measured field diffraction length is given by $L_{\mathrm{meas}}^{\mathrm{MPS}}=(f_{\mathrm{meas}}/f_{\mathrm{rad}})^2L_{\mathrm{rad}}^{\mathrm{MPS}}=12.48L_{\mathrm{Piston}}=65.05$ cm. The beam divergence rate is

$\theta_{meas}^{LW} = 2.02 \times 10^{-2}$. When compared to the piston beam, the measured efficiency ratio, $\Gamma_{meas}^{LW}/\Gamma_{meas}^{CW}$, of the MPS beam indicates an enhancement factor of 12.11, and the beam divergence rate, $\theta_{meas}^{LW}/\theta_{meas}^{CW}$, indicates a decrease factor of 5.11.

Both numerical simulations [Ziolkowski, 1991] and experiments [Ziolkowski & Lewis, 1990] were conducted to confirm the predicted results given above. In the numerical experiments, $L_{meas}^{MPS} = (f_{meas}/f_{rad})^2 L_{rad}^{MPS}$ lay in the 50-60cm region, $\Gamma_{meas}^{LW}/\Gamma_{meas}^{CW}$ was calculated to be 6.25, while $\theta_{meas}^{LW}/\theta_{meas}^{CW}$ indicates a decrease factor of 3.66. For the acoustic tank experiments, L_{Piston}=3.0cm, $L_{meas}^{MPS} = (f_{meas}/f_{rad})^2 L_{rad}^{MPS}$ lay in the 50-60cm region $\approx 25 L_{Piston}$, while $\theta_{meas}^{LW}/\theta_{meas}^{CW}$ indicates a decrease factor of 2.91. The numerical and experimental data compare extremely well, while the experimental and predicted values compare reasonably.

Ziolkowski [1991] points out that the experimental results from both the simple and folded arrays show that LW arrays can be designed to effectively outperform CW arrays in the context of multi-time-derivative transmit/receive systems. In his experimentation, Ziolkowski used the MPS pulse, which is by no means the optimal LW pulse. The MPS pulse was only chosen because it has interesting propagation characteristics, and its closed form expression allows it to be easily analyzed and simulated. Further optimization work on localized waves is essential in determining the waves with optimal propagation characteristics.

3 Predicted Backscatter Spectrum

3.1 Backscatter Spectrum Calculation

In what follows, the $e^{-i\omega t}$ time dependence will be suppressed on field quantities, and, for reasons that will become evident, it will be assumed that $\omega<0$. As such, if $\mathbf{k}$ denotes a vector whose spherical polar components are (k, ϑ, φ), then the plane wave

$$e^{i\mathbf{k}\cdot\mathbf{r} - i\omega t} \tag{3.1}$$

is not travelling in the direction of $\mathbf{k}$, as t increases. Writing

$$e^{i\mathbf{k}\cdot\mathbf{r} - i\omega t} = \left[e^{-i\mathbf{k}\cdot\mathbf{r} - i|\omega|t}\right]^* \tag{3.2}$$

it is evident that the plane wave $e^{-i\mathbf{k}\cdot\mathbf{r} - i|\omega|t}$ is travelling in the direction of $-\mathbf{k}$ as t increases, where the spherical polar components of $-\mathbf{k}$ are $(k, \pi-\vartheta, \varphi+\pi)$.

Morse and Ingard [1968] give an expression for the scattered field at a point (r,θ,ϕ) due to a plane wave of unit amplitude and wave number k, incident on a nonrigid sphere of radius a centred on the origin, in the direction of the positive z-axis. The medium outside the sphere is assumed to be homogeneous, isotropic, and have a velocity of wave propagation c. Symmetry considerations imply that this expression will also give the scattered field at a point whose Cartesian coordinates are $(0,0,-r)$, due to a plane wave travelling towards the centre of the sphere

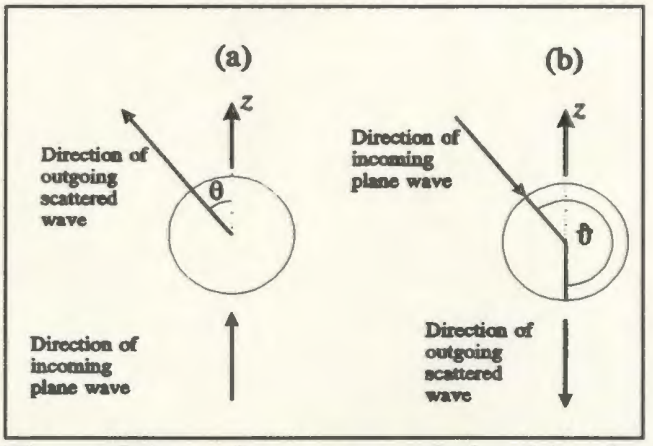

Figure 3.1: Symmetry relationship for scattering expression in (3.3).

from a direction whose spherical polar angles are ϑ & ϕ (figure 3.1). According to (3.2) above, this result may be modified to obtain the field at (0,0,-r) due to the plane wave $e^{i\mathbf{k}\cdot\mathbf{r} - i\omega t}$, where $\omega<0$. The result is, (suppressing the $e^{-i\omega t}$ time dependence):

$$-\left[\sum_{n=0}^{\infty}(i)^n(2n+1)\frac{j_n(ka) + i\alpha_n j_n(ka)}{h_n^{(1)\prime}(ka)+i\alpha_n h_n^{(1)}(ka)}h_n^{(1)}(kr)P_n(\cos\vartheta)\right] \qquad (3.3)$$

In (3.3) the term α_n is given by

$$\alpha_n = \frac{i\varrho c}{\varrho_e c_e}\left[\frac{j_n'(k_e a)}{j_n(k_e a)}\right] \qquad (3.4)$$

where ϱ is the density of the infinite medium surrounding the sphere, ϱ_e is the density of the sphere material, c_e is the speed of wave propagation in the sphere (so that $c_e = \sqrt{\varrho_e \kappa_e}$, where κ_e is the compressibility of the sphere material), $k=|\omega|/c$, $k_e=|\omega|/c_e$, a prime superscript on a function denotes the derivative of that function, j_n is the usual spherical Bessel function, $h_n^{(1)}$ is the spherical Hankel function of the first kind, and P_n is a Legendre polynomial. The expression in (3.3) may be compactly rewritten as

$$\sum_{n=0}^{\infty}\gamma_n h_n^{(2)}(kr)\,P_n(\cos\vartheta)\ , \qquad (3.5)$$

where

$$\gamma_n = -(2n-1)(-i)^n\left[\frac{j_n'(ka) + i\alpha_n j_n(ka)}{h_n^{(2)\prime}(ka) + i\alpha_n h_n^{(2)}(ka)}\right] \qquad (3.6)$$

and where $h_n^{(2)}$ is the spherical Hankel function of the second kind.

In principle then, one may obtain the scattered field at the point (0, 0, -r) on the negative z-axis, due to an arbitrary incident waveform, if it is composed of a weighted superposition of plane waves like (3.1). One merely takes the weighted superposition of (3.5) over each plane wave (i.e. Fourier) component of the incident waveform (the weighting being the spacetime Fourier transform of the incident waveform).

It will be assumed that the incident plane wave, $\psi(\mathbf{r},t)$, is a solution of the HWE for an infinite space filled with material such as that surrounding the sphere. The example used here will be the FWM solution discussed previously in chapter 2. The Fourier transform of the FWM is repeated here in (3.7) along with its support line projected onto the k_z, ω/c plane (figure 3.2)

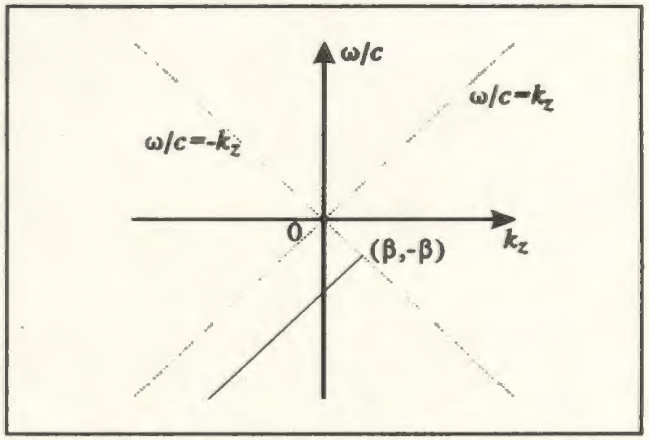

Figure 3.2: Projection of the support line of $\Psi_{\mathrm{FWM}}(\mathbf{k},\omega,\beta)$, as given in (3.7) onto the k_z, ω/c plane (projection shown as solid line segment).

$$\Psi_{\mathrm{FWM}}(\mathbf{k},\omega,\beta) = \frac{\pi^2}{i\beta} e^{-\kappa^2 z_0/4\beta}\, \delta[k_z-(\beta-\kappa^2/4\beta)]\, \delta[\omega+c(\beta+\kappa^2/4\beta)] \ . \qquad (3.7)$$

From figure 3.2 it is seen that the temporal Fourier transform of the FWM, $\mathcal{F}_t\{\psi_{\mathrm{FWM}}\}(\mathbf{r},\omega,\beta)$ will be an analytic signal, in that it contains only negative frequency components. The signal that is launched in a practical experiment is an approximation to $\mathbf{Re}\{\psi_{\mathrm{FWM}}\}(\mathbf{r},t,\beta)$, which has the two sided temporal Fourier transform $\frac{1}{2}[\mathcal{F}_t\{\psi_{\mathrm{FWM}}\}(\mathbf{r},\omega,\beta)+(\mathcal{F}_t\{\psi_{\mathrm{FWM}}\}(\mathbf{r},\omega,\beta))^*]$.

As discussed above then, the scattered field at the point whose Cartesian coordinates are (0,0,-*r*), due to an incident FWM of the form (2.9), will be given by a weighted superposition of the expression (3.5), for a single plane wave, over the plane wave [Fourier] decomposition (2.8) of the FWM. That is, the scattered field is given by

$$\Lambda_\beta(r,\omega) = \frac{\pi^2}{i\beta}\frac{1}{(2\pi)^3}\int_{\mathbf{R}^3} d\mathbf{k}\, e^{-\kappa^2 z_0/4\beta}\,\delta[k_z - (\beta - \kappa^2/4\beta)]\,\delta[\omega + c(\beta + \kappa^2/4\beta)] \times \gamma_n h_n^{(2)}(kr)\, P_n(\cos\vartheta) \tag{3.8}$$

where $\int_{\mathbf{R}^3} d\mathbf{k}$ denotes the integral over the three dimensional spatial Fourier transform domain.

The following identity, valid in the sense of generalized functions, is readily verified:

$$\delta[\omega + c\beta + c\kappa^2/4\beta] \equiv \frac{\sqrt{\beta}}{c\sqrt{|\beta + \omega/c|}}\, u(-\omega/c-\beta)\,\delta[\kappa - \sqrt{4\beta|\beta + \omega/c|}\,] , \tag{3.9}$$

where u, the unit step function, is needed to ensure $\omega+c\beta<0$. The volume integral $\int_{\mathbf{R}^3}$ in (3.8) may be broken down into separate integrations over cylindrical polar coordinate variables as $\int_0^{2\pi} d\varphi \int_{\mathbf{R}} dk_z \int_0^\infty d\kappa\,\kappa$. With the aid of the identity (3.9) the κ & φ integrations may be performed to give

$$\Lambda_\beta(r,\omega) = \frac{u(-\beta-\omega/c)}{2ic} e^{z_0(\beta+\omega/c)} \times \int_{\mathbb{R}} dk_z\, \delta[k_z - (2\beta + \omega/c)] \sum_{n=0}^{\infty} \gamma_n h_n^{(2)}(kr)\, P_n(\cos\vartheta)\big|_{\kappa=[4\beta|\beta+\omega/c|]^{1/2}} \cdot \tag{3.10}$$

Care must be exercised with the remaining k_z integral. With $\kappa = \sqrt{4\beta\,|\beta + \omega/c|}$, it is seen that the remaining delta function will set k_z so that k becomes

$$k = \sqrt{\kappa^2 + k_z^2} = \{4\beta|\beta + \omega/c| + (2\beta + \omega/c)^2\}^{1/2} = |\omega|/c \tag{3.11}$$

where the last equality followed from the step function $u(-\omega/c-\beta)$ in (3.10). Similarly, it can be shown that $\cos\vartheta = k_z/k = \{2\beta c/|\omega|\}-1$. Thus, (3.10) becomes

$$\Lambda_\beta(r,\omega) = \frac{u(-\beta-\omega/c)}{2ic} e^{z_0(\beta+\omega/c)} \sum_{n=0}^{\infty} \gamma_n\big|_{k=|\omega|/c}\, h_n^{(2)}(|\omega| r/c)\, P_n\left[\frac{2\beta c}{|\omega|} - 1\right] . \tag{3.12}$$

As was discussed chapter in 2, a LW finite energy solution to the HWE may be obtained by taking a weighted superposition over the arbitrary parameter β,

$$\int_0^{\infty} d\beta\, F(\beta)\, \psi_{\mathrm{FWM}}(\mathbf{r}, t, \beta) , \tag{3.13}$$

with appropriate conditions on the integrability of F. In particular, the weighting

$$F(\beta) = \begin{cases} 4\pi i \beta e^{-(B\beta - b)}, & \text{if } \beta > b/B; \\ 0 & \text{if } 0 \le \beta < b/B. \end{cases} \tag{3.14}$$

is chosen to obtain the MPS superposition (the parameters τ and T have been set to unity in equation (2.25)) [Ziolkowski, 1985].

With the waveform (2.25) incident on the sphere, the received signal at the point

(0,0,-r) on the negative z-axis is given by

$$\Lambda_{MPS}(r,\omega) = \int_0^\infty d\beta\, F(\beta)\Lambda_\beta(r,\omega)$$

$$= \frac{2\pi B u(-\omega/c - b/B)e^{z_0\omega/c+b}}{c} \sum_{n=0}^{\infty} \gamma_n|_{k=|\omega|/c}\, h_n^{(2)}(|\omega|r/c) \qquad (3.15)$$

$$\times \int_{b/B}^{|\omega|/c} d\beta\, e^{-\beta(B-z_0)} P_n\left((2\beta c)/|\omega| - 1\right)$$

If the change of variable $\zeta=\{2\beta c/|\omega|\}$-1 is made in (3.15), the result can be integrated by parts n times ($P_n^{(n+1)} \equiv 0$) to get

$$\Lambda_{MPS}(r,\omega) = \frac{\pi B|\omega|\, u(-\omega/c - b/B)}{c^2} \sum_{n=0}^{\infty} \gamma_n|_{k=|\omega|/c}\, h_n^{(2)}(|\omega|r/c)$$

$$\times \left[e^{-z_0(|\omega|/c - b/B)} \left[\frac{P_n(\zeta_0)}{\sigma} + \frac{P_n'(\zeta_0)}{\sigma^2} + \cdots + \frac{P_n^{(n)}(\zeta_0)}{\sigma^{n+1}} \right] \right. \qquad (3.16)$$

$$\left. - e^{-|\omega|B/c+b} \left[\frac{P_n(1)}{\sigma} + \frac{P_n'(1)}{\sigma^2} + \cdots + \frac{P_n^{(n)}(1)}{\sigma^{n+1}} \right] \right]$$

where

$$\sigma = \frac{|\omega|}{2c}(B - z_0) \qquad \zeta_0 = \frac{2bc}{B|\omega|} - 1. \qquad (3.17)$$

3.2 Backscatter Spectrum Analysis

Closer examination of (3.16) reveals that the predicted backscattered spectrum is a complicated function of the distance from the sphere, r, the sphere radius, a, and the sphere's material parameters, ϱ_e and $c_e = \sqrt{\varrho_e \kappa_e}$. For remote sensing purposes, the

ability to extract material parameters from the sphere's backscattered spectrum would be valuable. Here, emphasis will be placed on the extraction of the sphere radius. In figure 3.3, the predicted backscattered spectrum is illustrated in a two dimensional plot for sphere radius. In this example, the material parameters $c_e=3.0\times10^3$ m/s and $\varrho_e=7.8\times10^3$ kg/m^3, are used, similar to those of mild steel. The MPS parameters are set to $z_0=0.004$ m, $B=300$ and $b=750$ m^{-1} for this and all subsequent examples and experiments. For particular values of a, as illustrated in figure figure 3.4, the spectrum appears as a series of frequency peaks and dips beyond approximately 30 kHz. The spectral spacing of these dips changes with sphere radius; as the size of the sphere increases, the spacing between adjacent dips decreases. Hence, the sphere radius may be extracted by examining the frequency of these spectral peaks and dips.

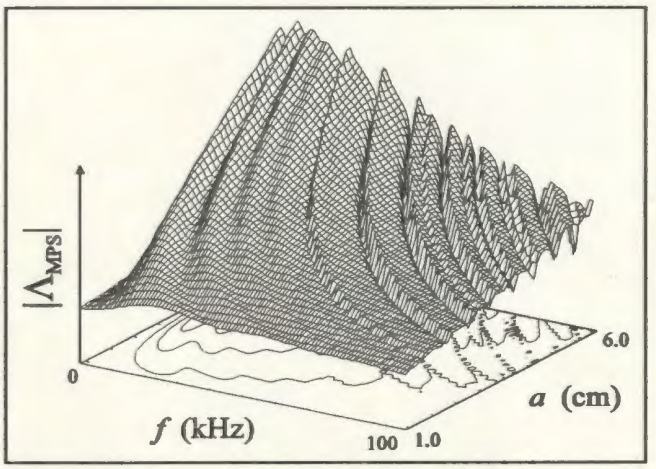

Figure 3.3: Surface plot of predicted backscattered spectra for varying sphere radius.

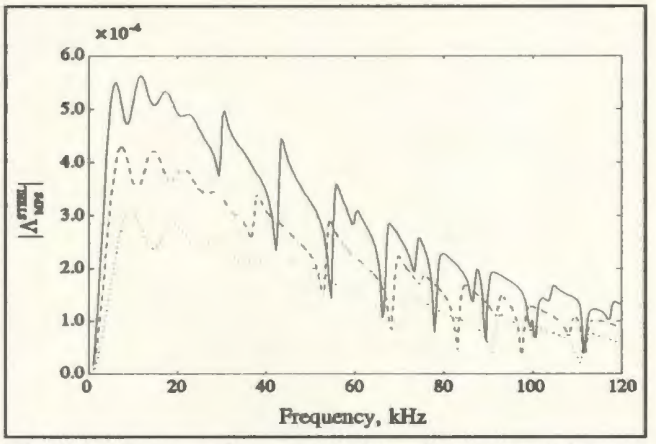

Figure 3.4: $|\Lambda_{MPS}(r,\omega)|$ for $r=150$mm, $c_e=3000$m/s, and $\varrho_e=7.8\times10^3$kg/m^3: $a=$[50 (solid), 40 (dashed), and 30 (dotted)] mm.

However, the variables c_e and ϱ_e also appear in (3.16); hence their effect on the spectral dip frequencies should be examined as well. In figure 3.5, the backscattered

spectrum is illustrated for varying ϱ_e. In this example the parameters a=0.3 cm and c_e=3.0×10³ m/s are used with ϱ_e in the range [3.0, 12.0]×10³ kg/m³. As the contour plot in this figure shows, a large change in ϱ_e does not greatly affect the spacing of the spectral dips.

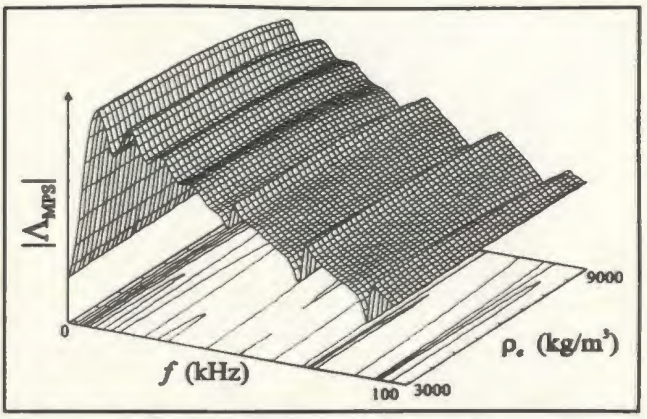

Figure 3.5: Surface plot of predicted backscattered spectra for varying sphere density.

In figure 3.6, the backscattered spectrum is illustrated for varying c_e. In this example, the sphere parameters a=0.3 cm and ϱ_e=7.8×10³ kg/m³ are used with of c_e varying in the range [2.0, 4.0]×10³ m/s. This figure shows that as c_e increases, the spacing of the spectral dips decreases. Hence, it seems that the backscattered spectrum changes with the sphere's speed of sound, yet doesn't change greatly with varying sphere density. This is illustrated more fully by fixing the frequency and changing both the sphere's density and speed of sound. The resulting surface plot is illustrated in figure 3.7. As this figure shows, the predicted backscattered spectrum does not change greatly as the density is changed yet changes abruptly as the speed of sound is changed.

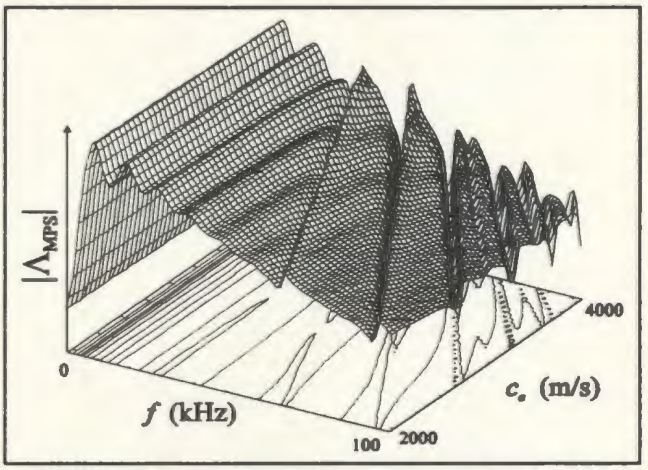

Figure 3.6: Surface plot of predicted backscattered spectra for varying c_e.

It is notable that many metals and hard materials have similar c_e values [Gray,

1972] (table I). Hence it should be possible to extract the sphere size from the backscattered spectrum if the sphere is assumed to be a material with c_e near 3100m/s. The accuracy of the extraction will of course degrade as the actual value of c_e varies away from the assumed value.

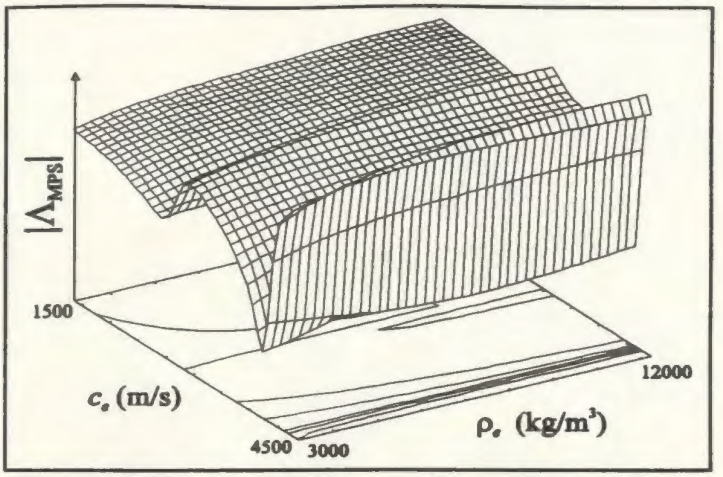

Figure 3.7: Surface plot of predicted backscattered spectra at 50kHz for varying ϱ_e and c_e.

Material	c_e (m/s)
Stainless Steel	3100
Aluminum (rolled)	3040
Titanium	3125
Nickel	3000
Magnesium	3050
Cast Iron	2809
Pyrex Glass	3280

Table I: Speed of Sound in Various Rigid Materials

4 Experimental Methodology

In order to obtain spherical backscatter signals for analysis, acoustic experiments were conducted in a large (3×4×5 m) tank. Three steel spheres with radii measuring 20, 40 and 60 mm, and a single aluminum sphere with a 40 mm radius, were used. The MPS pulses were launched using the double hydrophone system illustrated in figure 4.1 (next page).

The experimental setup is controlled using a single HP 9000 series PC and an IEEE-488 (GPIB) bus. This system allows for completely automated data aquisition. Digitized transmit signals are generated by the computer and sent via the GPIB to an arbitrary waveform generator and amplifier. Received signals are digitized and relayed back to the PC, again via the GPIB. A Kruger stepper motor/controller allows for movement of the transmitter through three axes.

4.1 Transmitter System

The transmitter (TX) system consists of a digital to analog converter (DAC), a power amplifier, and an ultrasonic transmitter. The DAC, a WaveTek model 275, has the ability to store a 2048 sample signal in memory and convert it using a definable sampling period (in the 267ns-267ms range). The WaveTek has a burst mode which allows a previously stored signal to be converted with a single GPIB command. The output analog signal consists of flat voltage steps which are smoothed by the filter in the power amplifier. The sampling frequency used throughout the experiments is 1MHz.

The power amplifier, a B&K model 2713, has a linear frequency response and

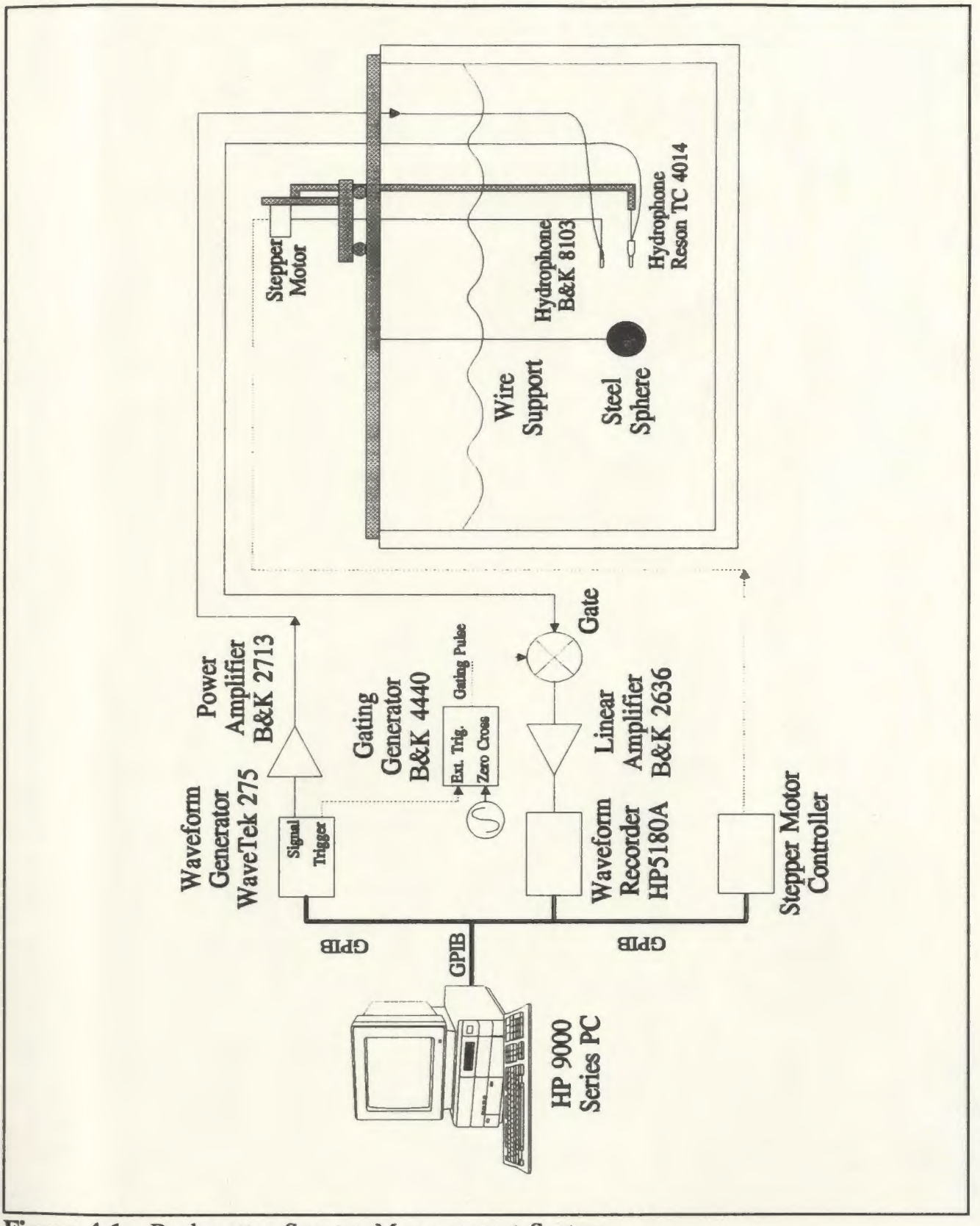

Figure 4.1: Backscatter Spectra Measurement System.

a bandwidth of 200kHz. The 200kHz cutoff in the amplifier provides anti-aliasing filtering for the WaveTek analog signal.

The MPS pulses are launched synthetically, using superposition, by a Bruel and Kyjer hydrophone (B&K 8103). A stepper motor is used to move the hydrophone to the required positions along the synthetic transmit aperture. The spheres are placed directly in front of the transmit aperture in line with the array's z-axis (figure 4.2). The receiver hydrophone is placed near the centre of the transmit array, offset by about 1cm from the z-axis. At this position, the receiver is assumed to be close enough to the centre of the array such that the signal it receives is approximately equal to the signal at the centre of the array (the backscattered signal).

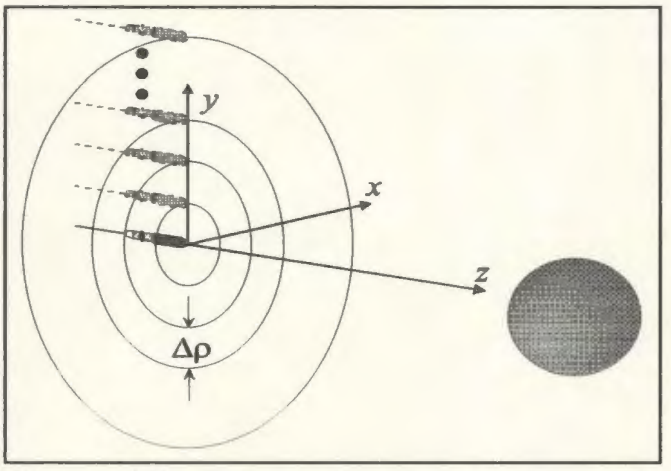

Figure 4.2: Sphere placed along the z-axis of the aperture.

In order to obtain a variety of spectra, the array was placed at distances of 150, 250, and 350 mm from the centre of each sphere. Because of the placement of the receiver, these distances represent the variable r given previously in (3.16). At the distance $r=150$ mm, the spheres are located in the *near field* of the transducer array. In this case, the near field of the array simply refers to where the approximation $z/R \approx 1$, discussed previously in chapter 2, is invalid (or where $z < \textit{size of aperture}$).

The frequency response of the transmit hydrophone, as measured 1 m away from the hydrophone, has a slope of approximately 40dB/decade (figure 4.3) 10-110kHz. In

the time domain, this translates into a double time derivative as the signal passes through the hydrophone into the far field of the hydrophone. This phenomenon is similar to the disk transducer behaviour described by previously in chapter 2 in which the conversion from electrical energy to far field pressure is described by two time derivatives. The transmitter is essentially omni-directional over the *x*-*y*, *y*-*z* and *x*-*z* planes below 110kHz.

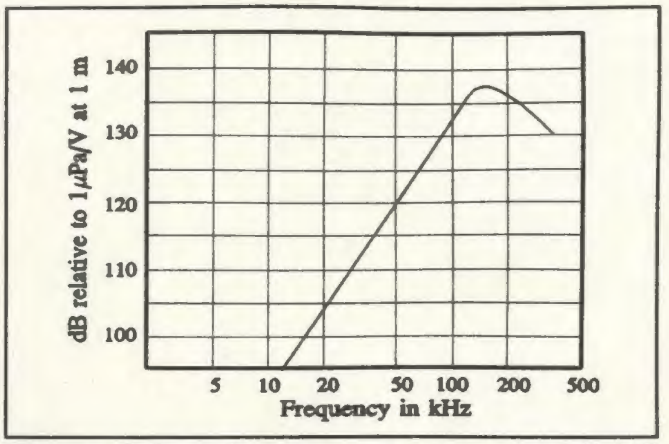

Figure 4.3: Frequency response of B&K 8103 measured in water 1 m away from the hydrophone [Brüel and Kjær, 1986].

4.2 Receiver System

The receiver (RX) system consists of an ultrasonic receiver, a gating system, and a waveform recorder. The receiver hydrophone, a Reson TC4104, senses both the direct and reflected signals from the transmitting hydrophone and the sphere, respectively. The frequency response of the receiver is approximately flat below 400kHz (figure 4.4). The receiver is omni-directional over 360° in the *x*-*y* plane and 310° in the *x*-*z*, *y*-*z* plane below 200 kHz.

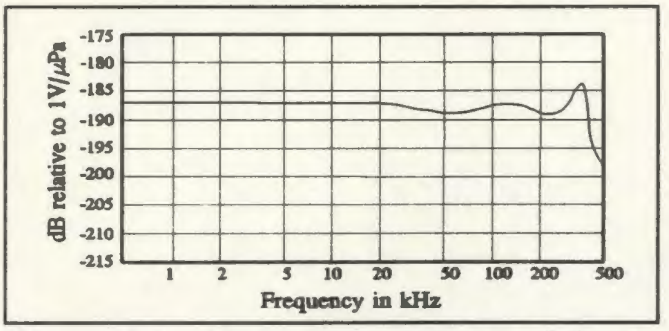

Figure 4.4: Frequency response of Reson TC-4104 [Reson System APS, 1988]

A gating system is used to remove a significant portion of the direct signal from

the receiver signal so as to avoid saturation of the waveform recorder's input amplifiers. The gate consists of a gating generator (B&K 4440) and an analog gate. The gating generator receives a trigger pulse from the DAC when the DAC starts sending its analog signal. Consequently, the generator produces an "on" voltage pulse that is fed into the analog gate. The delay and duration of the voltage pulse is controlled from the front panel of the gating generator. The waveform recorder converts the gated analog signal to digital form and relays it back to the PC via the GPIB.

The waveform recorder is used to convert the gated analog signals to digital form. The recorder was set up to receive 512 samples at a sampling rate of 1MHz. Waveform recording is initiated by a triggering pulse sent by the DAC when it starts to transmit. The delay between when the recorder receives the trigger pulse and when is starts recording a waveform is also user definable.

4.3 System Transfer Function

As described in the previous two sections, the TX system imparts a double time derivative on an input signal in the range 0-110 kHz. On the other hand, the RX system essentially has a flat frequency response below 400kHz. Hence, the TX/RX system in water will impart two time derivatives on any input signal in the 0-110kHz band. Analysis of system TX/RX transfer function was performed by inputting $(\sin 2Bt)/2Bt$ pulses of bandwidth B into the transmitter. A plot of the received signal from a 150 kHz sinc pulse is shown in figure 4.5.

Below approximately 110 kHz, the system transfer function, $H(\omega)$, can be

approximated by

$$H(\omega) = K\omega^2, \qquad (4.1)$$

where K is a constant. This confirms the two time derivative phenomenon expected from the total system. The transfer function block diagram is illustrated in figure 4.6.

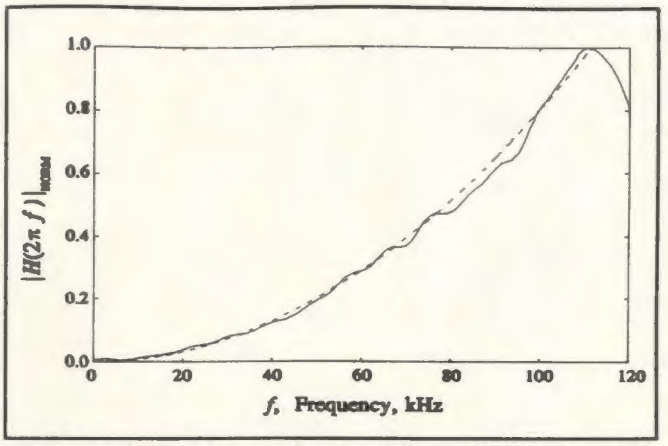

Figure 4.5: Magnitude Plot of the double hydrophone system transfer function, $H(\omega)$ (solid), and a least squares fitted second order polynomial, $K\omega^2$ (dotted).

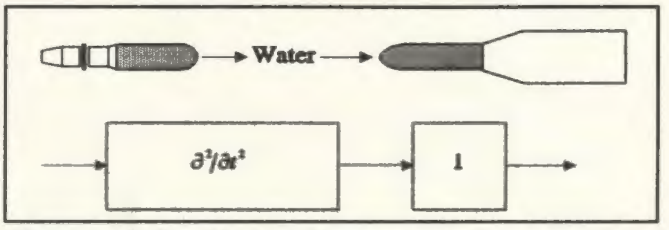

Figure 4.6: Hydrophone system response.

4.4 Signal Reconstruction

The axisymetric nature of both the MPS pulse and the reflecting sphere allows us to reduce the number of elements in the transmit array by using discrete, equally spaced annular sections (c.f. figure 4.2). If the receiver hydrophone is placed along the z-axis ($\rho=0$) then, assuming a flat band system transfer function, the backscattered signal may be reconstructed using the formula

$$v_{MPS}(r,t) = -\sum_{n=0}^{N} \varsigma_n(r,t)\, S(n) \qquad (4.2)$$

In (4.2), v_{MPS} is the reconstructed backscattered signal, ς_n are the spherically reflected signals originating from each of the N transmit elements, ρ_n is the radial location of the n^{th} element, $\Delta\rho$ is the spacing between adjacent annular elements, $S(1)=\pi\Delta\rho^2/4$ and $S(n)=\pi(\rho_n+\frac{1}{2}\Delta\rho)^2-\pi(\rho_n-\frac{1}{2}\Delta\rho)^2=2\pi\rho_n\Delta\rho$. Thus a complete aperture can be synthesized

by moving the transmit hydrophone to discrete positions along a single radius of the transmit aperture, corresponding to each discrete annular region. For these experiments, N=30 and $\Delta\rho$=4 mm, hence the aperture has a radius of 116 mm.

In order to obtain the relationship between the reconstructed and predicted backscattered spectra, (4.2) should be weighted with the system transfer function, $H(\omega)$. Hence, if the MPS pulse is designed such that the effective maximum frequency, f_{max} (chapter 2) [Ziolkowski, 1991], of each driving function is below 110kHz, then the backscattered spectrum, Λ_{MPS}, and the Fourier transform of the reconstructed signal, Υ_{MPS}, are approximately related by

$$\Upsilon_{MPS}(r,\omega) \approx K\omega^2\Lambda_{MPS}(r,\omega) \tag{4.3}$$

in the range [0-120] kHz. For the MPS parameters chosen, f_{max}=59.7 kHz.

4.5 Direct Signal Cancellation

The experiments discussed in this chapter are designed such that, theoretically, the direct and reflected signals do not overlap. However, practical experimentation showed that a small amount of residual direct signal overlapped the received signal, and in some cases completely overwhelmed the weak reflected signal. The residual direct signal is actually thought to be due to reflections from the conical shaped brass case that houses the receiver hydrophone. In order to remove this unwanted residual signal, a signal cancellation method is used. The residual plus spherically reflected signals are first measured by transmitting with the sphere present in the tank. The residual direct signal is then measured by transmitting with the sphere absent from the tank. The

residual signal is thus removed from the residual/sphere signal by subtraction. The effectiveness of this method is illustrated in figures 4.7 and 4.8 on the following pages. Figure 4.7 shows the residual direct signal superimposed over the residual/sphere signal. The reflected signal is calculated to arrive at approximately 0.06 ms. Figure 4.8 shows the reflected signal with the direct residual signal subtracted out. As expected, the reflected signal remains starting at approximately 0.06 ms. Note here that the time axis on figures 4.7 and 4.8 are referenced to the start of waveform recording and not to the start of direct signal transmission.

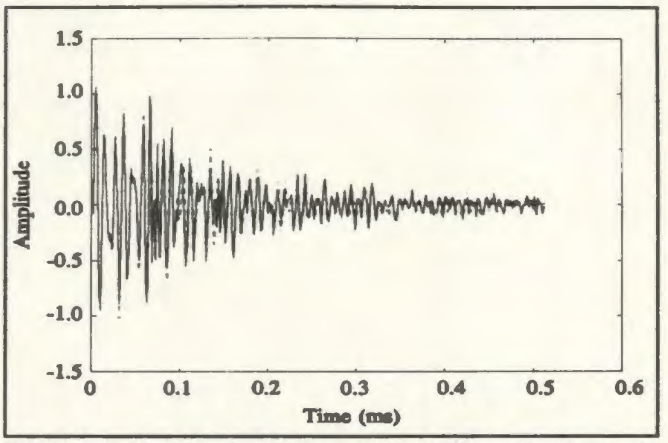

Figure 4.7: Typical residual signal (dotted) superimposed over the residual+spherically reflected signal. Notice that the difference between the two signals is noticable (barely) only after approximately 0.06ms.

4.6 Background Noise

The effect of background is reduced simply through signal averaging. The PC controller is capable of sending repeated signals through the system and averaging them. To demonstrate the effectiveness of this procedure, the background noise was measured by powering up the TX/RX amplifiers and

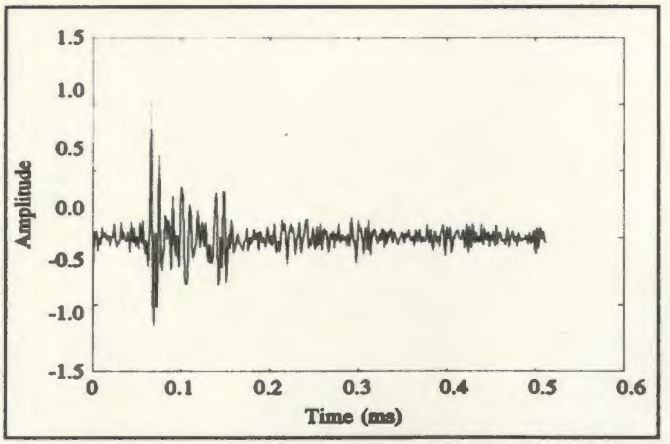

Figure 4.8: Spherically reflected signal obtained after the residual direct signal has been subtracted out.

measuring the amount of random noise present. The noise signals were then averaged M times to record the effective noise reduction. Figure 4.9 shows the effect of averaging 10 and 50 times. The FFT of the averaged signals shows a significant reduction of the noise power as the averaging is increased from 10 to 50 times. The ratio of signal energy between the $M_1=10$ and the $M_2=50$ signal is calculated using

$$\frac{\mathscr{E}_1}{\mathscr{E}_2} = \frac{\sum_{l=0}^{N-1} n_1(l)}{\sum_{l=0}^{N-1} n_2(l)} \qquad \textbf{(4.4)}$$

where $\mathscr{E}$ is the energy, n is the sample signal and N is the number of samples taken. For this example, the ratio is 4.7642, which is close to the expected ratio for gaussian white noise (5.0). For these experiments, the signals were averaged 50 times each. A 512 point Hanning window was applied to the reconstructed sampled signals in order to smooth the backscattered signal FFTs.

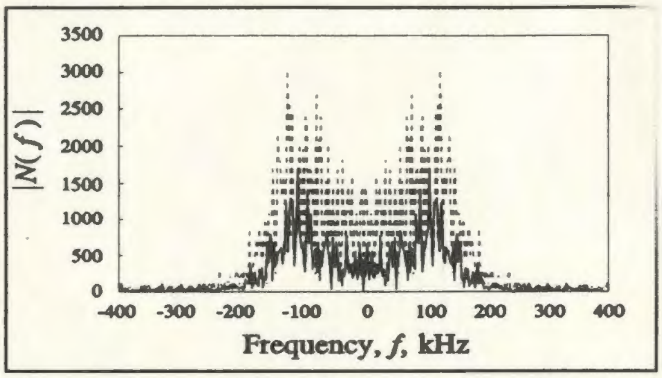

Figure 4.9: FFT of received background after 10 averages (dotted) and after 50 averages (solid)

5 Experimental Results

In the figures which follow, the reconstructed backscattered, Υ_{MPS} spectra are compared to the predicted backscattered spectra, Λ_{MPS}. The predicted spectra has been weighted with the system transfer function, $H(\omega)$, in order to account for two time derivatives. In figures 5.1-5.3, the predicted versus measured spectra is shown for steel sphere radii 20, 40 and 60 mm respectively for $r=15$ cm. In figure 5.4, the predicted versus measured spectrum is shown for the 40mm radius aluminum sphere for $r=15$ cm. Other plots of measured backscattered spectra for the cases $r=25$ cm and $r=35$ cm are contained in appendix C. In all cases, both the predicted and measured spectra contain *dips*. Although the locations of the dips are different in the measured and predicted spectra, the average spacing between the dips are

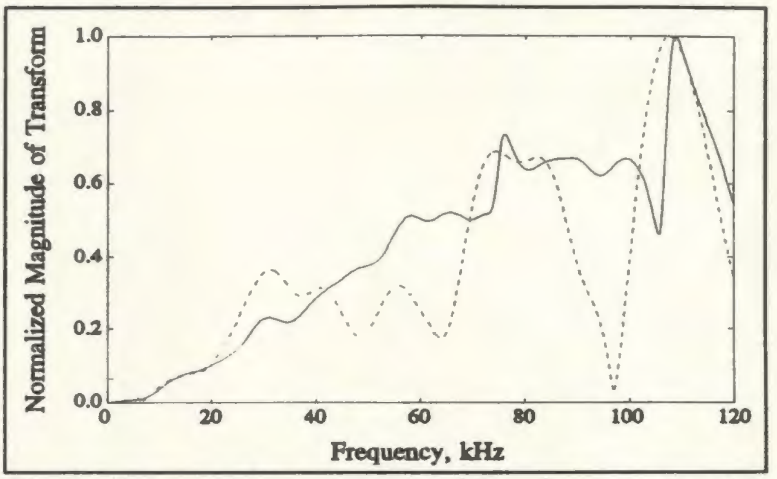

Figure 5.1: Comparison of $|\Upsilon_{MPS}|$ (dotted) with $|H\Lambda_{MPS}|$ (solid) for a 30 mm radius steel sphere at $r=150$ mm from the array.

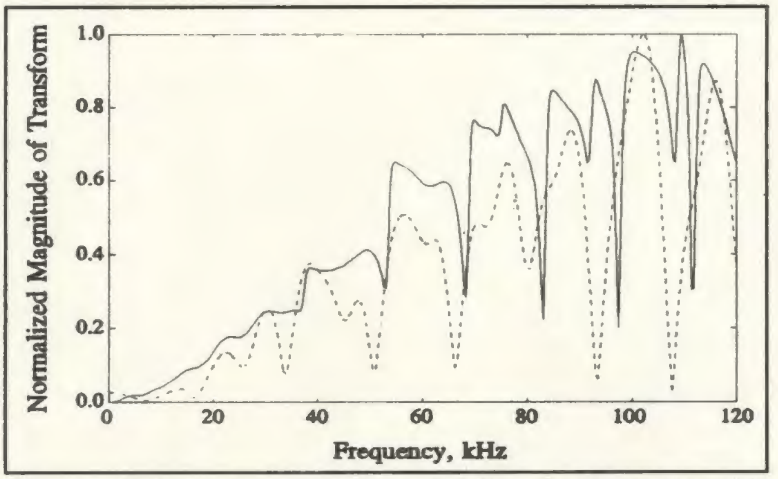

Figure 5.2: Comparison of $|\Upsilon_{MPS}|$ (dotted) with $|H\Lambda_{MPS}|$ (solid) for a 40 mm radius steel sphere at $r=150$ mm from the array.

approximately the same. The differences between both spectra may be due to the following:

- An approximation to the MPS pulse is launched from the array. As such the measured backscattered spectra will also be an approximation.

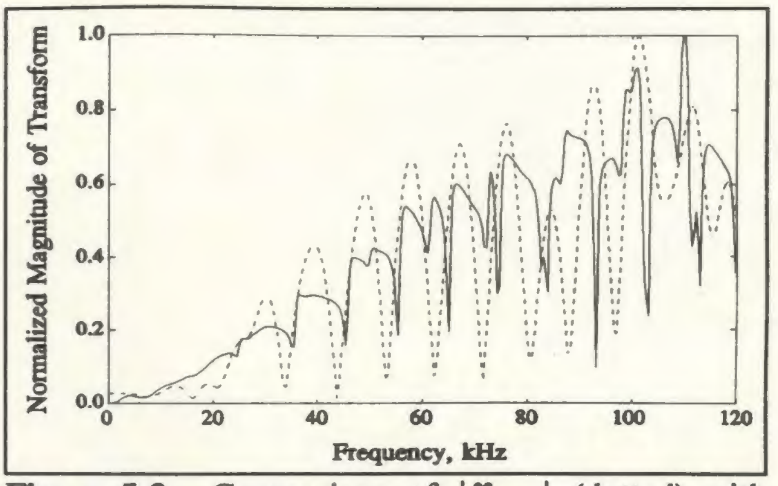

Figure 5.3: Comparison of $|\Upsilon_{MPS}|$ (dotted) with $|H\Lambda_{MPS}|$ (solid) for a 60 mm radius steel sphere at $r=150$ mm from the array.

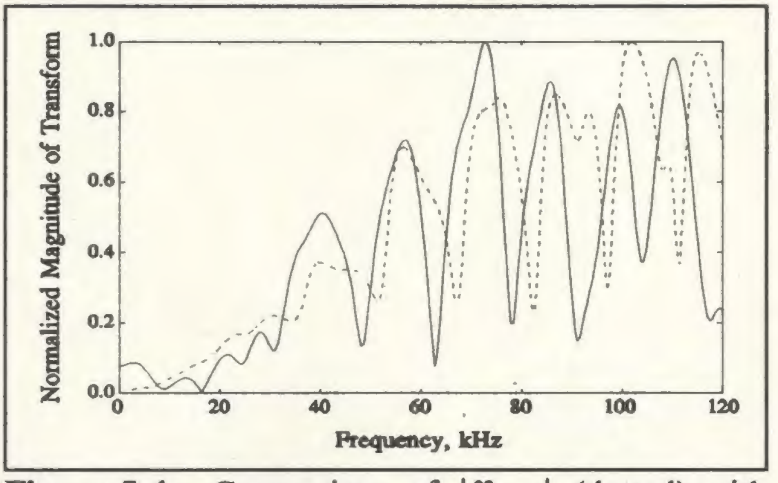

Figure 5.4: Comparison of $|\Upsilon_{MPS}|$ (dotted) with $|H\Lambda_{MPS}|$ (solid) for a 40 mm radius aluminum sphere at $r=150$ mm from the array.

- The material parameters used to generate the predicted spectra may not be the actual parameters of the spheres used in the experiments. Since accurate measurements of the material parameters of the steel and aluminum were not available, estimates of c_e and ρ_e were made based on the grade of steel and aluminum used.

- The receiver hydrophone was slightly offset from the z-axis. Although it was hoped that this offset would not greatly affect the results, it may have contributed to the difference in locations of the dips in the measured versus predicted spectra.

As was discussed in the previous chapter, a window function was applied to the measured reconstructed signals to impart spectral smoothing. It was determined that this window function has little effect on the location of the dips of the predicted spectra.

As was discussed in chapter 3, the frequency of the dips in the backscattered spectra may be used to determine the size of the sphere. In this case, the average spectral spacing of the dips will be used, since they are consistent between measured and predicted spectra. The spectral dips of five steel sphere spectra (2-6cm radii) were located and the differences between adjacent dips were calculated and averaged. Since the dips seem to be most prominent between 30kHz and 120kHz, only these dips were used in the calculation. The results are shown in figure 5.5 as the solid line. Since the curve appears to exhibit an inverse relationship, the extracted points were fitted with a $K_1/a+K_2$ curve via the least squares approach. The fitted curve is shown as the dashed line in figure 5.5. The maximum error in the fitted curve is 0.61% for points shown in the figure (radii of 2-6cm).

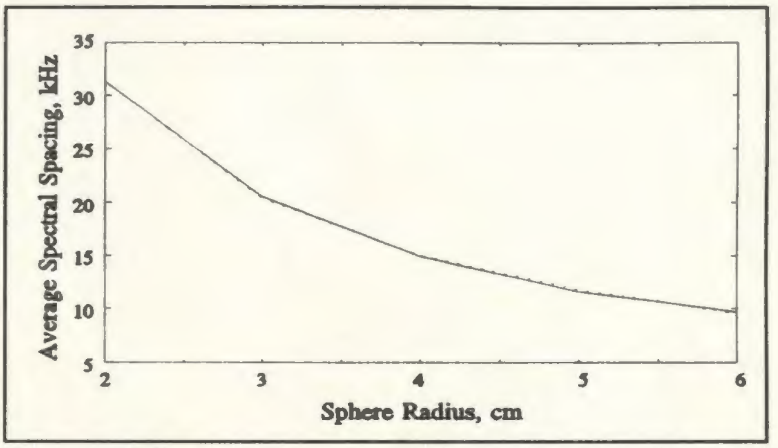

Figure 5.5: Average spectral spacing plot for steel spheres. Graph shows both extracted (solid) and modelled (dashed) data.

An identical analysis was performed on a set of aluminum sphere predicted backscattered spectra. As shown in figure 5.6, the modelled curve (dashed) agrees well with the predicted results (solid) with a maximum error of 1.65 percent for the points

shown in the figure (radii of 2-6cm).

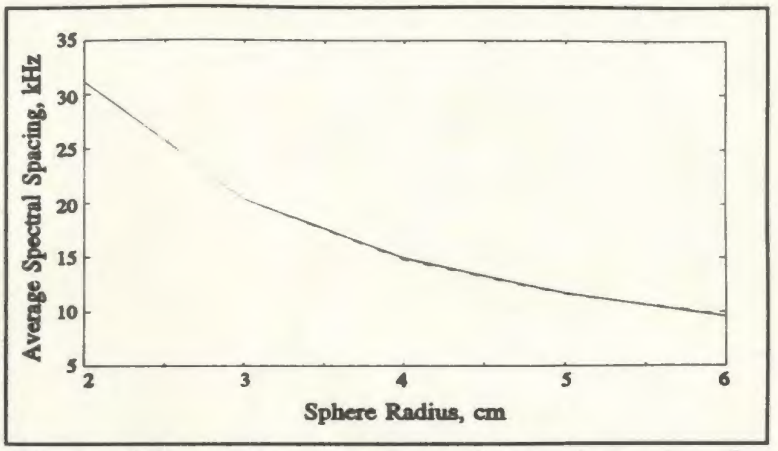

Figure 5.6: Average spectral spacing plot for aluminum spheres. Graph shows both extracted (solid) and modelled (dashed) data.

From the results above, it is seen that a method to extract the radius from a backscattered spectrum may be readily formulated. Using a number of spheres of known size, one may determine the constants in the $K_1/a+K_2$ curve from the dips in the backscattered spectra. This calibration eliminates the need to determine c_e or ρ_e of the spheres. In order to extract the radius of an unknown sphere, one may simply examine the dips of its backscattered spectra and extract the sphere radius from the calibrated curve, $K_1/a+K_2$.

This method was tested on the measured backscattered spectra of the steel and aluminum spheres. The constants K_1 and K_2 were determined using the three steel sphere spectra obtained at $r=150$ mm. In order to automate the extraction procedure, a simple algorithm was formulated to determine the locations of the spectral dips. This algorithm numerically differentiates the input spectrum to locate where the slope of the spectrum changes abruptly. The algorithm was implemented as a MatLab®[2] function and is listed in appendix B. Table II shows the extraction results for each of the spheres at the indicated distances. The maximum error is 3.5% for the steel spheres and 6.5% for the aluminum sphere. The percent error for the aluminum sphere is somewhat higher than

[2]MatLab is © copywrite 1984-1993 The Mathworks Inc.

that of the steel spheres. This is to be expected since the modelled curve was fitted using the steel sphere spectra. However, the results are still favourable since the error seems to be within acceptable limits.

Actual Size (cm)	Dist. from Array (cm)	Estimated Size (cm)	Percent Error
Steel			
2.0	15	1.9941	0.3
2.0	25	2.0044	0.2
2.0	35	1.9975	0.1
4.0	15	4.0968	2.4
4.0	25	4.0939	2.3
4.0	35	4.1403	3.5
6.0	15	5.8445	2.6
6.0	25	5.7954	3.4
6.0	35	5.8632	2.3
Aluminum			
4.0	25	4.1773	4.4
4.0	35	4.2610	6.5

Table I: Actual Vs. Extracted Sphere Radius

6 Qualitative Analysis of Two Ball Scattering

In chapter three, the predicted MPS backscatter was derived and supported with the experimental spectra presented in chapter five. In this chapter, experimentally obtained two ball scattering spectra will be presented. The experimental setup used to obtain the data is similar to the setup described in chapter four. Two identical 40mm radii steel spheres are separated by distance d and hung from wire supports. The array is positioned at distance r from the centre of the two-ball axis, such that the array and two-ball axes are perpendicular. This is illustrated in figures 6.1 and 6.2. The method used to reconstruct the MPS pulse is somewhat different than that used in the single ball case. The symmetry of the single ball set up allowed the use of a single line of transducers to reconstruct the MPS backscatter. However, symmetry of the two-ball setup requires a complete half array to reconstruct the two ball backscatter (figure 6.1). The measured backscatter spectra obtained at r=25cm for d=[4.0, 8.0, 14.0, 20.0]cm

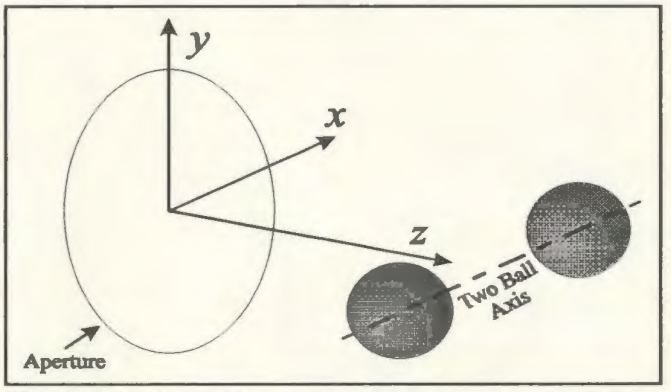

Figure 6.1: Placement of two spheres in from of acoustic array.

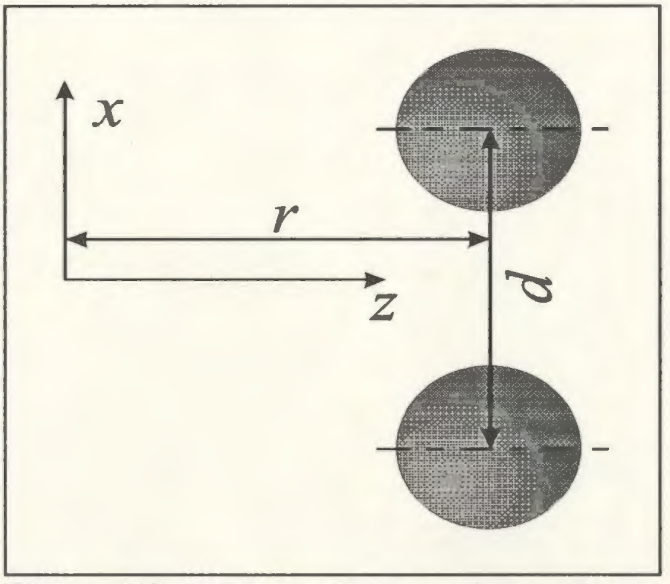

Figure 6.2: Two spheres, whose centres are separated by distance d, are placed at distance r from the array.

are illustrated in figures 6.3 to 6.6 respectively. Similar spectra obtained at r=35cm are given in appendix C.

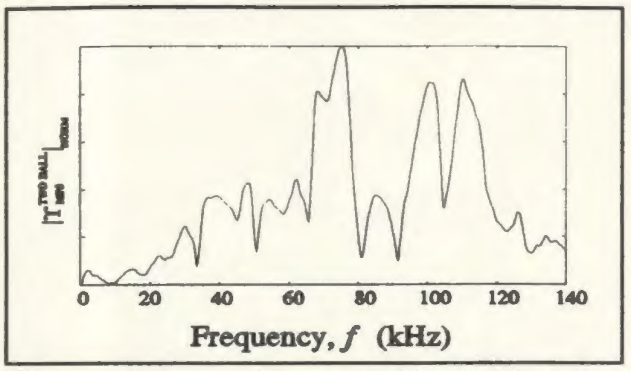

Figure 6.3: Two ball backscatter spectrum for r=25cm and d=4cm.

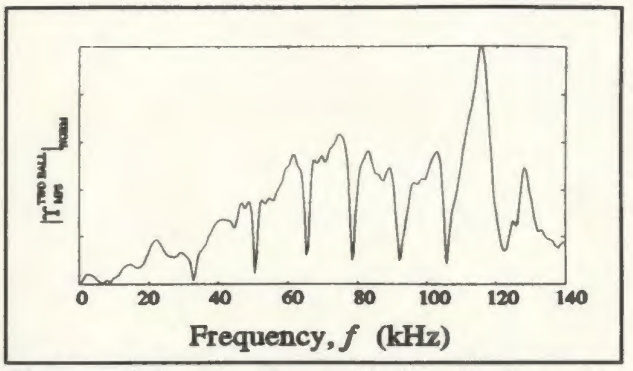

Figure 6.4: Two ball backscatter spectrum for r=25cm and d=8cm.

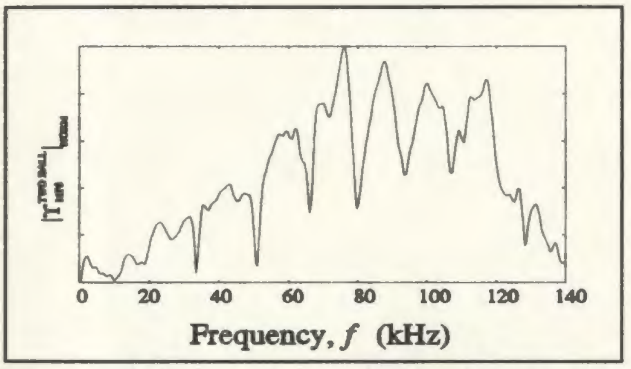

Figure 6.5: Two ball backscatter spectrum for r=25cm and d=14cm.

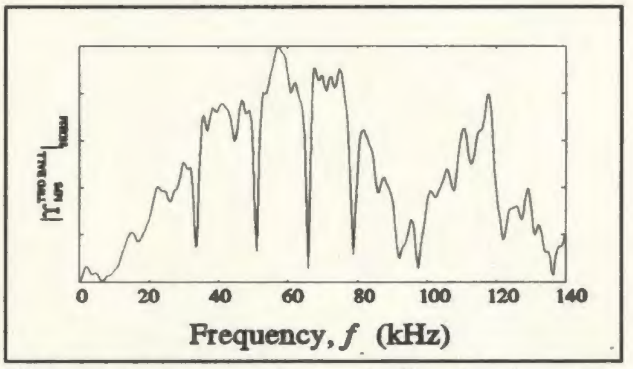

Figure 6.6: Two ball backscatter spectrum for r=25cm and d=20cm.

As these figures illustrate, the backscattered spectra contain the characteristic frequency dips at locations similar to those of the single ball backscattered spectra. The dips also appear at spectral locations similar to those of the 40mm radius single sphere backscattered spectrum, with slight differences.

The predicted backscattered spectrum may be obtained in a similar manner to the method outlined in chapter three. For instance, several authors have derived plane wave scattering from multiple spheres [Waterman & Truell, 1961; Brunning and Lo, 1971;

Peterson and Strom, 1973]. If the plane wave scattering expression is obtained, then it may be superposed over the plane wave decomposition of the LW; the result would be the two-sphere scattering expression. However, it may be difficult, if not impossible, to obtain the two ball LW scattering expression in closed form. As a first approximation, one may add the backscattered signals from two single spheres that are offset by angles of $\pm\theta$.

The practical significance of a two-ball backscattering expression is questionable due to its *apparent* complexity. For instance, the predicted spectra would only be valid for equal sized spheres with the same material parameters, with two-sphere axis perpendicular to that of the array. The analysis would not account for different sized spheres, spheres of differing materials, nor spheres whose axes are obliquely oriented to that of the array. In a practical sonar or radar system, one would launch a narrow waist LW in such a manner as to be able to discern single targets in a multi-target area using the single target backscatter expression. For instance, one may sweep an area using a pencil beam LW and obtain scattering signals from single targets if the targets are located far enough from one another to avoid spatial aliasing. In the case of closely spaced targets, the performance of a pencil beam LW system would depend on the size of the array and on the effective frequency of the LW pulse. Hence, the multiple sphere LW backscatter expression *may* not have any significance in a practical remote sensing system. However, further comments in this regard are deferred pending a complete analysis of the predicted two-sphere LW backscatter expression. This work will be completed at a later date.

Conclusions

In the context of multi-time-derivative transmit-receive systems (such as that present in the forward propagating section of our experimental setup), the superior focusing properties of the MPS pulse over equivalent CW pulses has been demonstrated [6]. It thus seems natural to try to use the extended near-field characteristics of the MPS pulse, coupled with its broadband nature, to extract information from backscattered signals; the broadband nature of the signals allows for parameter extraction, while it is the enhanced propagation properties of the LW pulses that ensures that a relatively large amount of energy reaches the target. Other broadband signals might not have desirable propagation properties, and more focused monochromatic pulses would not have the desirable spectral width.

The sphere radii have been successfully extracted from the MPS backscattered spectra of several different sizes of steel and aluminum spheres, using a relatively naive algorithm. In this algorithm, the speed of sound in the sphere is assumed known (and is approximately the same for a wide variety of metals), and the radius is extracted from the spectrum. It may be possible to estimate both the material properties and the radius from the backscattered spectrum. Work on this is ongoing.

References

Besieris, I. M., Shaarawi, A. M., & Ziolkowski, R. W., "A bidirectional travelling plane wave representation of exact solutions of the scalar wave equation," *J. Math. Phys.*, **30**, 1254-1269 (1989).

Bowman, J. J., Senior, T. B. A., Uslenghi, P. L. E., "Electromagnetic and Acoustical Scattering by Simple Shapes," (North-Holland Publishing Company: Amsterdam), 1969.

Brittingham, J. B., "Focus Wave Modes in homogeneous Maxwell's equations: transverse electric mode," *J. Appl. Phys.*, **54**, 1179-1189 (1983).

Brüel and Kjær, "Instruction Manual, Hydrophones Types 8101, 8103, 8104, 8105," 1986.

Brunning, J. H., & Lo, Y. T., "Multiple scattering of EM waves by spheres, part I and II," *IEEE Trans. Ant. Prop.*, **19**, 378-400 (1971).

Donnelly, R. K., & Ziolkowski, R. W., "Designing Localized Waves," *Proc. R. Soc. Lond. A*, **440**, 541-565 (1993).

Donnelly, R. K., & R. W. Ziolkowski, R. W., "A method of constructing solutions of homogeneous partial differential equations: localized waves," *Proc. R. Soc. Lond. A*, **437**, 673-692, (1992).

Donnelly, R., Power, D., Templeman, G., & Whalen, A., "Graphical Simulation of Superluminal Acoustic Localized Wave Pulses," *IEEE Trans. Ultrason., Ferroelec, Freq. Contr.*, To be published (1993).

Peterson, B., & Strom, S., "T-Matrix for electromagnetic scattering from an arbitrary number of scatterers and representation of E(3)," *Phys. Rev. D.*, **8**, 3667-3677 (1973).

Power, D., Donnelly, R., & Macisaac, R., "Spherical scattering of superpositions of localized waves," *Phys. Rev. E.* 8, 1410-1417 (1993).

Gray, D., ed., "American Institute of Physics Handbook," (McGraw Hill: New York), 1972.

Jones, D. S., "The Theory of Electromagnetism," (Pergamon: New York), 1964.

Lu, J., & Greenleaf, J. F., "Experimental verification of nondiffracting X waves," *IEEE Trans. Ultrason., Ferroelec, Freq. Contr.*, **39**, 441-446 (1992).

Morse, P., & Ingard, K. U., "Theoretical Acoustics," (McGraw Hill: New York), 1968.

Overfelt, P. L., "Bessel-Gauss pulses," *Phys. Rev. A*, **44**, 3941 (1991).

Reson System APS, "TC 4014 Reference Hydrophone," 1988.

Ristic, V., "Principles of Acoustic Devices," (Wiley: New York), 1983.

Waterman, P. C., & Truell, R., "Multiple scattering of waves," *J. Math. Phys.*, **2**, 700-734 (1961).

Wyld, H. W., "Mathematical Methods for Physics," (W. A. Benjamin Inc: Mass), 1976.

Ziolkowski, R. W, Lewis, D. K., & Cook, B, D., "Evidence of localized wave transmission," *Phys. Rev. Lett.*, **62**, 147-150 (1988).

Ziolkowski, R. W., "Localized transmission of electro-magnetic energy," *Phys. Rev. A*, **39**, 2005-2032 (1989).

Ziolkowski, R. W., & Lewis, D. K., "Verification of localized wave transmission effect," *J. Appl. Phys.*, **68**, 6083-6086 (1990).

Ziolkowski, R. W., "Localized wave physics and engineering," *Phys. Rev. A*, **44**, 3960-3984 (1991).

Ziolkowski, R. W., "Exact solutions of the wave equation with complex source locations," *J. Math. Phys.*, **26**, 861-865, (1985).

Appendix A: HP 9000 Controller Code

```
1     REAL Datum(1:512)
2     REAL Receiver(1:512)
3     INTEGER Receiver_i(1:512)
5     Zz=0
6     X=00
7     Y=00
8     Z=00
42    REAL C
43    INTEGER Errorcount
44    Errorcount=0
45    Cha_range=1.0
47    C=1500 ! SPEED OF SOUND IN WATER
48    DIM Stepmove$[2] BUFFER
49    ASSIGN @Stepper TO 714
50    ASSIGN @Stepresp TO BUFFER Stepmove
51    ASSIGN @Digitizer TO 704
53    CLEAR SCREEN
54    GOSUB 2000
55    ON ERROR GOSUB 20000
90    PRINT
91    PRINT
100   PRINT "WHAT KIND OF TEST DO YOU WANT TO DO"
110   PRINT "     1) RF PULSE WITH TRANSDUCER POSITION"
120   PRINT "     2) WAVEFORM WITH MULTI-POSITION AND DATA CAPTURE"
125   PRINT "     3) CONTINUOUS WAVE WITH TRANSDUCER POSITION"
126   PRINT "     4) LOCATE ZY HIGH POINT AS TRANSDUCER ORIGIN"
130   INPUT Choice
140   IF Choice<1 OR Choice>4 THEN
150     PRINT
151     PRINT "YOU HAVE ENTERED THE WRONG CHOICE"
152     PRINT "TRY AGAIN"
153     PRINT
154     GOTO 100
155   END IF
160   ON Choice GOSUB 10000,11000,12000,13000
170   REM NOW PROGRAM IS COMPLETE,
180   REM END
190   PRINT
191   PRINT TABXY(1,18),"************** PROGRAM NOW COMPLETE ***************"
192   PRINT "NUMBER OF ERRORS ENCOUNTERED DURING EXECUTION: ";Errorcount;"."
194   STOP
1000  REM ***********************************************
1001  REM OUTPUT ROUTINE FOR POSITIONING STEPPER MOTOR
1002  REM PASS X FOR MOVEMENT TO ABSOLUTE XE
1003  REM PASS Y FOR ABSOLUTE YO
1004  REM PASS Z FOR ABSOLUTE ZO
1010  REM ADDRESS IS 714
1011  REM
1013  REM ***********************************************
1014  GOSUB 16000  ! TURN ON MOTOR
1040  OUTPUT 714;"PW"&VAL$(X)  ! X IN UNITS
1060  OUTPUT 714;"PY"&VAL$(Y)  ! Y IN UNITS
1080  OUTPUT 714;"PZ"&VAL$(Z)  ! Z IN UNITS
1083  REM
1084  REM NOW WAIT FOR MOVEMENT TO STOP
1085  OUTPUT @Stepper;"FS01"
1086  OUTPUT @Stepper;"?"
1087  TRANSFER @Stepper TO @Stepresp
1088  WAIT FOR EOT @Stepper@
1089  IF Stepmove$<>"0@" THEN 1085 ! WAIT UNTIL MOTOR HAS STOPPED
1090  OUTPUT @Stepper;"FS01"
1093  GOSUB 13435  ! TURN OFF MOTOR
1094  RETURN 3
1100  REM
2000  REM ***********************************************
```

```
2001  REM SUBROUTINE TO RESET STEPPER MOTOR CONTROLLER
2010  REM SETS STEP RATE AT 500 STEPS PER SECOND
2011  REM ***********************************************
2012  REM
2020  OUTPUT 714;"AZ"
2030  OUTPUT 714;"AY"
2035  OUTPUT 714;"AW"

2040  OUTPUT 714;"RZ500"
2050  OUTPUT 714;"RY500"
2055  OUTPUT 714;"RW500"
2060  RETURN
2070  REM
3000  REM ***********************************************
3001  REM POSITION THE DISTANCE BETWEEN TRANSDUCERS
3002  REM THIS IS THE X AXIS
3010  REM ***********************************************
3020  INPUT "ENTER THE DISTANCE BETWEEN TRANSDUCERS IN CENTIMETERS ( <50 )",X
3021  IF X>50 THEN
3022    PRINT
3023    PRINT "PARAMETER OUT OF RANGE"
3025    PRINT "TRY AGAIN"
3027    GOTO 3020
3028  END IF
3029  Zz=X/100   ! OBSERVATION Z CO-ORDINATE
3030  INPUT "ENTER HOLDOFF BEFORE THE START OF RECEPTION (cm)",Ho
3032  Holdoff=Ho/100/C+Extrahold  ! HOLD OFF DELAY IN SECONDS"
3033  X=-INT(X*20000+.5)/10
3034  GOSUB 1000
3040  RETURN
4000  REM *****************************************************
4010  REM SET UP HP 5180A WAVEFORM RECORDER
4020  REM THIS WILL BE SET UP TO TAKE 'SAMPLES' NUMBER OF SAMPLES
4030  REM SPACED AT 1/'DFREQ' APARTK
4040  REM CHANEL A WILL BE SELECTED IN dc COUPLING
4050  REM BLOCK ONE WILL BE EXCLUSIVE MEMORY LOCATIONR
4060  REM BLOCK SIZE WILL BE SET AT 'SAMPLES'
4070  REM THE XYZ DISPLAY WILL BE ENABLED AS WELL IF A SCOPE IS
4080  REM TO BE CONNECTED TO THE WAVEFORM ANALYSER
4081  REM TRIGGER IS SET TO BE EXTERNAL FALLING EDGE
4082  REM TRIGGER LEVEL IS SET AT 2 VOLTS WITH 100mV HYSTERISIS
4090  REM POSITION OF TRIGGER WILL BE SET AT 'HOLDOFF'
4100  REM LOCATION OF HP5180A IS AT HPIB LOCATION 4
4101  REM VARIABLES (DFREQ,HOLDOFF,SAMPLES)
4110  REM ***********************************************
4120  REM
4130  REM SELECT CHANNEL
4140  OUTPUT 704;"CH2 "
4150  REM SELECT CHANNEL A RANGE (NOW SET TO 1)
4160  OUTPUT 704;"BR ",Cha_range
4165  REM SELECT dc COUPLING FOR CHANNEL A
4166  OUTPUT 704;"BC0 "
4170  REM SELECT CHANNEL OFFSET (NOW SET TO ZERO)
4180  OUTPUT 704;"BO ",
4190  REM SELECT SWEEP MODE TO SINGLE SWEEP
4200  OUTPUT 704;"SA1 "
4210  REM SELECT EXTERNAL SOURCE TRIGGER (VIA TRIGGER INPUT)
4220  OUTPUT 704;"SE1 "
4230  REM SELECT POSITION OF TRIGGER AS SO MANY SECONDSN
4240  OUTPUT 704;"PT",Holdoff
4250  REM TIME BASE SELECT AS 1/DFREQ SECONDS BETWEEN SAMPLES
4260  OUTPUT 704;"MM ",1/Dfreq
4270  REM SPECIFY MEMORY RECORD LENGTH 'SAMPLES'
4280  OUTPUT 704;"LE ",Samples
4290  REM SELECT INTERNAL 20 MhZ CLOCK RATE
4300  OUTPUT 704;"TE0 "
4301  REM SELECT TRIGGER LEVEL AS 2 VOLTS
4302  OUTPUT 704;"LV ",2
4303  REM SELECT FALLING EDGE TRIGGERO
```

```
4304  OUTPUT 704;"SLO "
4310  REM END THIS SUBROUTINE
4320  RETURN
7000  REM ******************************
7010  REM ANALYSE DATA
7020  REM ******************************
7030  REM
7032  FOR Iiii=1 TO Samples
7033    Receiver(Iiii)=Receiver(Iiii)+Datum(Iiii)
7047  NEXT Iiii
7048  RETURN i
9000  REM ********************************************
9010  REM THIS SUB TELLS WAVETEK TO TURN OFF
9020  REM ********************************************
9030  OUTPUT 709;"POI"
9040  RETURN 7
10000 REM ********************************************
10010 REM THIS SUB SETS UP WAVETEK FOR AN RF PULSE
10020 REM YOU SELECT THE FREQUENCY AND NUMBER OF CYCLESA
10030 REM ********************************************
10035 REM SEND INITIALIZING ARRAY
10040 OUTPUT 709;"A10 B3 D0 G0 Y4000 I"
10050 CLEAR SCREEN
10060 PRINT
10061 PRINT "DO YOU WISH TO SEND..."
10062 PRINT "   1) ARBITRARY"
10063 PRINT "   2) CONTINUOUS WAVE"
10064 PRINT
10065 INPUT Aaa
10066 IF Aaa>2 OR Aaa<1 THEN
10067   PRINT "ERROR: WRONG CHOICE"
10068   PRINT "TRY AGAIN..."
10069   PRINT
10070   GOTO 10061
10071 END IF
10072 SELECT Aaa
10073 CASE =2
10075   INPUT "INPUT THE WAVE FREQUENCY IN HZ (10mHz - 12MHz).",Freq
10076   IF Freq<1.0E-2 OR Freq>1.2E+7 THEN
10077     PRINT
10078     PRINT "FREQUENCY OUT OF RANGE!!!"
10079     PRINT "TRY AGAIN"
10080     PRINT
10081     GOTO 10075
10082   END IF
10090   INPUT "INPUT THE NUMBER OF CYCLES",Cycles
10091   IF Cycles<1 THEN
10092     PRINT
10093     PRINT "PARAMETER OUT OF RANGE, TRY AGAIN"
10094     PRINT
10095     GOTO 10090
10096   END IF
10110   PRINT "INPUT THE FUNCTION TYPE",
10120   PRINT "    0) SINE"
10130   PRINT "    1) TRIANGLE"
10140   PRINT "    2) SQUARE"
10141   PRINT "    3) SQUARE COMPLEMENT"
10150   PRINT
10160   INPUT Function
10170   IF Function>3 OR Function<0 THEN
10171     PRINT
10180     PRINT "WRONG RESPONSE, TRY AGAIN"
10190     PRINT
10200     GOTO 10110
10210   END IF
10230   PRINT
10240   PRINT "YOU WANT THE FOLLOWING BURST CHARACTERISTICS"
10250   PRINT "   A) FREQUENCY: ";Freq;" HZ."
10260   PRINT "   B) CYCLES: ";Cycles;"."
```

```
10270   IF Function=0 THEN A$="SINE"
10280   IF Function=1 THEN A$="TRIANGLE"
10290   IF Function=2 THEN A$="SQUARE"
10291   IF Function=3 THEN A$="SQUARE COMPLEMENT"
10300   PRINT "   C) FUNCTION: ";A$;"."
10310   PRINT
10320   INPUT "CORRECT [Y/N]",Yes$
10330   IF Yes$="N" OR Yes$="n" OR Yes$="no" OR Yes$="NO" THEN ,
10340     PRINT
10350     GOTO 10050
10360   END IF
10370   REM
10371   OUTPUT 709;"C",Function," F",Freq," R",Cycles," I "
10372   OUTPUT 709;"P1 I 'SETUP COMPLETE'"
10373   REM
10374   REM
10375   REM
10377 CASE =1
10378   PRINT "SELECT THE TYPE OF BURST..."
10379   PRINT "   1) SINC"
10380   PRINT "   2) GAUSSIAN"
10381   PRINT
10382   INPUT Bbb
10383   IF Bbb<1 OR Bbb>2 THEN
10384     PRINT "ERROR:  WRONG CHOICE"
10385     PRINT "TRY AGAIN"
10386     PRINT
10387     GOTO 10378
10388   END IF
10389   REM
10390   CLEAR SCREEN
10391   SELECT Bbb
10392   CASE =1
10393     REM SINC PULSE
10394     INPUT "ENTER THE MAXIMUM FREQUENCY IN THE SINC SPECTRUM",F0
10395     REM WE WILL HAVE 16 SAMPLES PER BUMP
10396     REM THUS THE MAXIMUM TIME SAMPLES ON EITHER SIDE
10397     REM OF ZERO IS 1024 / (32 * F0)
10398     REM AND THE SAMPLING FREQUENCY IS 32 * F0
10400     Ssamp=2048
10402     REM Sfreq=32*F0
10403     Sfreq=2.E+6       ! THIS IS FOR LARGE SINC SPECTRUMS
10405     IF (1/Sfreq)<2.67E-7 OR (1/Sfreq)>267 THEN
10406       PRINT "ERROR SINC FREQUENCY OUT OF RANGE"
10407       PRINT "TRY AGAIN"
10408       PRINT
10409       GOTO 10394
10410     END IF
10411     REM
10412     Tau=Ssamp/(Sfreq*2)
10417     REM
10418     REM LOAD SINC INTO WAVETEK
10419     GOSUB 22000
10420     PRINT "TOTAL SINC BURST IS ";2*Tau;" SECONDS."
10421     PRINT
10422     WAIT 3
10424   CASE =2
10425     REM GAUSSIAN PULSE
10426     REM
10427     INPUT "ENTER THE WIDTH IN ms OF THE GAUSSIAN PULSE",Bwidth
10430     Bwidth=Bwidth/1000
10440     Sfreq=1.E+6
10450     Ssamp=Sfreq*Bwidth
10460     IF Ssamp>2047 OR Ssamp<10 THEN
10470       PRINT "ERROR, WAVETEK SAMPLES OUT OF RANGE ";Ssamp;"."
10480       PRINT "ENTER THE PULSE WIDTH AGAIN"
10490       GOTO 10425
10500     END IF
10510     Rho=0F
```

```
10520      T0=-Bwidth/2
10530      Tau1=.5*Bwidth/SQRT(-LOG(.001))
10540      Tau2=1
10550      GOSUB 18000! LOAD INITIALIZING WAVEFORM ONTO WAVETEK
10600    END SELECT
10602  END SELECT
10604  REM SET UP DIGITIZER
10606  Holdoff=0
10608  Dfreq=1.E+6
10628  GOSUB 23000    ! FIX THE SAMPLING FREQUENCY OF DIGITIZER
10632  REM
10634  REM NOW ONTO THE SENDING OF THE BURST
10636  REM
10638  REM SET DISTANCE BETWEEN TRANSDUCERS
10640  GOSUB 3000
10641  GOSUB 4000     !SET UP DIGITIZER
10643  REM NOW WAIT FOR SETUP OF EQUIPMENT
10644  CLEAR SCREEN
10650  INPUT "NOW SET UP EQUIPMENT AND PRESS ENTER TO SEND BURST",Aaa$
10652  REM
10653  REM OUTPUT 709;"K0 P1 I"
10654  OUTPUT 709;"P1 I"
10656  OUTPUT 704;"LO ",1
10657  OUTPUT 704;"SA4"
10658  WAIT 1
10660  OUTPUT 709;"J"
10662  REM
10664  INPUT "DO YOU WISH TO SEND THE PULSE AGAIN",Aaa$
10666  IF Aaa$="n" OR Aaa$="N" THEN
10668    GOSUB 17000     !RESET TRANSDUCER POSITION,
10670    GOSUB 9000     !TURN OFF WAVETEK
10672    GOTO 10701
10674  ELSE
10676    INPUT "DO YOU WISH TO CHANGE THE DIGITIZER VALUES",Aaa$"
10678    IF Aaa$="" OR Aaa$="y" OR Aaa$="Y" THEN
10680      INPUT "ENTER RANGE IN VOLTS",Vv"
10682      OUTPUT 704;"AR ",Vv
10683      GOSUB 23000    ! CHANGE THE NUMBER OF SAMPLES
10684      OUTPUT 704;"LE ",Samples
10685      INPUT "ENTER HOLDOFF BEFORE THE START OF RECEPTION (cm)",Ho
10687      Holdoff=Ho/100/C+Extrahold! HOLD OFF DELAY IN SECONDS
10690      OUTPUT 704;"PT",Holdoff
10697    END IF
10698    GOTO 10644
10699  END IF
10700  REM
10701  REM NOW GET DATA FROM DIGITIZER
10702  INPUT "DO YOU WISH TO SAVE THE CAPTURED DATA",Aaa$
10703  IF Aaa$="y" OR Aaa$="Y" THEN
10704    REM HAUL DATA FROM DIGITIZER
10705    REM
10706    INPUT "ENTER THE NUMBER OF AVERAGES",Weight,
10707    REM ******************
10708    REM PUT AVERAGING IN HERE
10709    REM ******************
10710    FOR Flagaverage=1 TO Weight
10711      REM SET UP WAVETEK AND DIGITIZER
10712      OUTPUT 709;"K0 P1 I"
10713      OUTPUT 704;"LO ",1
10714      OUTPUT 704;"SA4"
10715      WAIT 1
10716      OUTPUT 709;"J"
10717      WAIT 1
10718      REM
10719      INPUT "IS THIS A GOOD SAMPLE",Yes$
10720      IF Yes$="Y" OR Yes$="y" THEN ,
10722        REM NOW GET DATA FROM THE DIGITIZER
10723        GOSUB 19000                    !GET DATA
10724        GOSUB 7000
```

```
10725     ELSE
10726       Flagaverage=Flagaverage-1
10727     END IF
10729   NEXT Flagaverage
10730   Integer_scale=32766/512/Weight
10733   GOSUB 25000l
10744   Recs=INT(3*Samples+.5)
10745   INPUT "ENTER THE NAME OF THE FILE YOU WISH TO SAVE",File$"
10746   CREATE File$,Recs
10747   IF ERRL(10746)=1 THEN
10748     INPUT "DATA FILE EXISTS, DO YOU WISH TO REPLACE IT?",Yes$
10749     IF Yes$="Y" OR Yes$="y" THEN
10750       PURGE File$
10751       CLEAR ERROR
10752       CREATE File$,Recs
10753     ELSE
10754       PRINT "YOU STUPID!!!! USE ANOTHER FILE NAME"
10755       GOTO 10745
10756     END IF
10757   END IF
10758   ASSIGN @Datafile TO File$
10760   OUTPUT @Datafile;Receiver_i(*)
10762   OUTPUT @Datafile;"    ********  THIS IS THE END OF THE FILE ********"
10763 END IF
10764 REM    SUBROUTINE NOW COMPLETE
10765 RETURN
11000 REM *********************************
11002 REM OUTPUT AN ARBITRARY BURST
11004 REM *********************************
11006 REM
11008 INTEGER Amplit
11009 REAL Tolfactor
11010 Tolfactor=1
11012 Amplit=10
11013 INPUT "ENTER THE NAME OF THE FILE",File$
11014 CREATE ASCII File$,1
11016 IF ERRL(11014)=1 THEN
11018   INPUT "DATA FILE EXISTS, DO YOU WISH TO REPLACE IT?",Yes$
11020   IF Yes$="Y" OR Yes$="y" THEN
11022     PURGE File$
11024     CLEAR ERROR
11026   ELSE
11028     PRINT "YOU STUPID!!!! COPY YOUR FILE YOU DUMMY"
11030     PRINT "PROGRAM TERMINATED"
11032     STOP
11034   END IF
11036 ELSE
11038   PURGE File$
11040 END IF
11042 CLEAR SCREEN
11044 PRINT "WHAT WAVEFORM DO YOU WISH TO PROCESS?"
11046 PRINT "     1) CONTINUOUS WAVE"
11048 PRINT "     2) PULSED ARBITRARY WAVE"
11050 INPUT Poa
11052 Poa=INT(Poa)
11054 IF Poa<1 OR Aaa>2 THEN
11056   PRINT
11058   PRINT "INVALID RESPONSE"
11060   PRINT "TRY AGAIN"
11062   GOTO 11044
11064 END IF
11066 IF Poa=2 THEN PRINT "ARBITRARY WAVEFORM IS AN MPS PULSE"
11068 SELECT Poa
11070 CASE =1
11072   REM CONTINUOUS WAVE INSTRUCTIONS
11074   INPUT "CHECK THAT HP TRIG IN GOES TO WAVETEK 'MAIN SYNC OUT'",Aaa$
11076   REM SET UP WAVETEK
11078   OUTPUT 709;"A",Amplit,"B3 D0 Y4000 C0 I"
11080   INPUT "INPUT THE CW FREQUENCY (RANGE 10E-3 < f < 1.5E5 Hz)",Wfreq
```

```
11082   IF Wfreq<1.0E-2 OR Wfreq>1.5E+5 THEN
11084     PRINT
11086     PRINT "WAVETEK FREQUENCY OUT OF RANGE ERROR"
11088     PRINT "INPUT FREQUENCY IN CORRECT RANGE"
11090     GOTO 11080
11092   END IF
11094   Msdcheck=1.0E-2
11096   Flag2=1
11098   WHILE Flag2=1
11100     Msd=Wfreq/Msdcheck
11102     IF Msd>=10 THEN
11104       Msdcheck=Msdcheck*10
11106     ELSE
11108       Flag2=0
11110     END IF
11112   END WHILE
11114   SELECT Msd
11116   CASE 5 TO 10
11118     Msd=5
11120   CASE 2 TO 4.99999999999999
11122     Msd=2
11124   CASE 1 TO 1.99999999999999
11126     Msd=1
11128   END SELECT
11130   Wfreq=Msdcheck*Msd
11132   PRINT "YOUR SELECTED FREQUENCY HAS BEEN ALTERED TO ";Wfreq;"Hz."
11134   OUTPUT 709;"PO F",Wfreq,"I"
11136   INTEGER Ncycle
11138   INTEGER Tcycle
11140   INTEGER Preamble
11142   INPUT "ENTER THE NUMBER OF CYCLES YOU WISH TO SAMPLE",Ncycle
11144   IF Ncycle<1 OR Ncycle>5 THEN
11146     PRINT "NUMBER OF CYCLES OUT OF RANGE"
11148     PRINT "USE THE RANGE [1,5]"
11150     GOTO 11142
11152   END IF
11154   INPUT "ENTER THE PREAMBLE CYCLES",Preamble
11156   INPUT "ENTER THE TOTAL NUMBER OF CYCLES",Tcycle
11158   IF Tcycle<(Ncycle+Preamble) THEN
11160     PRINT "ERROR:  YOU MUST ENTER A NUMBER GREATER THEN";Ncycle+Preamble
11162     GOTO 11154
11164   END IF
11166   OUTPUT 709;"R",Tcycle
11168   Extrahold=Preamble/Wfreq
11170   Btime=Ncycle/Wfreq          !  SAMPLE NCYCLE CYCLES
11172   Dfreq=100*Wfreq
11174 CASE =2
11176   INPUT "CHECK THAT HP TRIG IN GOES TO WAVETEK 'ARB SYNC OUT'",Aaa$
11178   REM BURST PARAMETERS
11180   REM
11182   REM CALCULATE WAVETEK PARAMETERS
11183   REM $$$$$$$$$$$$$$$$$$$$$$$$$$$$$$$$$$$$$$$$$$$$$$$$$$$$
11184   REM $$$$$$$$$$$$$$$$$$$$$$$$$$$$$$$$$$$$$$$$$$$$$$$$$$$$
11185   REM $$$   CHANGE ARBITRARY HP PARAMS HERE   $$$
11186   REM $$$$$$$$$$$$$$$$$$$$$$$$$$$$$$$$$$$$$$$$$$$$$$$$$$$$
11187   REM $$$$$$$$$$$$$$$$$$$$$$$$$$$$$$$$$$$$$$$$$$$$$$$$$$$$
11190   Extrahold=0
11191   Ssamp=200
11192   Sfreq=2.E+6
11193   Rho=0
11194   REM
11196   Btime=Ssamp/Sfreq
11198   Dfreq=1.E+6
11200 END SELECT
11202 REM NOW SET UP THE WAVEFORM RECORDER
11204 Sampletime=Btime*2.0
11208 Shortsamples=Dfreq*Sampletime
11210 Samples=2^(INT(LGT(Shortsamples)/LGT(2)+1))
11212 IF Samples<512 THEN Samples=512)
```

```
11214 PRINT "NUMBER OF SAMPLES WILL BE ";Samples;"."
11215 PRINT "REMEMBER TO CHANGE THE DIMENSIONING OF DATUM AND RECEIVER"
11216 PRINT "TO RELECT THIS NUMBER"
11218 WAIT 2
11219 REM NOW GET READY FOR CALIBRATION
11220 CLEAR SCREEN
11222 PRINT "YOU MAY NOW CALIBRATE YOUR RECEIVER PRE-AMP"
11224 PRINT "AND TRANSMITTER  POWER AMP POWER SETTINGS."
11226 PRINT "YOU CAN NOW ENTER THE TRANSDUCER SEPARATION FOR YOUR CALIBRATION"
11228 GOSUB 3000       ! POSITION X
11231 IF Poa=2 THEN
11232   Rn=Zz
11235   GOSUB 21000       !LOAD INITIALIZING WAVEFORM ONTO WAVETEK
11236 END IF
11239 GOSUB 4000
11240 OUTPUT 709;"K0 P1 I"         ! SET ARB ADDRESS TO 0
11241 OUTPUT 704;"LO ",1     ! SET THE LOCATION TO SEGMENT 1
11242 OUTPUT 704;"SA4"
11243 WAIT 1
11244 OUTPUT 709;"J"
11245 WAIT 1
11246 Weight=1
11248 GOSUB 19000    !GET MEAN AND VARIANCE
11249 CLEAR SCREEN
11250 PRINT "THE MEAN IS ";Meany
11251 PRINT "THE VARIANCE IS ";VaryV
11252 Vartol=VaryV
11254 INPUT "DO YOU WISH TO RE-SEND THE BURST FOR NEW CALIBRATION [Y/N].",Yes$
11255 IF Yes$="Y" OR Yes$="y" OR Yes$="YES" OR Yes$="yes" OR Yes$="Yes" OR Yes$="" THEN
11256   REM PRINT "THE WAVETEK AMPLITUDE IS SET FOR";Amplit;"V PEAK TO PEAK"
11257   PRINT "THE DIGITIZER IS SET FOR";Cha_range;"V PEAK TO PEAK"
11258   INPUT "DO YOU WISH TO CHANGE THIS",Yes2$
11259   IF Yes2$="Y" OR Yes2$="y" OR Yes2$="YES" OR Yes2$="yes" OR Yes2$="Yes" THEN
11260     REM INPUT "ENTER THE AMPLITUDE BETWEEN 1 AND 10",AmplitR
11261     INPUT "ENTER THE PEAK RANGE IN VOLTS",Cha_range"
11262     REM IF Amplit<1 OR Amplit>10 THENL
11263     REM   PRINT "INVALID RESPONSE, TRY AGAIN"
11264     REM   GOTO 11256
11265     REM END IF
11266     REM OUTPUT 709;"A",Amplit
11267     GOSUB 4000
11269   END IF
11270   GOTO 11240
11272 END IF
11274 REM
11275 REM SET THE VARIANCE TOLERANCE
11276 REM
11277 INPUT "ENTER THE TOLERANCE FACTOR FOR SEQUENCE REJECTION",Tolfactor"
11280 REM NOW ONTO THE TEST
11281 REM WE MUST NOW ASK QUESTIONS
11282 REM ABOUT THE SIZE OF THE ARRAY
11283 REM
11284 CLEAR SCREEN
11286 REM PRINT "YOU WILL NOW BE ASKED QUESTIONS "
11288 REM PRINT "ABOUT THE SIZE OF THE RECEIVING ARRAY "
11290 REM PRINT "THIS ARRAY WILL BE ROUND "I
11292 REM PRINT
11294 REM INTEGER Rside
11296 INTEGER Tsides
11298 REM INPUT "ENTER THE NUMBER OF TRANSDUCERS ALONG A RADIUS",Rside
11300 REM INPUT "ENTER THE SPACING BETWEEN TRANDUCERS (cm)",Rspace
11302 REM IF Rside*Rspace>45 THEN
11304 REM PRINT "ERROR:  YOU HAVE TOO MANY TRANSDUCERS OR TO A TOO LARGE SPACING"
11306 REM PRINT "RE-ENTER THE RECEIVER VALUES."
11308 REM GOTO 11298
11310 REM END IF
11322 REM PRINTF
11324 PRINT "YOU WILL NOW BE ASKED ABOUT THE TRANSMITTING ARRAY"
11326 INPUT "ENTER THE NUMBER OF TRANSDUCERS ALONG A RADIUS",Tside
```

```
11328 INPUT "ENTER THE DISTANCE BETWEEN TRANSDUCERS (cm)",Tspace
11331 IF Tside*Tspace>45 THEN
11332   PRINT "ERROR:  YOU HAVE TOO MANY TRANSDUCERS OR TO A TOO LARGE SPACING"G
11334   PRINT "RE-ENTER THE TRANSMITTER VALUES."
11336   GOTO 11322
11338 END IF
11340 CLEAR SCREEN
11341 REM Rspace=Rspace/100
11342 REM DELETE THIS NEXT LINE IF YOU WANT MORE THAN ONE RECEIVER IN ARRAy
11343 Rspace=0
11344 Rside=0
11346 Tspace=Tspace/100
11347 PRINT "YOU HAVE ENTERED THE FOLLOWING ARRAY PARAMETERS..."
11348 PRINT
11349 REM PRINT "RECEIVING ARRAY:"
11350 REM PRINT "   A) TRANSDUCERS ALONG RADIUS: ";Rside
11351 REM PRINT "   B) ELEMENT SPACING: ";Rspace;"m."
11354 REM PRINT
11356 PRINT "TRANSMITTING ARRAY"
11358 PRINT "   D) TRANSDUCERS ALONG SIDE: ";Tside
11360 PRINT "   E) ELEMENT SPACING: ";Tspace;"m."
11362 INPUT "IS THIS CORRECT [Y/n]",Aaa$
11364 IF Aaa$[1;1]="N" OR Aaa$[1;1]="n" THEN 11284
11366 GOSUB 9000      !TURN OFF WAVETEK
11368 REM
11370 CLEAR SCREEN
11375 Numtest=Tside
11376 CLEAR SCREEN
11381 PRINT "THERE WILL BE";Numtest;"POINTS TO PROCESS."
11382 REM
11383 REM BATTERY OF TESTS
11384 REM
11386 Recs=INT(3.5*Samples*Tside+.5)
11388 CREATE File$,Recs
11390 ASSIGN @Datafile TO File$;FORMAT OFF
11392 INPUT "ENTER THE NUMBER OF AVERAGES",Weight
11393 Integer_scale=32766/512/Weight
11395 Badcount=0
11396 Badaver=0
11398 REM ************************************
11399 REM THIS IS WHERE THE OUTER LOOP STARTED
11400 REM ************************************
11401 REM FOR Rr=0 TO (Rside-1)*Rspace STEP Rspace
11402 REM
11403 REM I HAVE ARBITRARILY CHOSEN THE OBSERVATION RHO CO-ORDINATE
11404 REM AS BEING IN THE OBSERVATION X DIRECTION
11405 REM THIS IS JUST THE CONVENTION FOR THIS EXPERIMENT
11406 REM SO IF SOURCE=(x',y',z') AND OBSERVATION=(x,y,z)
11407 REM THEN RR=SQRT(x^2+y^2)'
11408 REM OUR z IS ACTUALLY Zz
11409 REM      z' SET AT ORIGIN 0
11410 REM y = 0 AND x=Rr=RHO
11411 REM x', y' = Xx,Yy
11412 REM ALSO Rn CAN BA CALCULATED AS SQRT((x-x')^2+(y-y')^2+(z-z')^2)
11413 REM WE WILL BE CALCULATING Rn AS
11414 REM AN APPROXIMATE AT THE OBSERVATION RHO
11415 REM EQUAL TO ZERO.  IN THIS WAY
11416 REM THE WAVE WILL BE THE SAME
11417 REM REGARDLESS OF THE OBSERVATION CO-ORDINATES
11418 REM SO Rn=SQRT(Xx^2+Yy^2+Zz^2)
11419 FOR Xx=0 TO Tspace*Tside STEP Tspace
11420   REM CALCULATE RHO HERE AND OUTPUT MPS
11421   REM THE NEXT LINE SHOULD CHANGE YY=0 TO XX FOR SQUARE ARRAY)
11422   REM OTHER WISE ROUND ARRAY
11423   REM ****************************************
11424   REM THIS IS WHERE THE EXTRA LOOP STARTED BEFORE
11425   REM ****************************************
11426   REM FOR Yy=0 TO 0 STEP Tspace
11427   REM
```

```
11428   REM NOTE THAT SINCE x IS ARBITRARILY CHOSEN
11429   REM AS THE DIRECTION ON WHICH THE
11430   REM OBSERVATION RHO WILL LIE
11431   REM THEN THERE IS SYMMETRY ABOUT THE
11432   REM x,x' AXIS FOR THE SQUARE ARRAY
11433   REM SO WE NEED ONLY GO FROM 0 TO Yymax ON THE
11434   REM TRANSMITTER SIDE
11435   REM AND TAKE CARE OF THE REST IN THE DATA PROCESING
11436   REM SECTION
11437   REM
11438   PRINT TABXY(1,3),"PROCESSING FOR RECEIVER SPACE ";Rr;" cm.    "
11439   PRINT TABXY(10,4),"TRANSMITTER X SPACE ";Xx;" cm.    "
11440   PRINT TABXY(10,5),"TRANSMITTER Y SPACE ";Yy;" cm.    "
11441   REM
11442   REM Rn IS THE ABSOLUTE DISTANCE BETWEEN"
11443   REM RECEIVER AND TRANSMITTER AT x,y=0
11444   REM WHICH IS SQRT(x'^2 + y'^2 + (z-z')^2)
11445   Rn=SQRT(Xx^2+Yy^2+Zz^2)
11446   REM
11447   REM MUST CALCULATE THE SOURCE CO-ORDINATEY
11448   REM RHO WHICH IS SIMPLY SQRT((x'^2 + y'^2));
11449   Srho=SQRT(Xx^2+Yy^2)          ! SOURCE CO-ORDINATE RHO
11450   REM
11451   REM dx=TSPACE, dy=TSPACE
11452   REM WE MUST NOW CALCULATE THE RADIAL DISTANCE
11453   REM BETWEEN THE TRANSMITTER AND RECEIVER
11454   REM THE z DISTANCE (VARIABLE X) IS OF COURSE Zz
11455   REM THE PERPENDUCULAR RHO DISTANCE (VARIABLE Z)
11456   REM IS SQRT((x-x')^2+(y-y')^2)
11457   REM WHICH IS SQRT((Rr-Xx)^2+Yy^2)
11458   REM
11459   Trho=SQRT((Rr-Xx)^2+(Yy)^2)
11460   REM
11461   REM SO Trho IS THE PERPENDICULAR DISTANCE BETWEEN TRANSDUCERS"
11462   Z=-INT(2000000*Trho+.5)/10       ! SET STEPPER MOTOR Z DISTANCE
11463   GOSUB 1000                    !  (MOVE AXIS)
11464   GOSUB 4000
11465   GOSUB 21000
11466   REM
11467   REM DETERMINE THE VALUE OF THE VARIANCE FOR THIS EXPERIMENTN
11468   REM
11469   PRINT TABXY(10,9),"DETERMINING THE VARIANCE FOR SAMPLE REJECTION                "
11470   Number_aver=60
11471   Vartol2=0
11472   Flagaverage=10
11473   WHILE Flagaverage<=Number_aver
11474     REM SET UP WAVETEK AND DIGITIZER
11475     OUTPUT 709;"K0 P1 I"
11477     OUTPUT 704;"LO ",1
11478     OUTPUT 704;"SA4"
11479     WAIT 1.5
11480     OUTPUT 709;"J"
11481     WAIT 1
11482     REM
11483     REM NOW GET DATA FROM THE DIGITIZERR
11484     GOSUB 19000                    !GET DATA
11485     PRINT TABXY(10,8),"CURRENT SAMPLED VARIANCE IS";Vary
11486     IF Badsample_aver=1 THEN
11487       Badaver=Badaver+1
11489       PRINT TABXY(1,13),"BAD VARIANCE SAMPLE NUMBER";Badaver;"HAS OCCURED"
11490     ELSE
11491       Vartol2=Vartol2+Vary/Number_aver
11492       Flagaverage=Flagaverage+1
11494     END IF
11495   END WHILE
11496   Vartol=Vartol2
11497   REM
11498   PRINT TABXY(10,9),"VARIANCE FOR THIS AVERAGE SEQUENCE IS";Vartol;"     "
11499   REM RESET THE VALUE OF RECEIVER ARRAY
```

```
11500   REM
11501   FOR Bbb=1 TO Samples
11502     Receiver(Bbb)=0
11503   NEXT Bbb
11504   REM
11505   Flagaverage=1
11506   WHILE Flagaverage<=Weight
11507     PRINT TABXY(10,7),"CURRENT AVERAGE NUMBER IS";Flagaverage
11508     REM SET UP WAVETEK AND DIGITIZER
11509     OUTPUT 709;"K0 P1 I"
11511     OUTPUT 704;"LO ",1
11512     OUTPUT 704;"SA4"
11513     WAIT 2
11514     OUTPUT 709;"J"
11515     WAIT 1
11516     REM
11517     REM NOW GET DATA FROM THE DIGITIZER
11518     GOSUB 19000                        !GET DATA
11519     PRINT TABXY(10,8),"CURRENT SAMPLED VARIANCE IS";Vary
11520     IF Badsample=1 THEN
11521       Badcount=Badcount+1
11522       PRINT TABXY(1,12),"BAD SAMPLE NUMBER";Badcount;"ENCOUNTERED"
11523     ELSE
11524       Flagaverage=Flagaverage+1
11525       GOSUB 7000    ! ADD COLLECTED DATA TO RECEIVER SEQUENCE
11526     END IF
11527   END WHILE
11528   REM *****************************************
11529   REM THIS IS WHERE THE INNER LOOP ENDED BEFORE
11530   REM *****************************************
11531   REM NEXT Yy
11532   REM
11533   REM OUTPUTTING DATA
11534   REM
11535   PRINT TABXY(10,14),"****** OUTPUTTING DATA ********"
11536   GOSUB 25000
11537   OUTPUT @Datafile;Receiver_i(*)
11538   PRINT TABXY(10,14),"                                "
11542 NEXT Xx
11543 REM ****************************************
11544 REM THIS IS WHERE THE OUTER LOOP ENDED
11545 REM ****************************************
11546 REM NEXT Rr
11549 X=0
11550 Y=0
11551 Z=0
11552 GOSUB 1000     ! RESET THE AXIS
11553 GOSUB 9000     ! TURN OFF WAVETEK
11554 RETURN 0
12000 REM ************************************
12005 REM OUTPUTS A CONTINUOUS WAVEFOR*
12010 REM ************************************
12015 REM
12020 OUTPUT 709;"A1 B0 D0 Y4000 I"
12025 CLEAR SCREEN
12030 INPUT "INPUT THE FREQUENCY IN HZ (10mHz - 12MHz)",Sfreq
12035 IF Sfreq<1.0E-2 OR Sfreq>1.2E+7 THEN
12040   PRINT
12045   PRINT "WRONG RESPONSE, TRY ARAIN"
12050   PRINT
12055   GOTO 12030
12060 END IF
12065 PRINT "INPUT THE FUNCTION"
12070 PRINT "   0) SINE"
12075 PRINT "   1) TRIANGLE"
12080 PRINT "   2) SQUARE"
12085 PRINT
12090 INPUT Sfunc
12095 IF Sfunc>2 OR Sfunc<0 THEN
```

```
12100   PRINT "WRONG RESPONSE, TRY AGAIN"
12105   PRINT
12110   GOTO 12065
12115 END IF
12120 PRINT "YOU WANT THE FOLLOWING WAVE CHARACTERISTICS"
12125 PRINT "   A) FREQUENCY: ";Sfreq;" HZ."
12130 IF Sfunc=0 THEN A$="SINE"
12135 IF Sfunc=1 THEN A$="TRIANGLE"
12140 IF Sfunc=2 THEN A$="SQUARE"
12145 PRINT "   B) FUNCTION: ";A$;"."
12150 PRINT
12155 INPUT "CORRECT [Y/N]",Yes$
12160 IF Yes$="N" OR Yes$="n" OR Yes$="no" OR Yes$="NO" THEN
12165   PRINT
12170   GOTO 12025
12175 END IF
12180 REM NOW SET DISTANCE BETWEEN TRANSDUCERS
12185 GOSUB 3000
12190 OUTPUT 709;"C",Sfunc,"F",Sfreq
12195 OUTPUT 709;"P1 I'OUTPUTING WAVE'"
12200 REM NOW WE CAN OBSERVE THE CHARACTERISTICS
12205 REM
12210 CLEAR SCREEN
12215 PRINT "WAVETEK IS NOW OUTPUTTING A ";A$;" WAVE"
12220 INPUT "PRESS ENTER TO TURN OFF WAVE",Aaa$
12225 GOSUB 9000 !TURN OFF WAVETEK
12230 GOSUB 17000 !POSITION BACK TO ZERO
12235 RETURN
13000 REM ************************************
13005 REM LOCATE HIGH ZY AS ORIGIN
13010 REM ************************************
13015 REM
13020 CLEAR SCREEN
13025 Bside=20   ! SIDE OF SQUARE IN mm
13030 Bgap=1     ! DISTANCE BETWEEN MEASUREMENTS
13035 PRINT
13040 PRINT "THERE ARE ";Bside^2/Bgap^2;" POINTS TO PROCESS."
13045 PRINT
13050 REM NOW SET UP WAVETEK AND RECORDER
13055 INPUT "ENTER THE WIDTH IN ms OF THE GAUSSIAN PULSE",Bwidth
13060 Bwidth=Bwidth/1000
13065 Sfreq=1.E+6
13070 Ssamp=Sfreq*Bwidth
13075 IF Ssamp>2047 OR Ssamp<10 THEN
13080   PRINT "ERROR, WAVETEK SAMPLES OUT OF RANGE ";Ssamp;"."
13085   PRINT "ENTER THE PULSE WIDTH AGAIN"
13090   GOTO 13045
13095 END IF
13100 Rho=0
13105 T0=-Bwidth/2
13110 Tau1=.5*Bwidth/SQRT(-LOG(.001))
13115 Tau2=1
13120 GOSUB 18000   ! LOAD INITIALIZING WAVEFORM ONTO WAVETEK"
13125 REM
13130 Dfreq=1.E+6
13135 Sampletime=.00005*1.5
13140 Holdoff=0e
13145 Samples=1.E+6*Sampletime
13150 Samples=2^(INT(LGT(Samples)/LGT(2)+1))
13155 IF Samples<512 THEN Samples=512
13160 GOSUB 4000
13165 Weight=5
13170 Ocount=0
13175 Bhigh=0
13180 Ty=0
13185 Tz=0
13190 FOR Zz=-Bside/2 TO Bside/2 STEP Bgap
13195   Z=Zz*200
13200   FOR Yy=-Bside/2 TO Bside/2 STEP Bgap
```

```
13205     PRINT
13210     Ocount=Ocount+10
13215     PRINT "PROCESSING POINT ";Ocount;"."
13220     PRINT
13225     Y=Yy*200
13230     GOSUB 1000              !    POSITION CONTROLLER
13235     WAIT 10                 !    WAIT UNTIL BEAM HAS STOPPED SHAKING
13240     REM
13245     FOR Flagaverage=1 TO Weight
13250       REM SEND PULSE
13255       REM
13260       REM SET UP WAVETEK AND DIGITIZER
13265       OUTPUT 709;"K0 P1 I"
13270       OUTPUT 704;"LO ",1
13275       OUTPUT 704;"SA4"
13280       WAIT 1
13285       OUTPUT 709;"J"              ! TRIGGER WAVETEKS
13290       REM
13295       REM NOW GET DATA FROM THE DIGITIZERE
13300       GOSUB 19000           !HAUL DATA FROM DIGITIZER
13305     NEXT Flagaverage
13310     REM RECORD HIGH POINT
13315     Phigh=0
13320     FOR I=1 TO 512
13325       IF Datum(I)>Phigh THEN
13330         Phigh=Datum(I)
13335         Location=I
13340       END IF
13345     NEXT I
13350     PRINT
13355     PRINT "HIGH POINT FOR TRIAL ";Ocount;" IS ";Phigh;"."
13360     PRINT "LOCATION FOR HIGH POINT IS ";Location;"."
13365     PRINT
13370     IF Phigh>Bhigh THEN
13375       Bhigh=Phighh
13380       PRINT "NEW HIGH FOR TRIAL ";Ocount;"."
13385       Tz=Z
13390       Ty=Y
13395     END IF
13400   NEXT Yy
13405 NEXT Zz
13410 Z=Tz
13415 Y=Ty
13420 GOSUB 1000      ! MOVE TO ORIGIN
13425 GOSUB 2000      ! RESET TO ORIGIN
13430 RETURN
13435 REM ************************************
15000 REM SHUT OFF THE STEPPER MOTOR DRIVER
15005 REM ************************************
15010 OUTPUT 715;"Q0XM2"
15015 OUTPUT 715;"K5"
15020 OUTPUT 715;"B0"
15025 OUTPUT 715;"OI"
15030 WAIT 3
15035 RETURN
16000 REM ************************************
16005 REM TURN ON THE STEPPER MOTOR DRIVER
16010 REM ************************************
16015 OUTPUT 715;"Q0XM2"
16020 OUTPUT 715;"K5"
16025 OUTPUT 715;"B0"
16030 OUTPUT 715;"CI"
16035 WAIT 3
16040 RETURN
17000 REM ********************************************
17005 REM SEND TRANSDUCER BACK TO ITS ORIGINAL POSITION
17010 REM ********************************************
17015 X=0
17020 Y=0
```

```
17025 Z=0
17030 GOSUB 1000 ! NOW SEND 0,0,0 TO THE CONTROLLER
17035 RETURN
18000 REM ************************************
18005 REM LOOP TO LOAD ARBITRARY WAVEFORM
18010 REM DEFINED FUNCTION IS GAUSS
18015 REM VARIABLES (SSAMP,SFREQ,T0,TAU1,TAU2,RHO)
18020 REM ************************************
18025 REM
18030 OUTPUT 709;"A10 B3 R1 C6 D0 S",1/Sfreq,"Y4001 K0 P1 I 'LOADING WAVEFORM'"
18035 OUTPUT 709;"XB ",0," XH",Ssamp-1," G0 Q0 K0 I"
18040 FOR I=0 TO Ssamp-1
18045   T=T0+I/Sfreq
18050   J=INT(2047*(FNGauss(Rho/Tau2,T/Tau1))+.5)        !FULL SCALE IS 2047
18055   OUTPUT 709;"K",I,"L",J
18060 NEXT I
18065 OUTPUT 709;"K0 M1 I 'GAUSS BURST READY'"
18070 RETURN
19000 REM ************************************
19010 REM CONVERT STRING DATA TO INTGER DATUM
19020 REM CONVERTS TEST$[] INTO DATUM()
19030 REM VARIABLES(TEST$,DATUM,CHARPOINT,ARRAYCOUNT,NUMBER$,FLAG,SAMPLES
19040 REM IF FLAG2=1 THAT MEANS WE MUST BE AT THE BEGINNING OF OUR AVERAGING
19050 REM HENCE WE MUST RESET OUT ARRAY DATUM()
19060 REM WEIGHT IS THE WEIGHTING FACTOR OR NUMBER OF SAMPLES IN AN AVERAGE
19070 REM ************************************
19080 REM
19081 REAL Sumy
19082 REAL Susmsq
19090 Badsample=0
19091 Badsample_aver=0
19100 Sumy=0
19110 Sumysq=0
19120 OUTPUT @Digitizer;"OB ",1
19130 FOR Iii=1 TO Samples
19140   ENTER @Digitizer;Tmp1
19150   Datum(Iii)=Tmp1-512
19160   Sumy=Sumy+Datum(Iii)
19170   Sumysq=Sumysq+Datum(Iii)^2
19180 NEXT Iii
19190 Meany=Sumy/Samples
19200 Vary=Sumysq/Samples-Meany^2
19210 IF (Vary>(Vartol*Tolfactor)) OR (Vary<(Vartol/Tolfactor)) OR (ABS(Meany)>25) THEN
19220   Badsample=1
19230 END IF
19231 IF Vary>Vartol*Tolfactor OR (ABS(Meany)>25) THEN
19232   Badsample_aver=1
19233 END IF
19240 RETURN
20000 REM ***********************
20010 REM      ERROR ROUTINE
20020 REM ***********************
20030 PRINT ERRM$
20040 Errorcount=Errorcount+1
20050 ERROR RETURN
21000 REM ************************************
21010 REM LOOP TO LOAD ARBITRARY WAVEFORM
21020 REM DEFINED FUNCTION IS MPS
21030 REM VARIABLES (SSAMP,SFREQ,T0,RHO)
21040 REM ************************************
21050 REM
21060 REAL Tmp33
21070 REAL Scalefactor
21080 REM WE MUST SCALE THE MPS FOR UNITY AT ITS MAXIMUM POINT
21090 REM WE MUST FIND THE MAXIMUM FOR Scalefactor=ABS(FNMps(t,0,Zz,Zz))
21100 REM FOR RHO = 0
21110 REM USE SCALEFACTOR = -20E-4 FOR AN ESTIMATE OF THE MAXIMUM ONLY
21120 Scalefactor=8.E+4
21130 OUTPUT 709;"XB0 XH",Ssamp-1," G0 Q0"
```

```
21140 OUTPUT 709;"A10 B3 R1 C6 D0 S",1/Sfreq,"Y4001 K0 P1 I 'LOADING WAVEFORM'"
21150 FOR Iii=0 TO Ssamp-1
21160   T=(Iii-Ssamp/2)/Sfreq
21170   Tmp33=FNMps(T,Srho)e
21180   J=INT(2047*(Tmp33/Scalefactor)+.5)        !FULL SCALE IS 2047
21190   OUTPUT 709;"K",Iii,"L",J
21200 NEXT Iii
21210 OUTPUT 709;"K0 M1 I 'MPS BURST READY'"
21220 RETURN 7
22000 REM ***********************************
22010 REM LOOP TO LOAD ARBITRARY WAVEFORM
22020 REM DEFINED FUNCTION IS SINC
22030 REM VARIABLES (SSAMP,SFREQ,TAU,F0)
22040 REM ***********************************
22050 REM
22060 OUTPUT 709;"XB0 XH",Ssamp-1," G0 Q0 I"
22070 OUTPUT 709;"A10 B3 R1 C6 D0 S",1/Sfreq,"Y4001 K0 P1 I 'LOADING WAVEFORM'"
22080 FOR I=0 TO Ssamp-1
22090   T=I/Sfreq
22100   Tmp33=FNSinc(T,F0,Tau)
22110   J=INT(2047*(Tmp33)+.5)        !FULL SCALE IS 2047
22120   OUTPUT 709;"K",I,"L",J
22130 NEXT I
22140 OUTPUT 709;"K0 M1 I 'SINC BURST READY'"
22150 RETURN
23000 REM **************************
23010 REM CHANGE THE SAMPLING FREQUENCY
23020 REM OF DIGITIZER
23030 REM **************************
23040 INPUT "ENTER THE AMOUNT OF TIME YOU WISH TO SAMPLE IN ms",Sampletime
23050 Sampletime=Sampletime/1000
23060 Shortsamples=Sampletime*Dfreq
23070 Samples=2^(INT(LGT(Shortsamples)/LGT(2)+1))
23080 IF Samples<512 THEN Samples=512)
23090 IF Samples>16900 THEN
23100   PRINT "ERROR, TOO MANY SAMPLES."
23110   PRINT "TRY A SMALLER SAMPLE TIME"
23120   PRINT
23130   GOTO 23040
23140 END IF
23150 RETURN
25000 REM ************************************************
25010 REM * CONVERT RECEIVER REAL DATA INTO INTEGERS   ***
25020 REM ************************************************
25030 REM
25040 FOR Ccc=1 TO Samples
25050   Receiver_i(Ccc)=INT(Integer_scale*Receiver(Ccc)+.5)
25060 NEXT Ccc
25070 RETURN
29000 ENDU
30000 REM ************************************
30010 REM DEFINE THE GAUSS PULSE
30020 REM ************************************
30030 DEF FNGauss(R1,T1)
30040   Arbit=-EXP(-T1^2)*EXP(-R1^2)
30050   RETURN Arbit
30060 FNEND
30070   REM ************************************
30080   REM DEFINE THE MPS PULSE
30090   REM ************************************
30100 DEF FNMps(T1,Rho)
30110   REM T1 IS THE TIME ABSOLUTELY
30120   REM RHO IS THE SOURCE (x'^2+y'^2)
30130   REM Oz IS THE OBSERVATION Z CO-ORDINATE
30140   REM Rnn IS SQRT((x-x')^2+(y-y')^2+(z-z')^2)
30150   COMPLEX Eye
30160   REAL Arbit,A,B,Alph,C,Z0,Beta,Zmct,Rphi)
30170   COMPLEX S,Dzs,Dzf,Dts,Dtf,F,Phim
30180   Eye=CMPLX(0,1)
```

```
30190    Z0=4.E-3
30200    C=1.5E+3
30210    A=1.
30220    B=750E
30230    Alph=1
30240    Beta=300
30250    Zmct=(-C*T1)
30260    S=Rho^2/(Z0+Eye*Zmct)-Eye*(Zmct+2*C*T1))
30270    Dts=Eye*(Rho^2/(Z0+Eye*Zmct)^2-1)
30280    Dtf=(-1/Beta*(B+Alph/(S/Beta+A))*Dts+Eye/(Z0+Eye*Zmct))
30290    F=(1/(Z0+Eye*Zmct)*1/((S/Beta)+A)^Alph)*EXP(-B*S/Beta)
30300    Phi=F*(Dtf)
30310    Rphi=REAL(Phi)
30320    RETURN Rphi
30330  FNEND
30340    REM *************************
30350    REM DEFINE SINC
30360    REM ***********************
30370  DEF FNSinc(T,F,T1)
30380    IF T-T1=0 THEN
30390      RETURN 1
30400    ELSE
30410      RETURN SIN(2*PI*(T-T1)*F)/(2*PI*F*(T-T1))
30420    END IF
30430  FNEND
```

Appendix B: Matlab Algorithm for Extraction of Sphere Radius

```
function b=ballsize(spectrum, ff, weight)
%  usage:  b=ballsize(spectrum, ff, weight)
%  This program tries to extract the ball parameters by examining
%  the spectrum of he MPS backscatter.

if nargin~=3,
        error('Number of arguements must be three for ballsize');
end

location=peaks(spectrum, ff, weight);
flag=1;
loc=location;
count=0;
difference=0;

while flag==1,
        olddif=difference;
        count=count+1;
        flag=0;
        difference2=filter([1, -1], 1, location);
        difference=remove(difference2, 1);
        [Y I]=sort(difference);
        median_dip=median(Y);
        size(location);
        ii=0;
        secondflag=1;
        while(ii<max(size(Y)) & secondflag==1),
                ii=ii+1;
                if Y(ii)>1.2*median_dip,
                        secondflag=0;
                        flag=1;
                        location=insert(location, I(ii)+1, location(I(ii))+Y(ii)/2);
                elseif Y(ii)<median_dip/1.2,
                        if I(ii)==1,
                                location=remove(location, I(ii));
                        elseif I(ii)==max(size(Y)),
                                if difference(I(ii))+difference(I(ii)-1)>median_dip,
                                location=remove(location, I(ii)+1);
                                else
                                location=remove(location, I(ii));
                                end
                        else
                                if difference(I(ii)+1)>difference(I(ii)-1),
                                location=remove(location, I(ii));
                                else
                                location=remove(location, I(ii)+1);
                                end
                        end
                        flag=1;
                        secondflag=0;
                end
        end
end

b=7.3717/(mean(difference)/1e4+0.3654);
```

Appendix C
Measured Backscattered Spectra
Plots not included in text

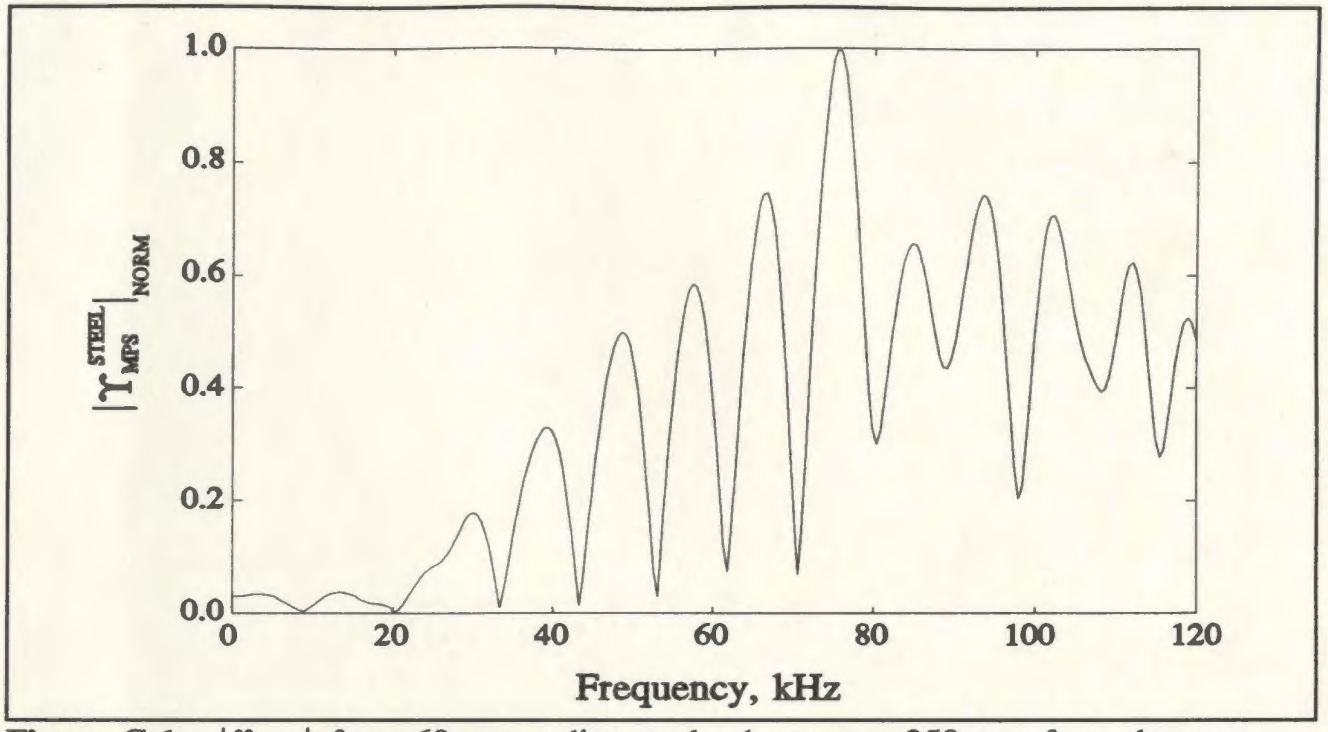

Figure C.1: $|\Upsilon_{MPS}|$ for a 60 mm radius steel sphere at r=250 mm from the array.

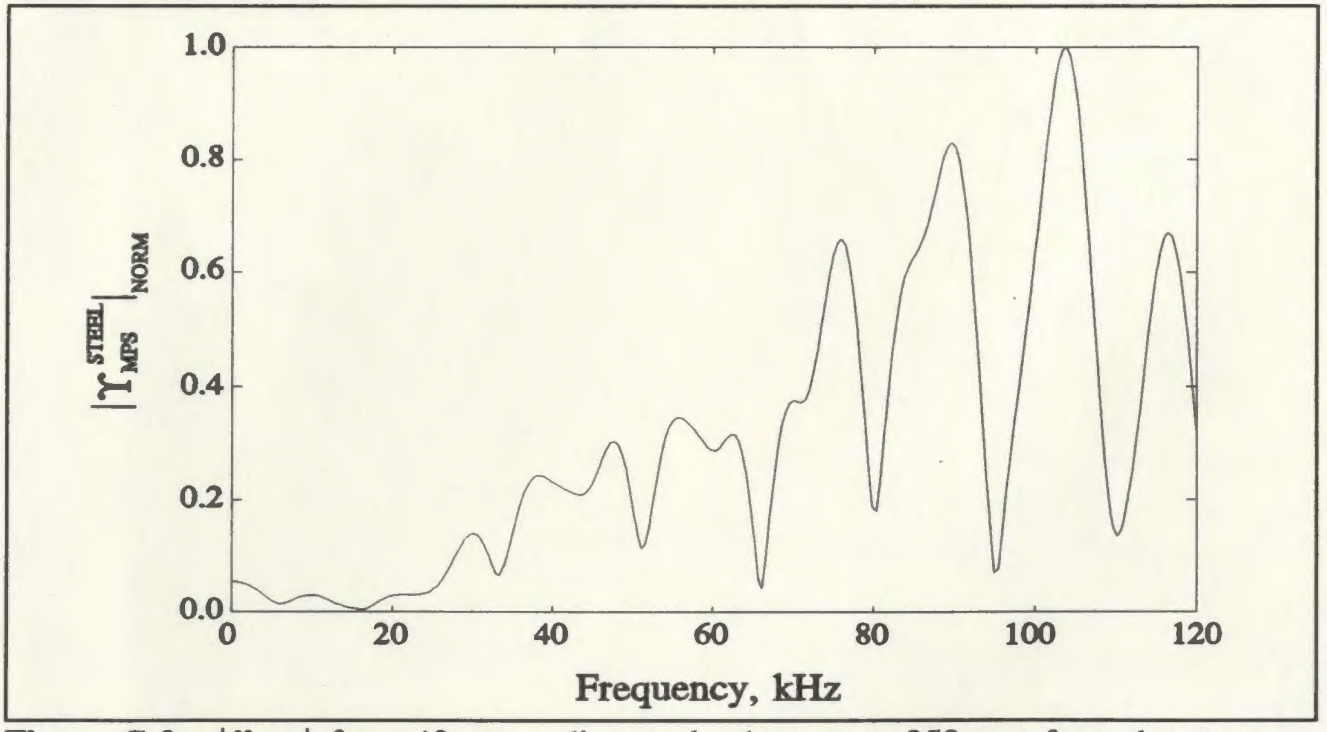

Figure C.2: $|\Upsilon_{MPS}|$ for a 40 mm radius steel sphere at r=250 mm from the array.

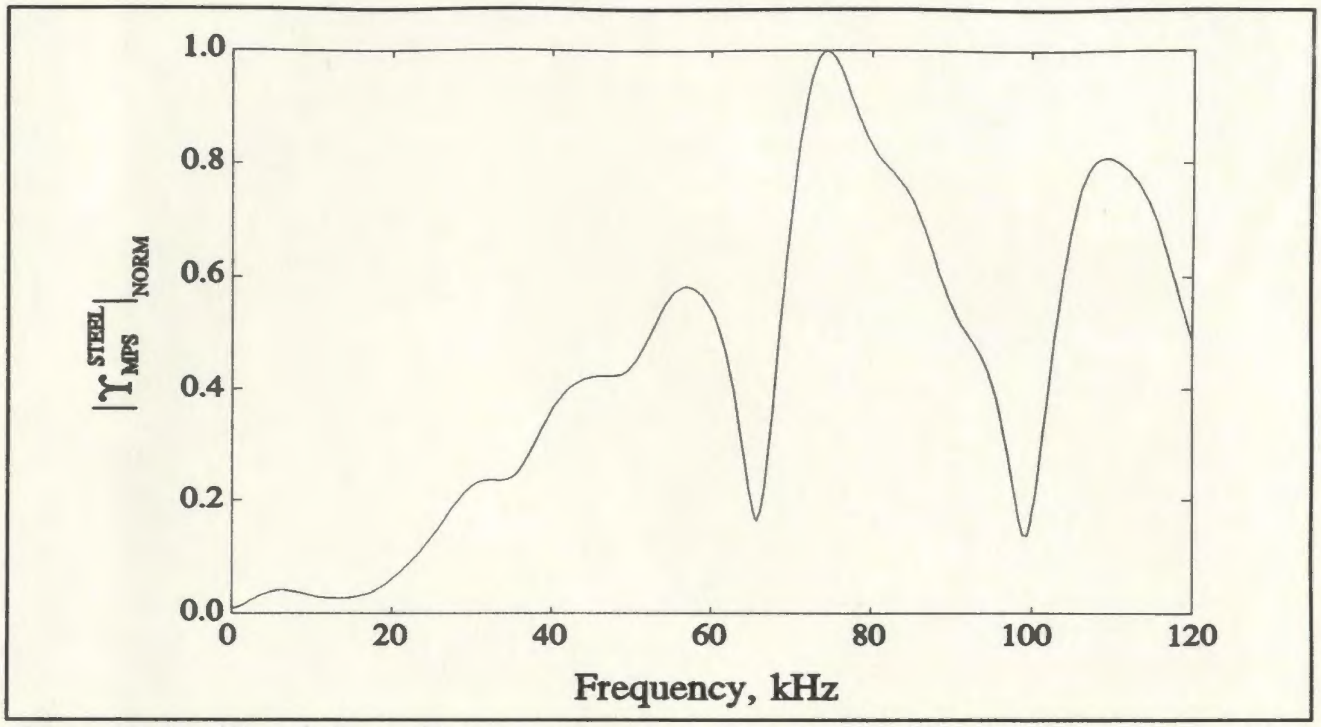

Figure C.3: $|\Upsilon_{MPS}|$ for a 30 mm radius steel sphere at r=250 mm from the array.

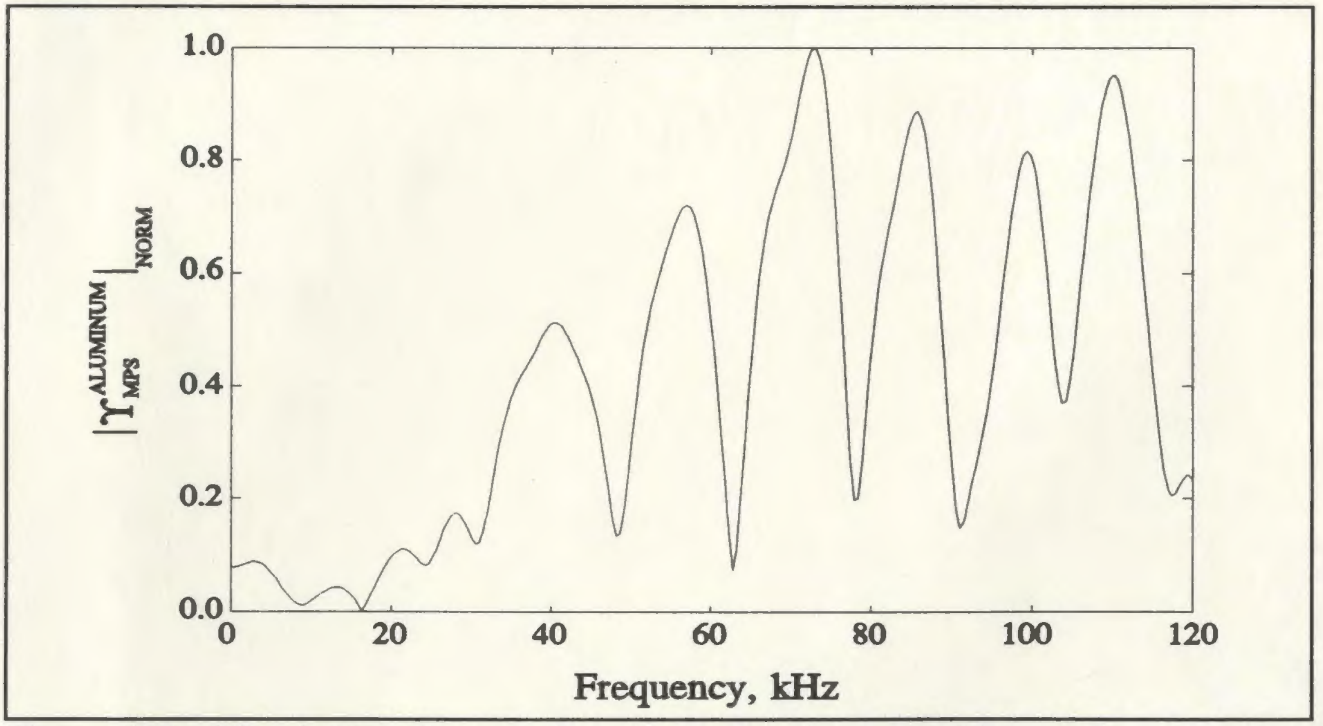

Figure C.4: $|\Upsilon_{MPS}|$ for a 40 mm radius aluminum sphere at r=250 mm from the array.

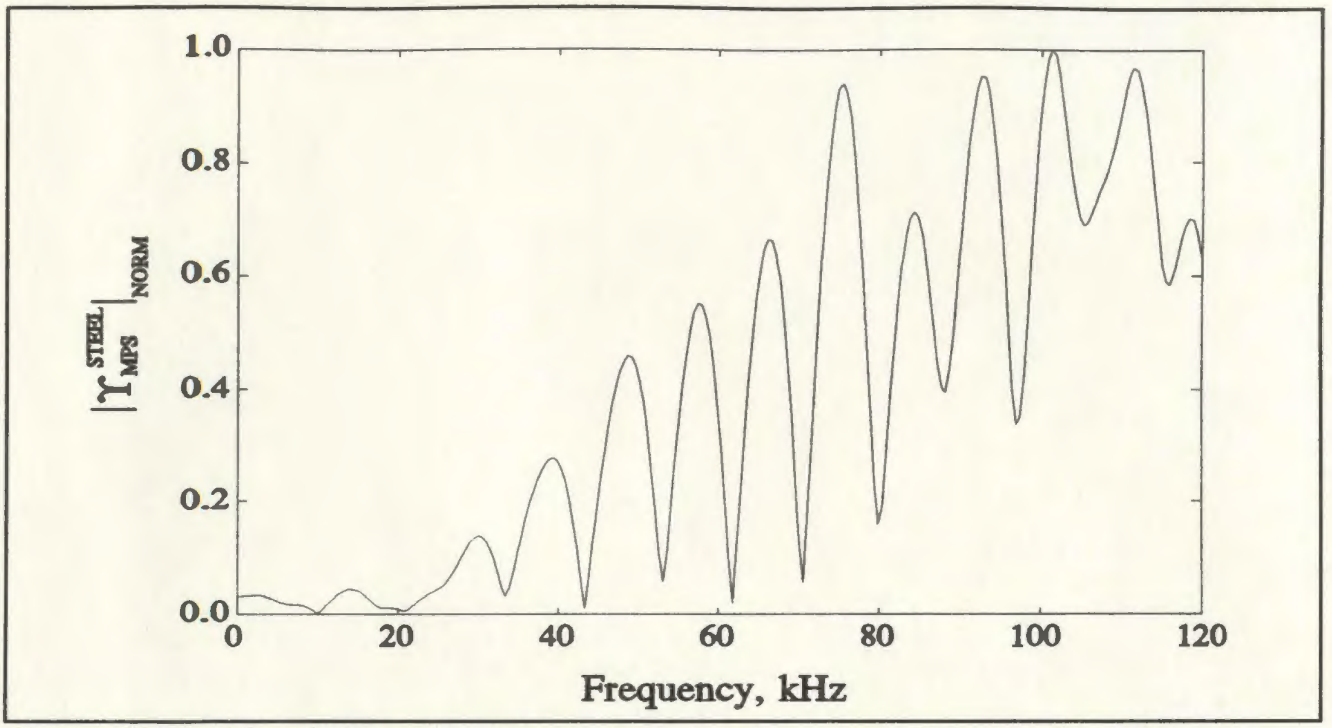

Figure C.5: $|\Upsilon_{MPS}|$ for a 60 mm radius steel sphere at r=350 mm from the array.

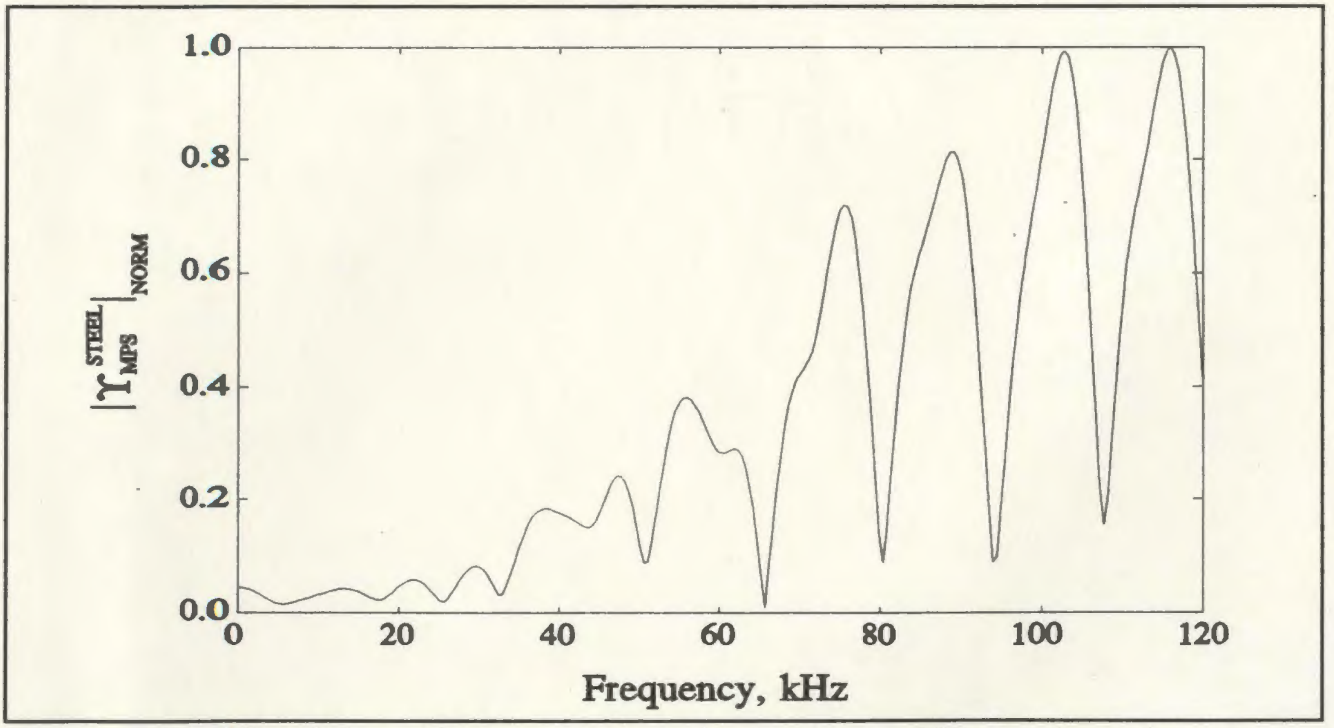

Figure C.6: $|\Upsilon_{MPS}|$ for a 40 mm radius steel sphere at r=350 mm from the array.

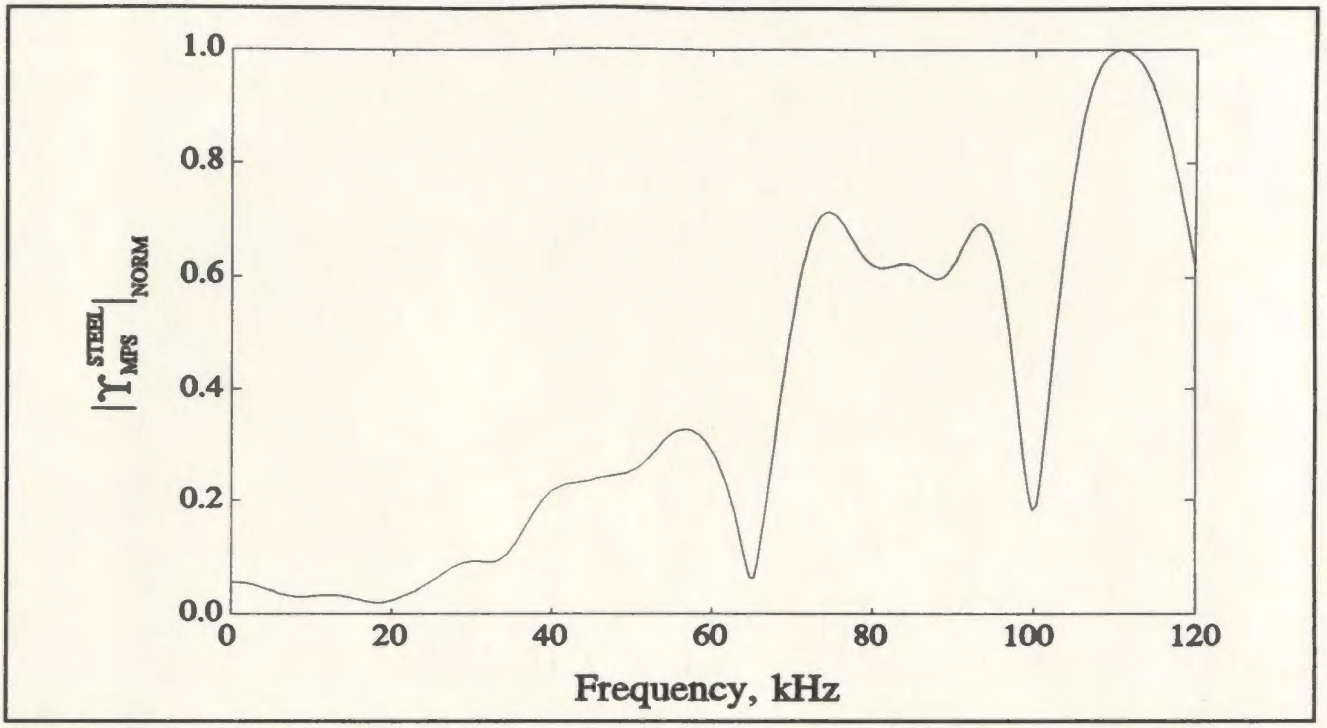

Figure C.7: $|\Upsilon_{MPS}|$ for a 30 mm radius steel sphere at r=350 mm from the array.

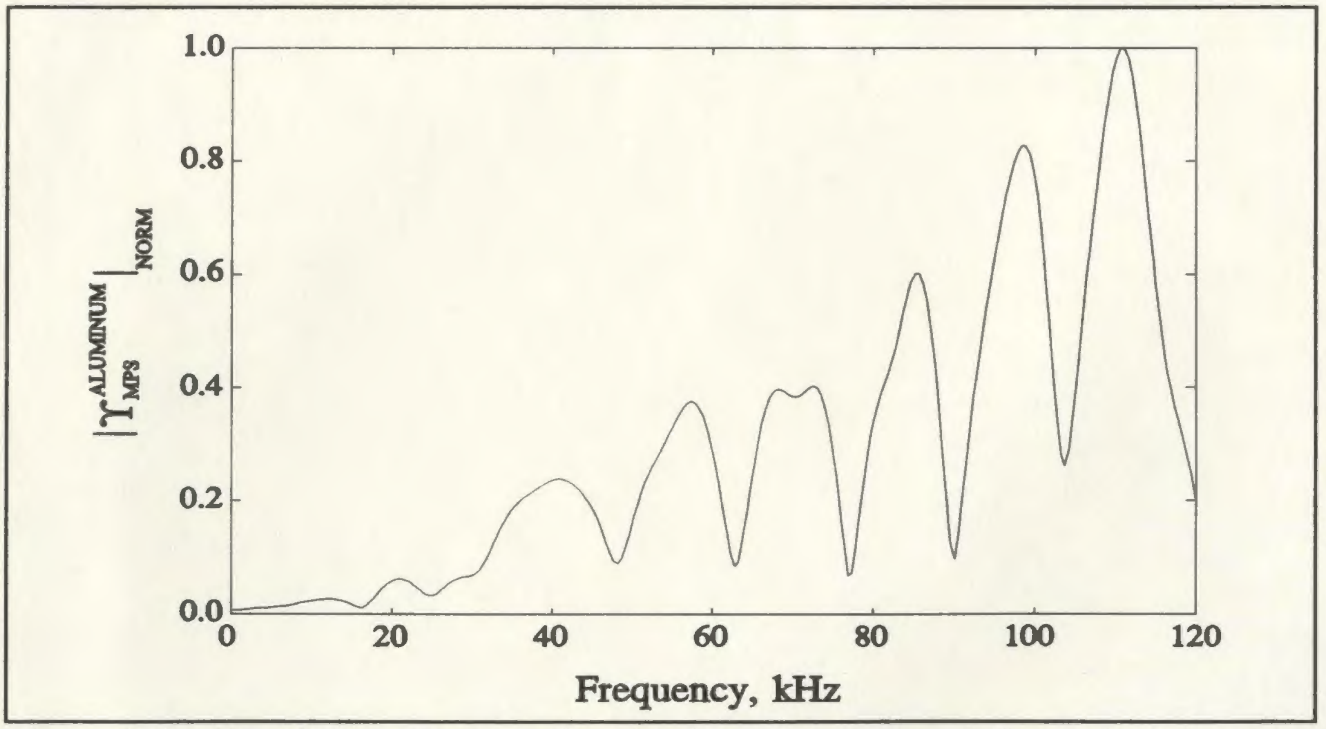

Figure C.8: $|\Upsilon_{MPS}|$ for a 40 mm radius aluminum sphere at r=350 mm from the array.

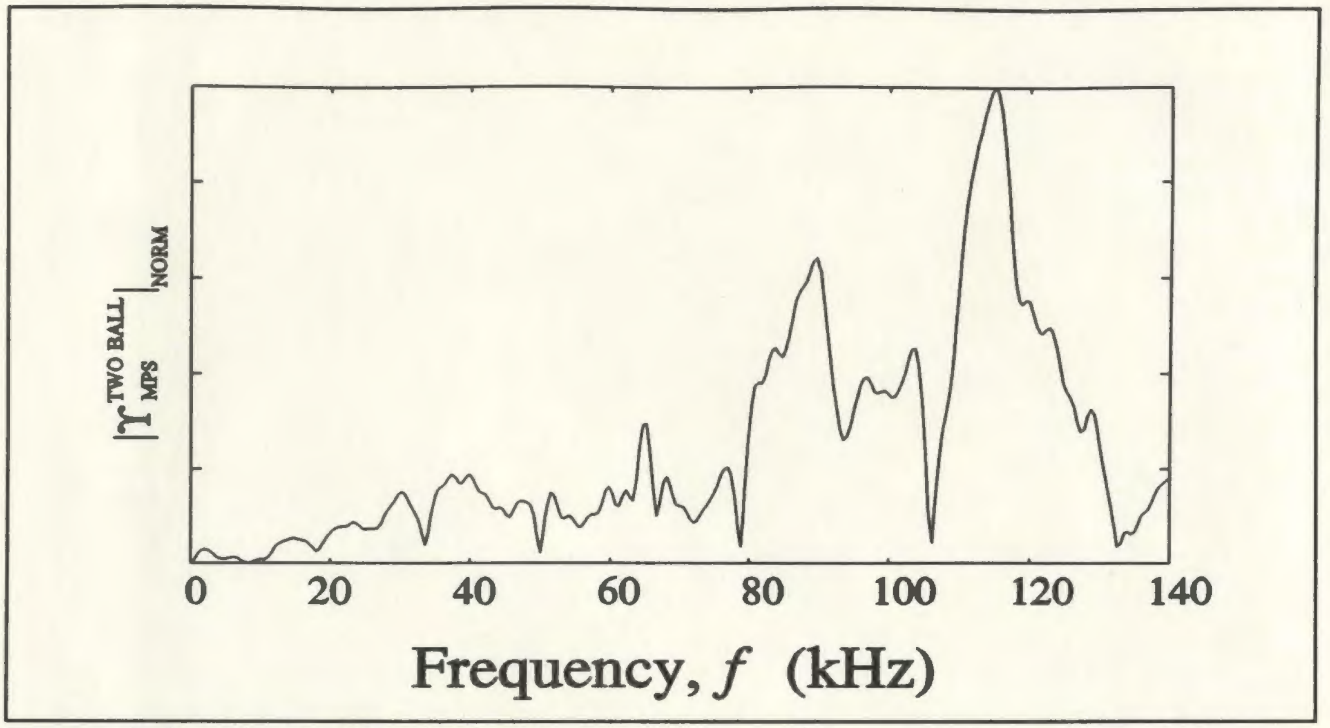

Figure C.9:: Two ball backscatter spectrum for r=35cm and d=4cm.

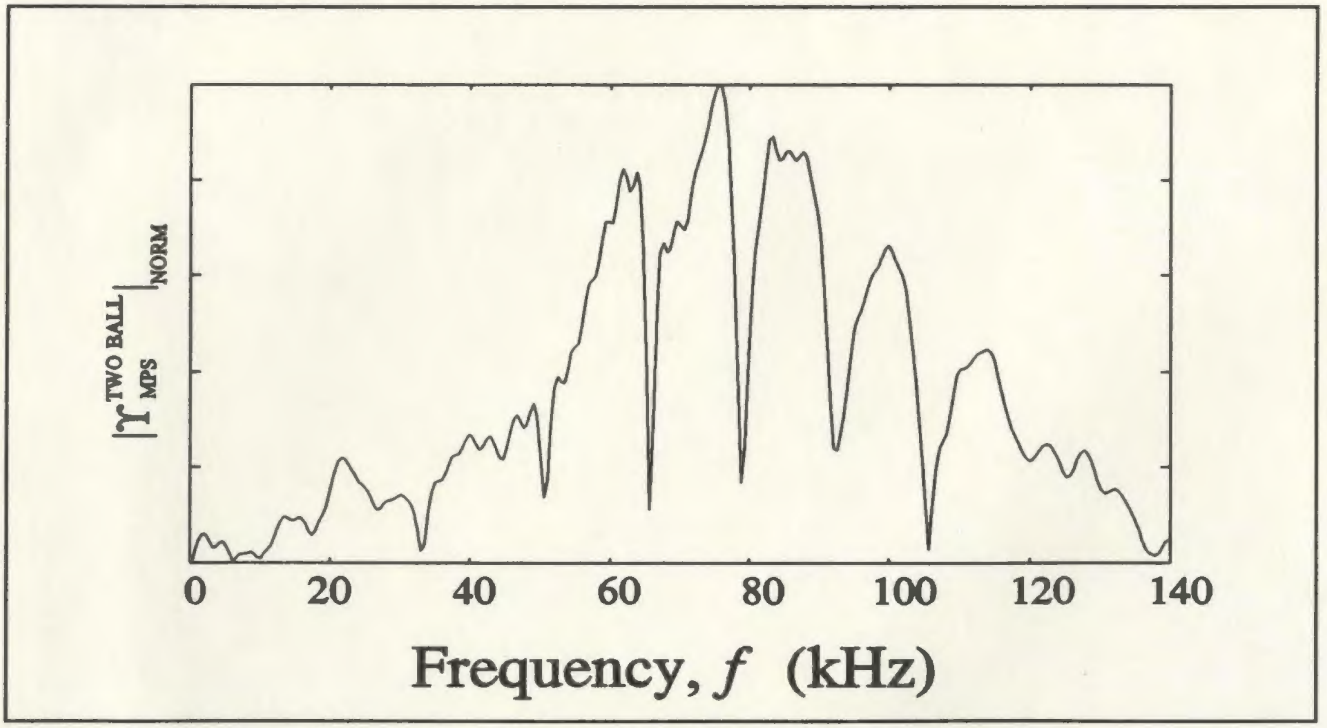

Figure C.10: Two ball backscatter spectrum for r=35cm and d=8cm.

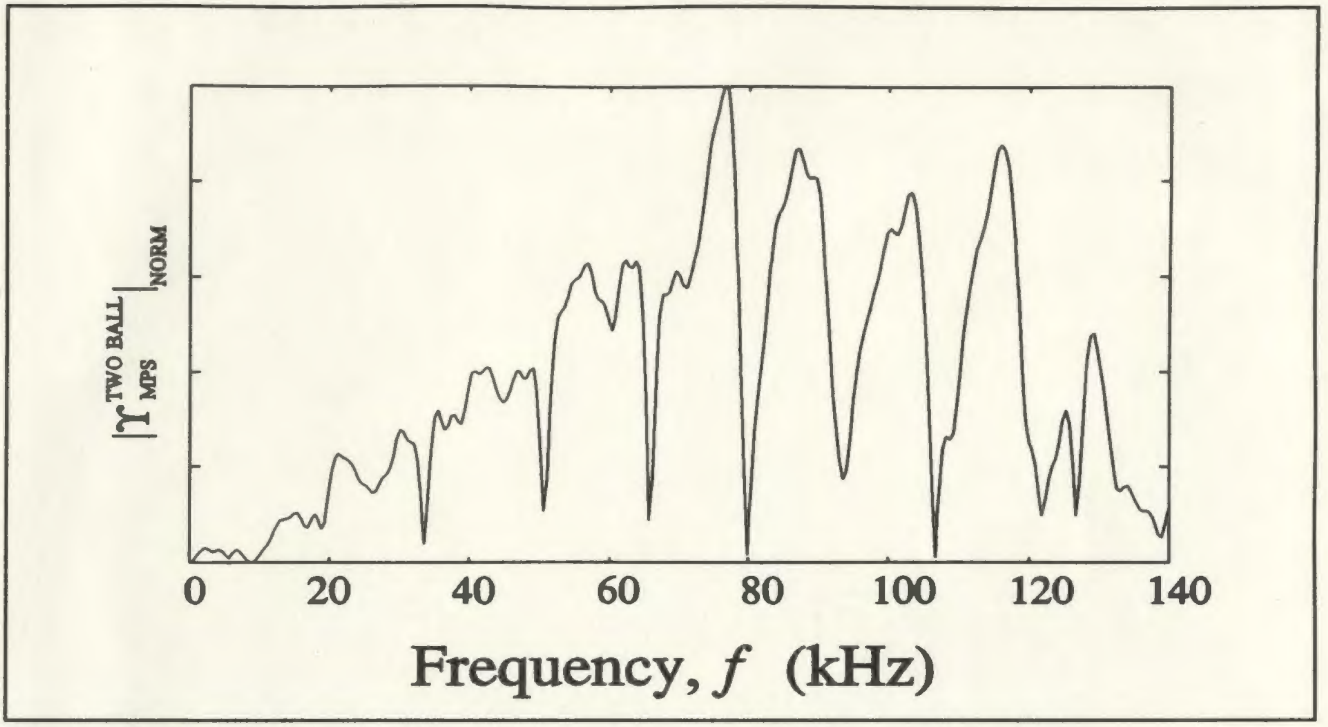

Figure C.11: Two ball backscatter spectrum for r=35cm and d=14cm.

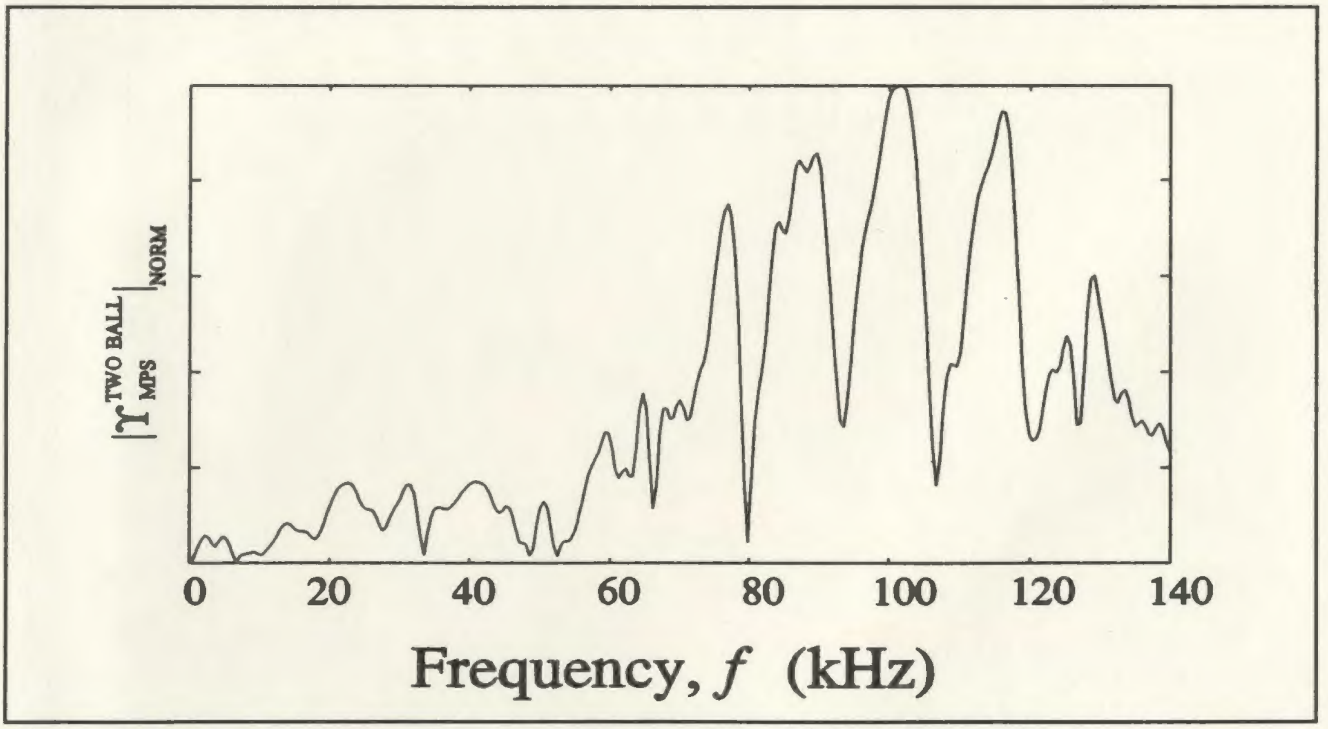

Figure C.12: Two ball backscatter spectrum for r=35cm and d=20cm.